Universidade de Aveiro
Departamento de Electrónica, Telecomunicações e Informática,
2015

Vítor Manuel Costa Ribeiro

Técnicas de Monitorização e Processamento Totalmente Óptico para Redes Transparentes

Monitoring and All-Optical Signal Processing Techniques for Transparent Networks

Vítor Manuel Costa Ribeiro

Técnicas de Monitorização e Processamento Totalmente Óptico para Redes Transparentes

Monitoring and All-Optical Signal Processing Techniques for Transparent Networks

This PhD Thesis was supervised by Prof. Dr. António Luís Jesus Teixeira, Associate Professor w/ Aggregation of the Departamento de Electrónica, Telecomunicações e Informática (DETI) of Universidade de Aveiro and co-supervised by Mário José Neves Lima Auxiliary Professor of the Departamento de Electrónica, Telecomunicações e Informática (DETI) of Universidade de Aveiro. .

Apoio financeiro da Fundacão para a Ciência
e a Tecnologia através da bolsa
SFRH/BD/69577/2010

o júri / the jury

presidente / president

Doutor Armando da Costa Duarte
Professor Catedrático da Universidade de Aveiro (por delegação do Reitor da Universidade de Aveiro)

vogais / examiners committee

Doutor António Luís Jesus Teixeira
Professor Associado com Agregação da Universidade de Aveiro (orientador)

Doutora Maria Inês Barbosa Carvalho
Professora Associada da Faculdade de Engenharia da Universidade do Porto

Doutor Paulo Miguel Nepomuceno Pereira
Professor Associado da Universidade de Aveiro

Doutor Luis Manuel Sousa Pessoa
Investigador Sénior da Faculdade de Engenharia da Universidade do Porto

Doutora Berta Maria Barbosa Neto
Consultora

Acknowledgements

First of all I want to thank my supervisor António Teixeira. His knowledge and technical skills are extremely high, but I believe that at the same level is his ability to deal and lead a team with different personalities. I want to thank him all his understanding, patience with me and encouragement to the realization of this thesis. I want also to thank my co-supervisor Mário Lima, who gave me the opportunity, 6 years ago to work in the optical communications group of IT-Aveiro.

I want to thank to Fundação para a Ciência e Tecnologia for giving the financial support to complete this thesis. I also wnat to thank to the projects Real-PON, MOTION, and PANORAMA, in which i was involved during the realization of this Ph.D. thesis. I want also to thank to IT-Aveiro in the name of its president Prof. José Neves for giving me the conditions to realize this thesis and its secretariat group for always giving me the appropriate support.

I also want to thank National Institute of Information and Communications Technology, Japan, specially the optical communications group and its leader Naoya Wada, for giving me the great opportunity to work in one of the best laboratories in the world. In there I had the pleasure to work with talented scientists such as Ruben Luís, Benjamin Puttnam, José Manuel Delgado Mendinueta, among others. I want to thank them all for teaching me so many thinks.

I want to thank my colleagues in IT, namely Ali Shahpari, Nelson Muga, Abdalla, Wael Dghais, Ana Rocha, Nuno Silva, Gil Fernandes, Zoran Vujicic, Álvaro Almeida, André Albuquerque, Fátima Domingues, Carlos Vicente, Artur Sousa, Fernando Guiomar, Nelson Rodrigues, Lucas Guardalben, Wonhoon Jang, among others. For them my total gratitude.

I also want to thank Sérgio Magalhães from Instituto Tecnológico e Nuclear and José Filipe Carvalho for being my friends at so many years. I apologize for not being with you more often.

Last but for sure not the least I want to specially thanks to my parents, for always giving the love and support, even in bad times, when the things look hopeless. For them my unconditional love. My thanks also to my sisters and nephews.

Palavras Chave Desempenho de redes ópticas, processamento totalmente óptico

Resumo As redes ópticas estão em constante desenvolvimento. A crescente demanda por dinamismo das mesmas requer cada vez mais, dispositivos que possam albergar diversos tipos de tráfego. Dessa forma surge o estudo sobre redes ópticas transparentes. Este tipo de abordagem torna as redes ópticas mais 'elegantes', devido a um uso mais eficiente dos recursos da rede. Nesta tese o autor propõe dispositivos que pretendem formar alternativas quer no estado da arte destas mesmas tecnologias quer no encaixe das mesmas em redes ópticas transparentes. Dado que a transparência total é dificil de alcançar com as tecnologias atuais (talvez com computação óptica mais desenvolvida isso seja possível), o autor propõe técnicas com diferentes níveis de transparência. No âmbito da monitoria de desempenho óptico o autor propôe duas técnicas para a monitoria da dispersão cromática com diferentes niveis de transparência.

No Capítulo 3 a técnica proposta parece fazer mais sentido para transmissões ópticas de longo curso e a elevadas taxas de transmissão, não só devido à sua moderada complexidade, mas também ao seu potencial custo. No entanto esta, é proposta para vários formatos de modulação, especialmente aqueles que têm uma componente de relógio bem saliente.

No Capítulo 4, o nível de transparência não foi testado para vários formatos de modulação, no entanto alguma transparência é obtida através da não inclusão de nenhum dispositivo eléctrico após o receptor (excepto um conversor analógico-digital). Isto permite que esta técnica possa operar a elevadas taxas de transmissão acima de 100 Gbit/s, se for utilizada amostragem electro-óptica assíncrona antes do receptor. Dessa forma pode ser utilizado um fotodetector de baixo custo e de baixa largura de banda.

No capítulo 5 é demonstrada uma técnica para monitoria em simultâneo de vários impedimentos da rede óptica atráves de um novo método para gerar diagramas de análise de desempenho com redes neuronais artificiais.

No capítulo 6 o autor demonstra uma técnica para controlo da polarização, totalmente processada no domínio óptico assim como um exemplo de como o processamento totalmente óptico pode cooperar com o monitoria do desempenho óptico.

Keywords Optical performance monitoring, All-optical signal processing

Abstract

Optical networks are under constant evolution. The growing demand for dynamism require devices that can accommodate different types of traffic. Thus the study of transparent optical networks arises. This approach makes optical networks more "elegant" , due to a more efficient use of network resources. In this thesis, the author proposes devices that intend to form alternative approaches both in the state of art of these same technologies both in the fitting of this technologies in transparent optical networks. Given that full transparency is difficult to achieve with current technology (perhaps with more developed optical computing this is possible), the author proposes techniques with different levels of transparency. On the topic of performance of optical networks, the author proposes two techniques for monitoring chromatic dispersion with different levels of transparency.

In Chapter 3 the proposed technique seems to make more sense for long-haul optical transmission links and high transmission rates, not only due to its moderate complexity but also to its potential moderate/high cost. However it is proposed to several modulation formats, particularly those that have a protruding clock component.

In Chapter 4 the transparency level was not tested for various modulation formats, however some transparency is achieved by not adding any electrical device after the receiver (other than an analog-digital converter). This allows that this technique can operate at high transmission rates in excess of 100 Gbit / s, if electro-optical asynchronous sampling is used before the optical receiver. Thus a low cost and low bandwidth photo-detector can be used.

In chapter 5 is demonstrated a technique for simultaneously monitoring multiple impairments of the optical network by generating novel performance analysis diagrams and by use of artificial neural networks.

In chapter 6 the author demonstrates an all-optical technique for controlling the optical state of polarization and an example of how all-optical signal processing can fully cooperate with optical performance monitoring.

Contents

List of Figures

List of Tables

List of Acronyms

AAH asynchronous amplitude histograms

ADC analog to digital converter

AM amplitude modulated

ANN artificial neural network

AOPC all-optical polarization control

AOR all-optical regeneration

AOSP all-optical signal processing

ASE amplified spontaneous emission

ATDD asynchronous time-delay diagrams

BER bit-error rate

BL bandwidth-distance

BPF band-pass filter

BPSK binary phase-shift keying

BTB back-to-back

CD chromatic dispersion

DCF dispersion compensating fiber

DGD differential group delay

DOP degree of polarization

DSF dispersion-shifted fiber

DSP digital signal processing

ECL external cavity laser

EDFA erbium-doped fiber amplifier

EON elastic optical networks

ESP electrical signal processing

FOPA fiber optical parametric amplifier

FWM four-wave mixing

HNLF highly non-linear fiber

MZI Mach-Zehnder interferometer

MZM Mach-Zehnder modulator

NOLM nonlinear optical loop mirror

NRZ non-return to zero

OADM optical add-drop multiplexers

OBS optical burst switching

OFC optical fiber conference

OGF optical gaussian filter

OOK on-off keying

OPM optical performance monitoring

OPS optical packet-switched

OSNR optical signal to noise ratio

PAED parametric asynchronous eye diagram

PAPR peak to average power ratio

PC polarization controller

PLS partial least squares

PM phase modulated

PMD polarization mode dispersion

PMF polarization maintaining fiber

PPG pulse-pattern generator

PRBS pseudo-random bit sequence

PSK phase-shift keying

PSP principal states of polarization

PT pilot-tone

PTP point-to-point

QoS quality-of-service

QPSK quadrature phase-shift keying

RF radio-frequency

RMSE root-mean-square-error

RZ return-to-zero

SBS stimulated brillouin scattering

SDM space division multiplexing

SED synchronous eye diagram

SEMF spectrally efficient modulation formats

SMF single-mode fiber

SOA semiconductor optical amplifier

SOP state of polarization

SPM self-phase modulation

TPA two-photon absortpion

VDC variable dispersion compensator

VOA variable optical attenuator

WDM wavelength division multiplexing

XGM cross-gain modulation

XPM cross-phase modulation

CHAPTER 1

Introduction

1.1 Historical overview and motivation

Optical networks are evolving to become more complex and thus more difficult to operate [1]. This complexity increases with the bandwidth demand, pushing the network operators and service providers to re-scale the physical layer infrastructure [1]. Wavelength division multiplexing (WDM) technology along with low spectrally efficient modulation formats (SEMF) were able during the so called WDM era [2] to satisfy the required bandwidth demand. Although in the mid 90's, when all the optical bandwidth was occupied and the first 1 Tb/s transmission was experimentally demonstrated, researchers started to look for ways to transmit and receive optical modulation formats with higher spectral efficiency [2, 3]. Phase, polarization and more recently space division multiplexing (SDM) have been proposed since then. This multiplexing techniques were already known by the academic and industrial societies. Particularly phase multiplexing or coherent optical communications as it is generally known, received great attention in the 80's as a solution to circumvent the limitation of

electronic repeaters [4]. Although this attention stopped, since erbium-doped fiber amplifier (EDFA) has become commercially available in the beginning of the 90's. It returned recently with the availability of digital coherent receivers using digital signal processing (DSP) techniques along with advancements in analog to digital converters (ADC), which by mitigating fiber impairments increased the bandwidth-distance (BL) product[5]. Currently it is expected that the fiber capacity limit with the current available technologies will be reached in the year of 2015 [2, 3]. Therefore two options are being considered for the near future of optical networks: increase the one fiber capacity limit (e.g. by using SDM) along with the BL product [2] or/and fine the optical networks granularity in order to avoid over design and efficiently allocate network resources in a per-demand basis [6]. Operators provide fixed bandwidth allocation for the worst case scenario, when most of the time it is not being used [7].

Regarding the second option since optical add-drop multiplexers (OADM) have become available optical networks went from opaque to transparent [7] (the term translucent is more adequate since optical-electrical-optical conversions may occur at the border nodes of the network). Efficiency on the use of network resources has been further increased, by introducing reconfigurable OADM and optical cross-connects which have enabled to adapt network resources remotely, accordingly to dynamic changes of network traffic [7]. Over the last years several efforts have been carried to improve network efficiency. One obvious solution is to introduce a finer granularity in to optical networks by increasing the number of dimensions for which the network can be adapted. Optical burst switching (OBS) and optical packet-switched (OPS) networks are the finer granularity solutions although its enabling technologies are not yet mature [8, 9], but still they are envisioned for the optical communications network of the future, when full transparency is implemented, which will require advanced all-optical signal processing (AOSP). A mean-term solution have received great attention recently: elastic optical networks (EON), which by adapting the spectrum allocation and modulation level dimensions in a per-demand basis, improve flexibility and introduce finer granularity in to the network. Traditional routing and wavelength assignment algorithms are no longer valid in this situation. Therefore it is transformed in to a routing, modulation level and spectrum allocation problem where for all connection requests is assigned a spectrum fraction[7].

Two enabling technologies are envisioned as key requirements for the optical communications networks of the future, such as EON, OBS and OPS: optical performance monitoring (OPM) [10–13] and AOSP [9, 14–16].

OPM is very important, but will be a key requirement in future optical networks, since with finer granularity, comes also higher number of parameters, for which OPM techniques must be able to adapt to achieve fully transparent optical networks. OPM is important for a robust and stable operation of optical networks, accommodate transparency, route traffic accordingly to impairment information (impairment-aware routing) and secure links [12]. AOSP provides transparency and scalability for future optical networks [17]. Is expected that all-optical routers, build over AOSP, can exploit a new wavelength domain available in switching and contention resolution in future OPS networks [9]. In current demonstrations of OBS and OPS networks, polarization dependent devices such as semiconductor optical amplifiers or nonlinear waveguides, have been used extensively [9] for AOSP. Therefore is important a careful adjustment of the state of polarization, to reduce the packet loss ratio.

OPM techniques shall accommodate transparency [12]. However, fully transparent optical performance monitoring techniques is difficult to achieve, with the current available technologies. Therefore, it is expected that OPM techniques are able to accommodate a limited amount of modulation formats and bit rates. Available techniques have demonstrated the capability to monitor several modulation formats, [18–22], although to achieve this goal, tuning of the OPM technique is required. This tuning is not necessarily done in hardware, which is not desirable [12], but by adapting the output impairment value to the traffic type. This can be achieved by first detecting the bit rate and modulation format [23–25] and afterwards evaluating the impairment value. In Figure 1.1, it is demonstrated how this can be achieved.

AOSP is an enabling technology for the next generation optical networks. OBS and OPS, require fast processing of bursts/packets. Electronic signal processing is limited in bandwidth, therefore if one wants to fast process optical packets or bursts, all-optical signal processing is required for fast switching in OPS [26] and OBS, respectively. Such OPS use intensively a number of photonic devices that are polarization dependent. Therefore carefull adjustment of the state of polarization (SOP) is required. In Chapter 6, the author demonstrates, all-optical

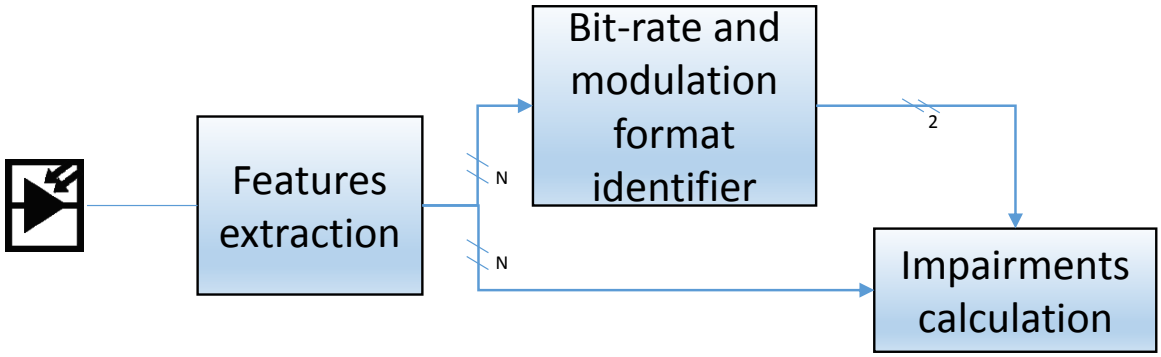

Figure 1.1: Strategy for impairment calculation in distinct traffic scenarios

polarization alignment in order to carefully adjust the SOP of packets, into the transmission fiber. The motivation of this thesis is to discuss and propose novel enabling technologies and methodologies for transparent optical networks, in the subfields of OPM and AOSP.

1.2 Thesis Outlook

The following chapters present solutions to accommodate the problems of OPM and AOSP.

Chapter 2 makes a general overview of OPM techniques. Within there is an overview of the state of the art of the monitoring strategies used in novel proposed techniques of Chapters 3 to 5. Within each chapter related with OPM (Chapter 3 to Chapter 5) there is a more detailed state of the art involving the proposed techniques. Chapter 3 and Chapter 4 analyze the problem of estimating chromatic dispersion (CD) in distinct scenarios (long-haul and short-haul communication links, respectively). Chapter 5 extends this study to polarization mode dispersion (PMD) and optical signal to noise ratio (OSNR) study and modelling in fiber.

Chapter 3 deals with the problem of estimating CD with a large monitoring window (2040 ps/nm) in long-haul communication links in a dynamical environment. The author analyzes the usage of Q-factor estimation together with radio-frequency (RF) clock-tone monitoring in order to achieve this goal.

Chapter 4 analyzes the substitution of an RF filter, required in RF spectral analysis (see Chapter 2), by an optical filter and electro-optical sampling, in order to estimate residual CD at 10 Gbit/s. This chapter analyzes this substitution

and studies if it allows that a low bandwidth photo-detector can be installed in the receiver.

Chapter 5 deals with multi-impairment optical performance monitoring. In this chapter is proposed a novel technique to monitor simultaneously CD, PMD and OSNR. Moreover the accuracy of the proposed model and the impact of inter-correlations between impairments is analyzed. The proposed diagram is compared with synchronous eye diagram (SED) in terms of description of anomalies in the optical signal.

Chapter 6 analyzes AOSP for the specific area of OPS. A general overview of the state of the art motivates the analysis of all-optical polarization control using the polarization attraction effect in OPS networks.

Chapter 7 draws the conclusions and prospects for future work.

1.3 Main Achievements

In the author opinion the main achievements reported in this thesis are:

- Proposal of a new method to monitor CD in long reach optical communications systems at $40\,\mathrm{Gbit/s}$. The achieved monitoring range at $40\,\mathrm{Gbit/s}$ of $2040\,\mathrm{ps/nm}$ is to the best of the author knowledge a record if we do not take into account low frequency pilot-tone (PT)s methods, which give higher monitoring range but at the price of much lower monitoring sensitivity.

- Proposal of a new method to monitor residual dispersion without requiring post-detection electrical components. Therefore this enables the possibility to use optical domain processing techniques allowing OPM at high data rates.

- Demonstration of a novel methodology to obtain performance diagrams such as the parametric asynchronous eye diagram (PAED) developed and named by the author of this thesis. The novelty resides in the ability to draw diagrams similar to an eye diagram, not only in on-off keying (OOK) modulation formats, as in previous methods, but also in coherent modulation formats such as quadrature phase-shift keying (QPSK). Simulations show that QPSK modulation format using direct detection also produces comprehensible diagrams with the ability to recognize important features

of the signal such as phase shifting caused by CD. Simultaneous estimation of impairments such as CD, PMD and OSNR is also achieved. This resulted in a patent and an award.

- Proposal of a fast all-optical polarization control using the polarization attraction effect in fibers, to manage the SOP in polarization sensitive OPS networks. Since optical packets may have duration as short as some nanoseconds and the SOP may vary in a packet-by-packet basis, a polarization control mechanism with that time response is required. This time response is not available with electro-optical devices such as the ones based in lithium niobate. The author found an AOSP solution suitable for solving this issue.

1.4 List of Publications

1.4.1 Journal Articles

6. **V. Ribeiro**, R. S. Luís, J. M. D. Mendinueta, B. Puttnam, A. Shahpari, N. Muga, M. Lima, S. Shinada, N. Wada and A. Teixeira, "All-Optical Packet Alignment using Polarization Attraction Effect," Photonics Technology Letters, IEEE, Vol. 27, No. 5, Mar. 2015. doi:10.1109/LPT.2014.2384592

5. **V. Ribeiro**, M. Lima and A. Teixeira, "Comparison of optical performance monitoring techniques using artificial neural networks," Neural Computing and Applications, Springer, Vol. 23, pp. 583-589, 2013
doi:10.1007/s00521-013-1405-z

4. **V. Ribeiro**, L. Costa, M. Lima and A. Teixeira, "Optical performance monitoring using the novel parametric asynchronous eye diagram," Opt. Express, OSA, Vol. 20, No. 9, pp. 9851 - 9861 , Apr. 2012.
doi:10.1364/OE.20.009851

3. **V. Ribeiro**, A. Teixeira, M. Lima, "Experimental validation of a chromatic dispersion monitoring technique using optical asynchronous sampling and double sideband filtering," Optical Fiber Technology, Elsevier, Vol. 17, No. 2, pp. 135 - 137, Mar. 2011.
doi:10.1016/j.yofte.2011.01.007

2. **V. Ribeiro**, A. Teixeira, M. Lima, "Chromatic dispersion monitoring technique using optical asynchronous and double sideband filtering," Optical Fiber Technology, Elsevier, Vol. 16, No. 2, pp. 124 - 127, Mar. 2010. doi:10.1016/j.yofte.2010.01.006

1. **V. Ribeiro**, L. Costa, A. Teixeira, R. Nogueira, M. Lima, "Chromatic Dispersion Monitoring Scheme Using Mach-Zehnder Interferometer and Q-factor Calculation," Journal of Optical Communications and Networking, IEEE/OSA, Vol. 2, No. 1, pp. 10 - 19, Jan. 2010. doi:10.1364/JOCN.2.000010

1.4.2 Conference Articles

5. **V. Ribeiro**, R. S. Luís, J. M. D. Mendinueta, B. Puttnam, A. Shahpari, N. Muga, M. Lima, S. Shinada, N. Wada and A. Teixeira, "Sub-microsecond packet polarization alignment using all-optical polarization attraction," Proc Optoelectronics and Communications Conf. - OECC Melbourne, Australia, Jul. 2014, paper TU4A-3.

4. **V. Ribeiro**, M. Lima, A. Teixeira, "Artificial Neural Networks in the scope of Optical Performance Monitoring," Proc. of Controlo 2012- Funchal, Madeira, Jul. 2012.

3. **V. Ribeiro**, M. Lima, A. Teixeira, "Parametric Asynchronous Eye Diagram For Optical Performance Monitoring," in Optical Fiber Communications , OSA Conference, Los Angeles, United States, pp. 1 - 3, Mar. 2012, paper JW2A.33. doi:10.1364/NFOEC.2012.JW2A.33

2. **V. Ribeiro**, A. Teixeira, M. Lima, "Chromatic Dispersion Monitoring by means of peak to average power calculation with NRZ an RZ modulation," Proc. European Conf. on Networks and Optical Communications - NOC, Algarve, Portugal, Vol. 15, pp. 181 - 184, Jun., 2010.

1. **V. Ribeiro**, M. Lima, A. Teixeira, R. Nogueira, "Chromatic dispersion monitoring scheme with very high dispersion monitoring window at 40 Gbit/s," Proc Conf. on Telecommunications - ConfTele, Santa Maria da Feira , Portugal, Vol. 7, May 2009.

1.4.3 Patents

1. V. Ribeiro, M. Lima, A. Teixeira, 'Método de geração de diagramas de olho em modo assíncrono', Patent PT 105360A Apr. 2012, see Appendix A.

1.4.4 Awards due to PhD work

1. 1^{st} prize in entrepreneurship course of technological basis (CEBT), Iberian , sponsored by University of Aveiro, University of Coimbra and University of Beira Interior.

References

[1] J. Berthold, A. A. M. Saleh, L. Blair, and J. M. Simmons, "Optical networking: Past, present, and future," *Lightwave Technology, Journal of*, vol. 26, pp. 1104–1118, May 2008.

[2] D. J. Richardson, J. M. Fini, and L. E. Nelson, "Space-division multiplexing in optical fibres," *Nature Photonics*, vol. 7, no. 5, pp. 354 – 362, 2013.

[3] R. Essiambre and R. Tkach, "Capacity trends and limits of optical communication networks," vol. 100, pp. 1035–1055, May 2012.

[4] T. Okoshi, *Coherent optical fiber communications*, vol. 3. Springer, 1988.

[5] S. Savory, "Digital coherent optical receivers: Algorithms and subsystems," *Selected Topics in Quantum Electronics, IEEE Journal of*, vol. 16, pp. 1164–1179, Sep. 2010.

[6] K. Christodoulopoulos, I. Tomkos, and E. A. Varvarigos, "Elastic bandwidth allocation in flexible ofdm-based optical networks," *Lightwave Technology, Journal of*, vol. 29, pp. 1354–1366, May 2011.

[7] I. Tomkos, M. Angelou, R. J. Duran Barroso, I. de Miguel, R. M. Lorenzo Toledo, D. Siracusa, E. Salvadori, A. Tymecki, Y. Ye, and I. Tafur Monroy, "Next generation flexible and cognitive heterogeneous optical networks," in *The Future Internet*, vol. 7281 of *Lecture Notes in Computer Science*, pp. 225–236, Springer Berlin Heidelberg, 2012.

[8] S. Yoo, "Energy efficiency in the future internet: The role of optical packet switching and optical-label switching," *Selected Topics in Quantum Electronics, IEEE Journal of*, vol. 17, pp. 406–418, Mar. 2011.

[9] S. J. B. Yoo, "Optical packet and burst switching technologies for the future photonic internet," *Lightwave Technology, Journal of*, vol. 24, pp. 4468–4492, Dec. 2006.

[10] L. Dittmann, C. Develder, D. Chiaroni, F. Neri, F. Callegati, W. Koerber, A. Stavdas, M. Renaud, A. Rafel, J. Sole-Pareta, W. Cerroni, N. Leligou, L. Dembeck, B. Mortensen, M. Pickavet, N. Le Sauze, M. Mahony, B. Berde, and G. Eilenberger, "The european ist project david: a viable approach toward optical packet switching," *Selected Areas in Communications, IEEE Journal on*, vol. 21, pp. 1026–1040, Sep. 2003.

[11] I. de Miguel, R. Duran, T. Jimenez, N. Fernandez, J. Aguado, R. Lorenzo, A. Caballero, I. Tafur Monroy, Y. Ye, A. Tymecki, I. Tomkos, M. Angelou, D. Klonidis, A. Francescon, D. Siracusa, and E. Salvadori, "Cognitive dynamic optical networks [invited]," *Optical Communications and Networking, IEEE/OSA Journal of*, vol. 5, pp. A107–A118, Oct. 2013.

[12] A. Willner, X. Wu, and J.-Y. Yang, "1 - optical performance monitoring: Perspectives and challenges," in *Optical Performance Monitoring* (C. C. Chan, ed.), pp. 1 – 19, Oxford: Academic Press, 2010.

[13] X. Cai, K. Wen, R. Proietti, Y. Yin, D. Geisler, R. Scott, C. Qin, L. Paraschis, O. Gerstel, and S. Yoo, "Experimental demonstration of adaptive combinational qot degradation restoration in elastic optical networks," *Lightwave Technology, Journal of*, vol. 31, pp. 664–671, Feb. 2013.

[14] D. Blumenthal, J. Bowers, L. Rau, H. F. Chou, S. Rangarajan, W. Wang, and H. Poulsen, "Optical signal processing for optical packet switching networks," *Communications Magazine, IEEE*, vol. 41, pp. S23–S29, Feb. 2003.

[15] J. Kurumida and S. Yoo, "Nonlinear optical signal processing in optical packet switching systems," *Selected Topics in Quantum Electronics, IEEE Journal of*, vol. 18, pp. 978–987, Mar. 2012.

[16] L. Liu, R. Kumar, K. Huybrechts, T. Spuesens, G. Roelkens, E.-J. Geluk, T. de Vries, P. Regreny, D. Van Thourhout, R. Baets, and G. Morthier, "An ultra-small, low-power, all-optical flip-flop memory on a silicon chip.," *Nature Photonics*, vol. 4, no. 3, pp. 182 – 187, 2010.

[17] L. Yan, A. Willner, X. Wu, A. Yi, A. Bogoni, Z. Y. Chen, and H. Y. Jiang, "All-optical signal processing for ultrahigh speed optical systems and networks," *Lightwave Technology, Journal of*, vol. 30, pp. 3760–3770, Dec. 2012.

[18] J. Zhao, Z. Li, D. Liu, L. Cheng, C. Lu, and H. Y. Tam, "Nrz-dpsk and rz-dpsk signals signed chromatic dispersion monitoring using asynchronous delay-tap sampling," *Lightwave Technology, Journal of*, vol. 27, no. 23, pp. 5295–5301, 2009.

[19] H. Takara, I. Shake, T. Ohara, and B. Kozicki, "Optical performance monitoring using asynchronous amplitude histogram," in *Optical Internet, 2007 and the 2007 32nd Australian Conference on Optical Fibre Technology. COIN-ACOFT 2007. Joint International Conference on*, pp. 1 –3, 2007.

[20] V. Ribeiro, L. Costa, A. Teixeira, R. Nogueira, and M. Lima, "Chromatic-dispersion-monitoring scheme using a mach-zehnder interferometer and q-factor calculation," *J. Opt. Commun. Netw.*, vol. 2, pp. 10–19, Jan. 2010.

[21] B. Kozicki, A. Maruta, and K. ichi Kitayama, "Experimental demonstration of optical performance monitoring for rz-dpsk signals using delay-tap sampling method," *Opt. Express*, vol. 16, pp. 3566–3576, Mar. 2008.

[22] T. Anderson, S. Dods, A. Kowalczyk, J. Bedo, and K. P. Clarke, "Method and apparatus for sampled optical signal monitoring, patent application," Jan. 2009.

[23] Y. Zhou, T. B. Anderson, K. Clarke, A. Nirmalathas, and K. L. Lee, "Bit rate identification using asynchronous delay-tap sampling," in *Proc. 34th European Conf. Optical Communication ECOC 2008*, pp. 1–2, 2008.

[24] F. N. Khan, Y. Zhou, A. P. T. Lau, and C. Lu, "Modulation format identification in heterogeneous fiber-optic networks using artificial neural networks," *Opt. Express*, vol. 20, pp. 12422–12431, May 2012.

[25] V. Ribeiro, L. Costa, M. Lima, and A. L. J. Teixeira, "Optical performance monitoring using the novel parametric asynchronous eye diagram," *Opt. Express*, vol. 20, pp. 9851–9861, Apr. 2012.

[26] M. Spyropoulou, N. Pleros, and A. Miliou, "Soa-mzi-based nonlinear optical signal processing: A frequency domain transfer function for wavelength conversion, clock recovery, and packet envelope detection," *Quantum Electronics, IEEE Journal of*, vol. 47, pp. 40–49, Jan. 2011.

CHAPTER 2

Optical performance monitoring

This chapter elaborates a general overview of optical performance monitoring techniques, that the author considers of most relevance due to its relative simplicity, low cost and that have been historically reproduced in different ways by several papers and authors. Recently there have been a major concern about phase-shift keying (PSK) modulation formats, although the author will not address them, since most of the schemes to estimate impairments are included as part of coherent digital signal processing (DSP) compensation mechanisms, which are not the focus of this review.

2.1 What is optical performance monitoring?

Optical performance monitoring (OPM) is a widespread research topic in optical communications. Its research started in the early 90s and the term itself has taken several definitions [1].

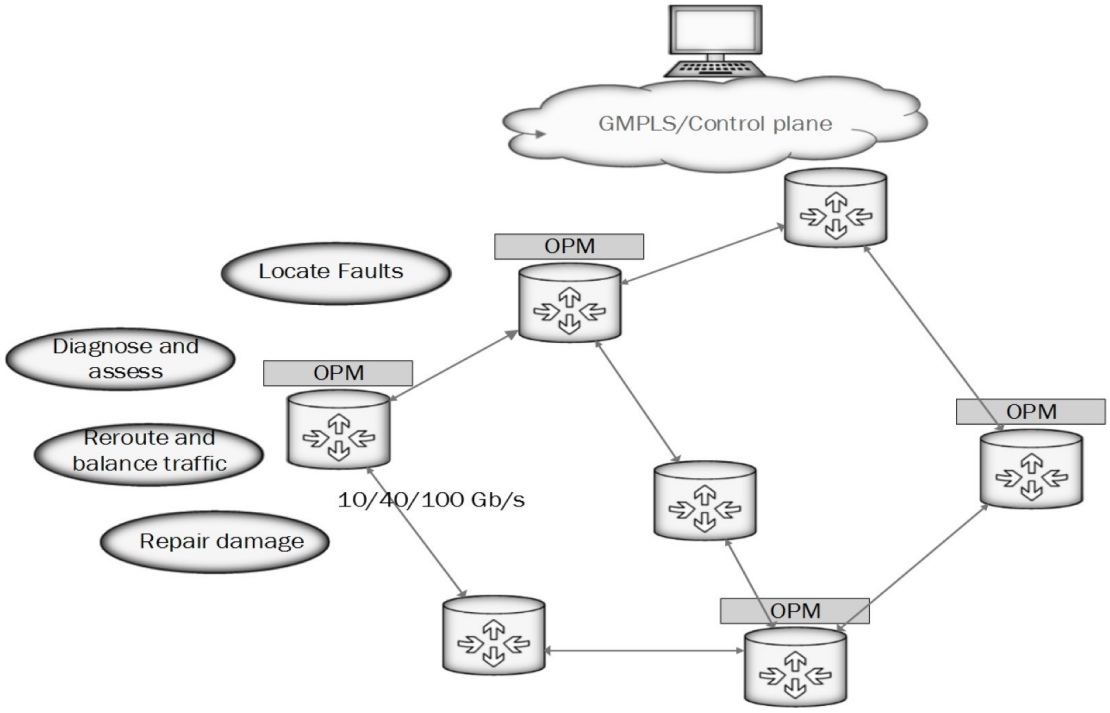

Figure 2.1: Optical performance monitors placement along the network with its functionalities. Locate faults, diagnose and assess, repair damage and reroute and balance traffic (based on [2])

In Figure 2.1 we can see an optical network where some nodes include optical performance monitoring. The optimum placement of optical performance monitors along the network is subject of research [3, 4] by the scientific community, since the placement of one optical performance monitor per link is not efficient [4]. The functionalities of optical performance monitors are demonstrated in Figure 2.1: locate faults, diagnose and assess, reroute and balance traffic and repair damage [2]. These functionalities act as a reaction to natural disasters or network malfunctions due to aging of the network or lack of maintenance. OPM is devoted to the monitoring of the signal quality in the physical layer, for the purpose of providing information about the signal integrity in the optical domain. OPM is not strictly related to quality-of-service (QoS) measures. Its pri-

mary performance monitoring application is to certify service level agreements between the networks operators and their clients [1]. Besides that, OPM may also be used in other applications such as routing decisions and compensation of signal degradation, by tuning, for instance, optical amplifiers or dispersion compensators [1].

While the demand for superior data rates and bandwidth creates increasingly complex networks, with much more variables varying through time [2], the introduction of OPM in the physical layer allows a smart operation of the network, capable of managing the network as parameters vary. From a large set of impairments we can distinguish three that are of major concern:

- Chromatic dispersion (CD). Single-mode optical fibers cause pulse broadening, due to the impact of frequency-dependent group velocities. The shape of the pulse becomes wider creating intersymbol interference. It is usually measured in picoseconds per nanometer (ps/nm) and increases linearly with the length of the fiber and its impact on the signal worsens with high transmission rates. Moreover environment conditions such as temperature may also cause residual CD increment or decrement [5].

- Polarization mode dispersion (PMD). PMD is a linear electromagnetic propagation effect occurring in single mode optical fiber due to the random change of birefringence along the fiber which results in random coupling between the two polarization modes. These two modes of propagation travel at different group velocities, resulting in a mean differential group delay (DGD) between the two principal states of polarization PSPs. DGD causes pulse broadening and intersymbol interference reducing the quality of transmission (QoT). The mean DGD is usually given in picosecond (ps) and it is proportional to the square root of the length of the fiber [6].

- Optical signal to noise ratio (OSNR). The amplification of an optical signal in wavelength division multiplexing (WDM) optical communications system is provided by an erbium-doped fiber amplifier (EDFA). Amplified spontaneous emission (ASE) noise in conjunction with attenuation (0.2 dB/km) of the optical fiber is a serious impairment to the transmission of the optical signal. OSNR gives a measure of the impact of this impairment and is usually given in dB [7].

2.2 Optical performance monitoring based on RF spectrum analysis

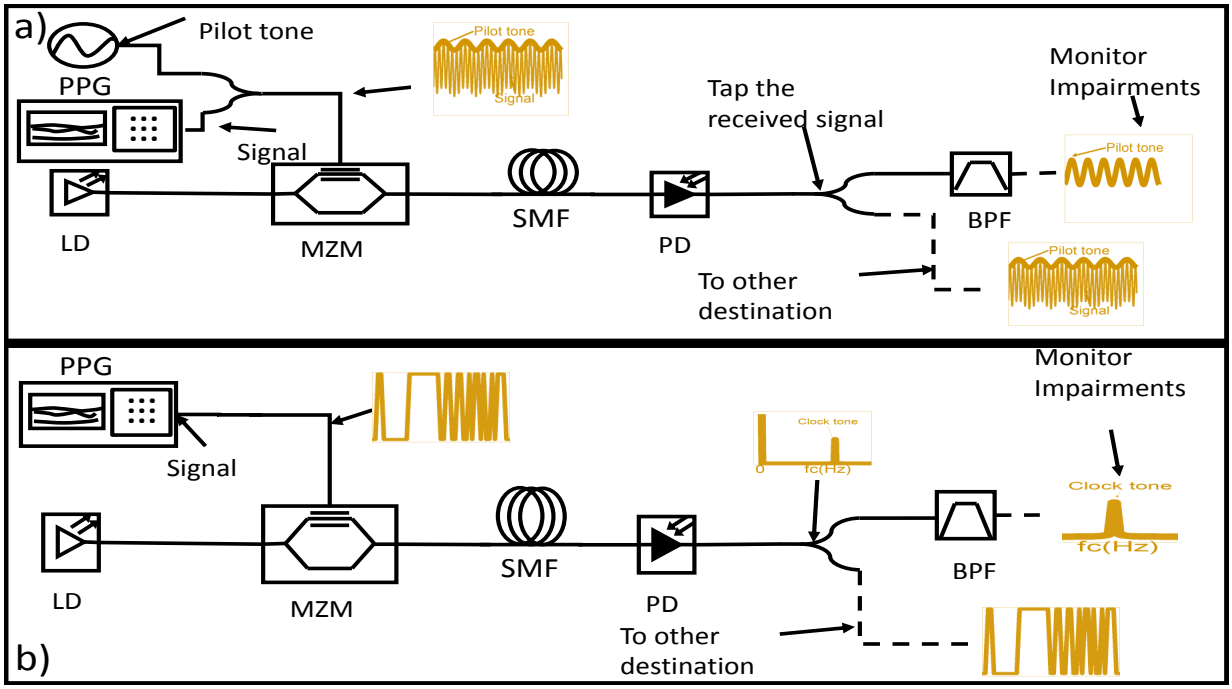

Figure 2.2: Optical performance monitoring based on a) pilot tones and b) clock tones (based on [8]). At the receiver the tone is filtered, after being tapped.PPG-pulse pattern generator, MZM-Mach-Zehnder modulator, PD-photo-diode, LD-laser-diode, BPF- band pass filter

Radio-frequency (RF) spectrum analysis method, comprises techniques that measure the amplitude of one low frequency RF pilot-tone (PT) described in Figure 2.2 a) and techniques that measure the amplitude of the clock tone of the signal described in Figure 2.2 b). Figure 2.2 a) shows the setup configuration of one optical performance monitor, using a low frequency RF PT.

A low frequency RF PT is added at the transmitter. After passing through a dispersive medium, like a single-mode fiber (SMF), the low frequency RF tone, suffers fading, due to impact of CD and PMD. The RF PT is filtered by a band-pass RF filter centered in the frequency of the RF PT. Several approaches have demonstrated that by measuring the carrier-to-noise ratio of an high frequency RF PT, it is possible to establish a relationship between the fading of the RF PT and optical signal to noise ratio (OSNR) [8, 9]. Although the measurements are

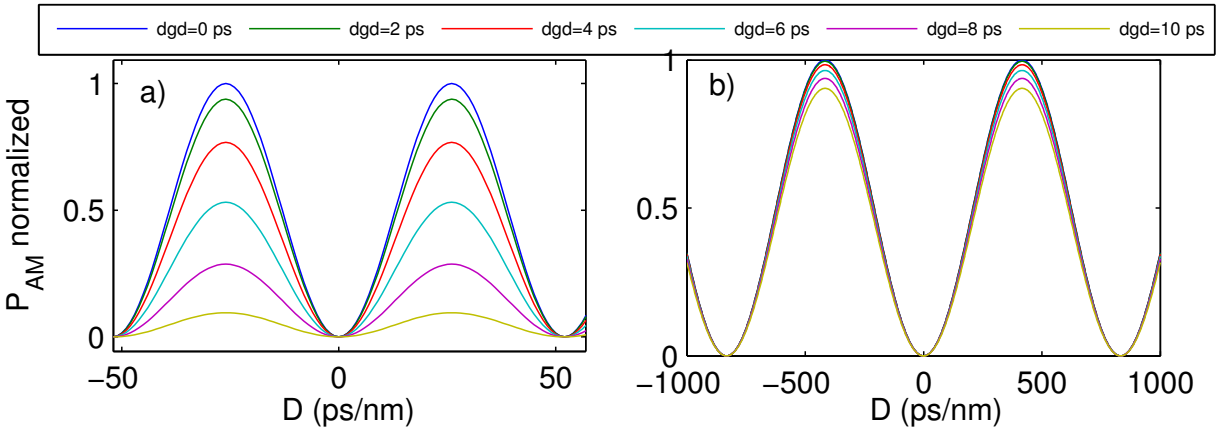

Figure 2.3: Examples of the application of Eq. (2.2) a) f_c =40 GHz, b) f_c =10 GHz

dependent of CD and PMD impact on the signal.

Figure 2.2 b) uses similar approach. However instead of changing the transmitter, which can be very undesirable for the network operator and sometimes not possible (directly modulated lasers), the average power of the RF clock tone is measured. The average electrical power is related with CD by Eq. (2.1) [5]:

$$P_{AM} = \frac{1}{2}\left\{\Re P_o m \left| cos\left(\frac{\pi\lambda^2 DL}{c} f_c^2\right)\right|\right\}^2 R_L \tag{2.1}$$

where P_{AM} is the RF power, P_o is the averaged received optical power, before the photodetector, $\Re$ is the responsivity of the photodetector, R_L is the resistive load of the photodetector, m is the root mean square (rms) modulation index of the amplitude modulator, c is the speed of light in vacuum, λ is the operating wavelength, D is the accumulated CD in the fiber and f_c is the frequency of the clock tone. Similar expression is obtained for the RF PT, simply by substituting f_c by f_p, where f_p is the frequency of the RF PT.

A more general expression can be obtained demonstrating the interdependence between CD and PMD, as show in Eq. (2.2) [10]:

$$P_{AM} = \left[1 - 4\gamma(1-\gamma)\sin^2(\pi f_c DGD)\right]\sin^2\left(\frac{\pi c D f_c^2}{f_0^2}\right) \tag{2.2}$$

where γ is the splitting ratio between the two principal states of polarization (PSP), f_0 is the frequency of the optical carrier and dgd is the 1^{st} order PMD. The same expression can be used for RF PT, by substituting f_c by f_p. In Figure 2.3 is shown some examples of the application of Eq. (2.2) for distinct clock

frequencies and for $\gamma = 0.5$, $\lambda_0 = c/f_0 = 1550$ nm and for several values of dgd. The parameter dgd increases the fading of the power of the clock tone as the value of dgd also increases. This is more evident for higher clock tone frequencies. The monitoring range is also decreased from about ±400 ps/nm in the case of f_c =10 GHz to about ±25 ps/nm in the case of f_c =40 GHz. By using single side band amplitude modulated (AM) PTs, it has been shown that it is possible to measure DGD independent of CD [11]. Moreover by using phase modulated (PM) PTs it has been demonstrated that is possible to monitor CD independent of DGD and self-phase modulation (SPM)[12]. The AM PT, can modulate the refractive index, and therefore modulate the phase of the PT. Thus the AM PT will create an additional AM component due to PM-AM conversion due to CD, causing monitoring errors. This issue is best addressed by a PM PT, which almost completely erases this problem.

In Table 2.1 is demonstrated a summary of the above discussion. It can be concluded by this summary, that if one can change the transmitter, which due to the lower cost of direct modulation, does not occur so often, one shall use low frequency RF PT analysis, such as AM PT or PM PT. If this is not possible one shall use clock tone analysis. In Chapter 3 as we will see later the author choose to use clock tone analysis, which is not dependent of the transmitter type.

2.3 Optical performance monitoring based on asynchronous sampling methods

Asynchronous sampling methods are a set of methods, that sample the data waveform, in asynchronous mode. The most relevant techniques in the scope of

Table 2.1: RF spectrum analysis techniques: summary

	Bit rate independent?	Modulation format independent?	Sensitive to SPM?	Interdependence between impairments?
Clock tone analysis	no	no	yes	yes
RF AM PT analysis	yes	yes	yes	may not have
RF PM PT analysis	yes	yes	no	may not have

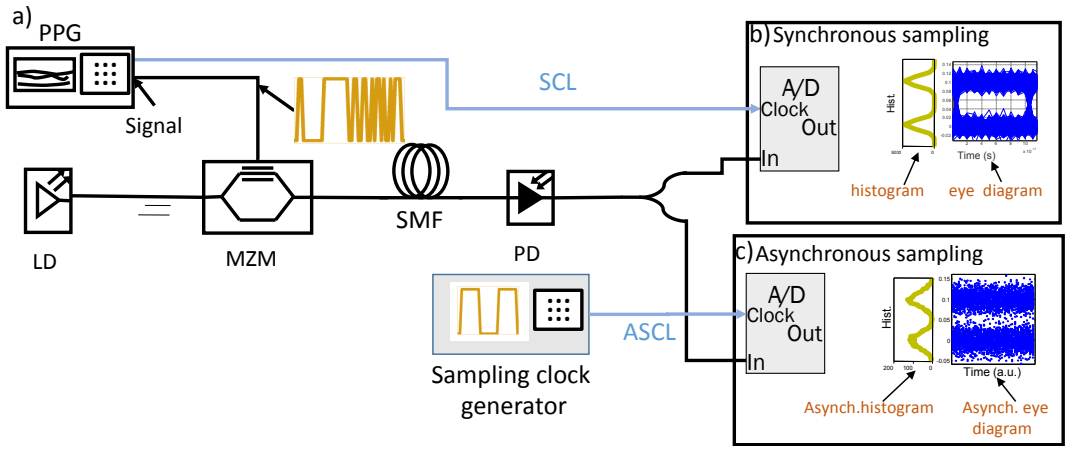

Figure 2.4: AAH configuration setup (based on [13]). SCL-synchronous clock line, ASCL-asynchronous sampling clock line. a) transmission of a modulated signal through fiber b)synchronous sampling and c) asynchronous sampling.

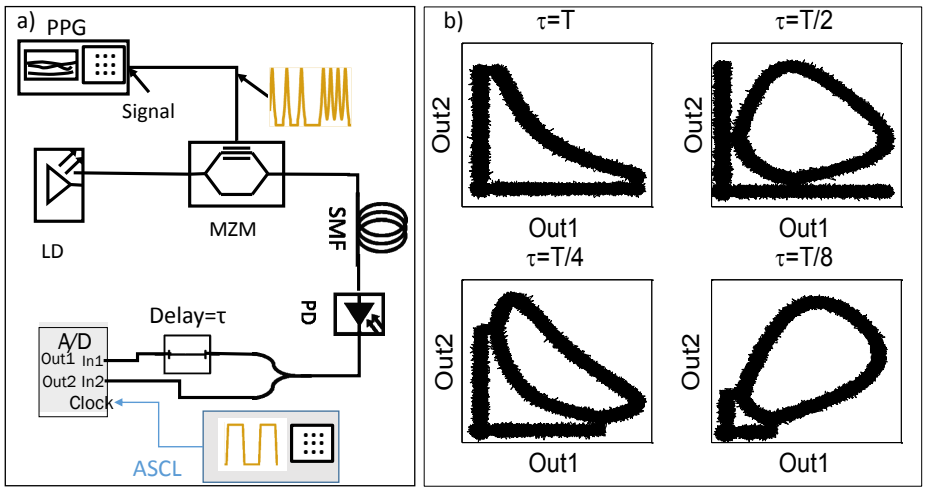

Figure 2.5: a) Configuration setup of ATDD(based on [14]). b) Asynchronous time delay diagrams generated for several time delays τ. T =bit period. The diagrams are generated by plotting $Out2$ versus $Out1$, where $Out1$ and $Out2$ are the outputs of the analog to digital converter in a). $Out1$ and $Out2$ are the outputs of the inputs of the analog to digital converter, $In1$ and $In2$, respectively.

this method are AAH and ATDD.

2.3.1 Asynchronous amplitude histograms

Figure 2.4 shows the setup configuration of the AAH technique for monitoring purposes. The configuration used in Figure 2.4 c) comprises a sampling

clock generator and an analog to digital converters (ADC) in the receiver. The synchronous sampling receiver in Figure 2.4 b) is also shown for comparison purposes. The frequency of the internal sampling clock shown in Figure 2.4 c) is not correlated with the bit rate, and the clock of the signal is not synchronized with the clock of ADC. Therefore the sampling is completely asynchronous. This reduces cost, since an expensive clock recovery device is not required.

Figure 2.4 c) also shows the asynchronous eye diagram which demonstrates a higher concentration of points in two areas correspondent to the binary zeros and ones. This is mathematically demonstrated in the asynchronous amplitude histograms on the left of the asynchronous eye diagram. The asynchronous Q factor can be calculated, using this information, and some monitoring parameters can be measured, relating this quantity with the value of impairments [15–17] . The Q-factor is given by [15]:

$$Q_{avg} = \frac{\mu_{1,avg} - \mu_{0,avg}}{\sigma_{1,avg} + \sigma_{0,avg}} \tag{2.3}$$

where $\mu_{1,avg}$ and $\sigma_{1,avg}$, are the mean and standard deviation of the 1-bit level and $\mu_{0,avg}$ and $\sigma_{0,avg}$ are the mean and standard deviation of the 0-bit level.

AAH based techniques suffer from non-ideal sampling, which produces middle level samples, that affect the calculation of the Q-factor. This can be demonstrated by comparing the generated histograms and eye diagrams of Figure 2.4 b) and c). Figure 2.4 b) shows a synchronous histogram that as generally a clearer separation between binary zeros and ones than its asynchronous counterpart on Figure 2.4 c). This is a result of the non-ideal sampling mentioned above. This is sometimes called the averaging effect [18]. This has impact on the accuracy of the AAH-based techniques as shown in [15]. AAH has demonstrated the capability to monitor several impairments such as OSNR [16], CD [13, 19, 20] and PMD [19].

2.3.2 Asynchronous time-delay diagrams

In Figure 2.5 the setup to reproduce ATDD is presented [14]. In Figure 2.5 a) the configuration setup of the optical performance monitor is presented. It is composed by the transmission part plus fiber and the receiver side comprising a photo-detector, a RF splitter that splits the power of the signal in two equal parts, and a time-delay which delays the signal with a certain amount of time,

which usually is correlated with the bit-rate ($\frac{1}{T}$) of the signal. In Figure 2.5 b) several ATDD are obtained while changing the time-delay.

In the literature some approaches were developed to monitor many impairments simultaneously, such as OSNR, PMD, CD [21–24]. These approaches include the use of machine learning by extracting features from histogram analysis [24] and from splitting the ATDD in to four quadrants and deriving the mean and standard deviation for each quadrant [21]. Several other approaches does not require artificial neural network (ANN). As an exemple Zhao et al., have used the distance scatter plots [20], to monitor OSNR and CD, however not simultaneously. Kozicki et al. have used the Hough transform to monitor OSNR and CD [23]. In Table 2.2 is demonstrated a summary of the above discussion with additional details relatively to the accommodation of traffic type by the asynchronous sampling techniques. One can conclude that they do not present clear advantages relatively to one another. However the two dimensional plot provided by ATDD is more rich in terms of information about the quality of the signal. This allowed to distinguish a large number of impairments such as jitter or filter offset [25]. The author in Chapter 5 also uses a two dimensional plot to characterize the optical signal [26], however he has used a differentiator in the place of a time-delay. This gives a certain number of advantages, such as the ability to discriminate high frequency components with the differentiator. Dispersion either CD or PMD is more severe at this higher frequencies, causing the power fading of this components. Another advantage is that [26] it is not bit-rate dependent.

Table 2.2: Asynchronous sampling analysis techniques

	Bit rate independent?	Modulation format independent?	Interdependence between impairments?	Distinguish impairments?
AAH	yes	limited	yes	yes
ATDD	no	limited	yes	yes

2.4 Optical performance monitoring based on nonlinear optics

Nonlinear optics based techniques, make use of nonlinear effects, like four-wave mixing (FWM) [27], cross-phase modulation (XPM) [28] or SPM [29], to monitor different impairments, such as OSNR [27] and CD [29]. In general the nonlinear optics-based monitor works with a nonlinear optical medium or device, such as an highly non-linear fiber (HNLF), a nonlinear optical loop mirror (NOLM), a parametric optical amplifier, or a semiconductor optical amplifier (SOA). The great advantage of these methods is that they are all-optical, which means that the opto-electronic conversion, only occurs, for sampling purposes, and the critical signal processing is done in the optical domain favouring largely the acquisition speed obtained. One clear drawback is that nonlinear optics-based effects require high power to be considered effective.

FWM based OPM has been used to CD [30–32] and OSNR [27] monitoring. In one approach the pulse-width of the pump signal is related with the average power of the idler. All the quantities involved in the process are known except the pulse-width that is dependent on CD. Therefore by measuring the average power of the idler is straightforward to determine the pulse-width and CD.

XPM is a nonlinear phenomena, where the intensity of the electric field of the beam (1) (pump), modulates the phase of the beam (2) (probe), by the Kerr Effect:

$$\Delta n^{(2)} = 2n_2 I^{(1)} \tag{2.4}$$

where $\Delta n^{(1)}$ is the index of refraction variation of the optical beam (2), caused by the intensity of the optical beam (1) $I^{(1)}$. n_2 is the nonlinear index of refraction of the material [33]. In general a probe is phase modulated by the pump signal which generates ghost tones in the probe at the data rate frequency of the pump. This ghost tones are faded by the increase in CD, allowing to provide a relationship between the power of this tones and CD. XPM-based OPM has been used to CD[28, 34, 35] and simultaneous CD, OSNR[36] monitoring.

SPM is a nonlinear phenomena in which the intensity of the optical beam (1) has effect on its own refractive index [37]:

$$\Delta n^{(1)} = n_2 I^{(1)} \tag{2.5}$$

A remarkable paper from Westbrook et al, exploits this effect [29]. Positive CD causes pulse broadening and therefore causes spectrum narrowing. On the other hand SPM, causes pulse narrowing and therefore causes spectrum broadening. CD and SPM interact being opposite forces. A simple optical power meter and a detuned optical filter located before it, measure the portion of the optical power, that is inside one optical filter bandwidth located in the receiver, which is high when CD is low and vice versa.

2.5 Conclusions

In this chapter the author made a general overview over several techniques and methods in the OPM field. Static networks can estimate the impairments by assumptions of input power in the fiber, its length and number of amplifiers. As we move to long-haul transmission systems we must consider that some impairments may vary in a considerable dynamic range due to temperature changes, weather conditions, fiber stress, among others. This justifies the use of an OPM technique, to estimate residual variations in the impairments value, even if the traffic is a static point-to-point (PTP) transmission link. Based on this, one can conclude that the choice of the appropriate OPM technique depends on the specific network. Some networks require that the OPM technique be bit rate transparent (not the case of a static PTP), therefore techniques such as ATDD or based on the XPM effect shall not be used, since they depend on the bit rate of the signal. Some networks may have restrict requirements in terms of costs so one should consider a multi-impairment OPM technique. Although some networks, such as optical burst switching (OBS) networks, may require that the OPM technique be not just be transparent to the bit rate but to the modulation format (limited to a number of modulation formats), including phase modulation formats such as quadrature phase-shift keying (QPSK). One should study other options. In this thesis the author proposed a multi-impairment, bit rate and modulation format transparent (limited to a number of modulation formats) OPM technique in Chapter 5.

References

[1] D. C. Kilper, R. Bach, D. J. Blumenthal, D. Einstein, T. Landolsi, L. Ostar, M. Preiss, and A. E. Willner, "Optical performance monitoring," *Lightwave*

Technology, Journal of, vol. 22, p. 294, Jan. 2004.

[2] A. Willner, X. Wu, and J.-Y. Yang, "1 - optical performance monitoring: Perspectives and challenges," in *Optical Performance Monitoring* (C. C. Chan, ed.), pp. 1 – 19, Oxford: Academic Press, 2010.

[3] S. Azodolmolky, J. Perello, M. Angelou, F. Agraz, L. Velasco, S. Spadaro, Y. Pointurier, A. Francescon, C. Saradhi, P. Kokkinos, E. Varvarigos, S. Al Zahr, M. Gagnaire, M. Gunkel, D. Klonidis, and I. Tomkos, "Experimental demonstration of an impairment aware network planning and operation tool for transparent/translucent optical networks," *Lightwave Technology, Journal of*, vol. 29, pp. 439–448, Feb. 2011.

[4] L.-K. Chen, M.-H. Cheung, and C.-K. Chan, "From optical performance monitoring to optical network management: research progress and challenges," in *3rd Int. Conf. Optical Communications and Networks (ICOCN), Hong Kong,*, 2004.

[5] K. T. Tsai and W. Way, "Chromatic-dispersion monitoring using an optical delay-and-add filter," *Lightwave Technology, Journal of*, vol. 23, pp. 3737–3747, Nov. 2005.

[6] J. P. Gordon and H. Kogelnik, "Pmd fundamentals: Polarization mode dispersion in optical fibers," *Proceedings of the National Academy of Sciences*, vol. 97, no. 9, pp. 4541–4550, 2000.

[7] V. Ribeiro, M. Lima, and A. Teixeira, "Comparison of optical performance monitoring techniques using artificial neural networks," *Neural Computing and Applications*, vol. 23, no. 3-4, pp. 583–589, 2013.

[8] H. Ji, K. Park, J. Lee, H. Chung, E. Son, K. Han, S. Jun, and Y. Chung, "Optical performance monitoring techniques based on pilot tones for wdm network applications," *J. Opt. Netw.*, vol. 3, pp. 510–533, Jul. 2004.

[9] G. Rossi, T. Dimmick, and D. Blumenthal, "Optical performance monitoring in reconfigurable wdm optical networks using subcarrier multiplexing," *Lightwave Technology, Journal of*, vol. 18, pp. 1639 –1648, Dec. 2000.

[10] S. Nezam, Y.-W. Song, C. Yu, J. McGeehan, A. Sahin, and A. Willner, "First-order pmd monitoring for nrz data using rf clock regeneration techniques," *Lightwave Technology, Journal of*, vol. 22, pp. 1086 – 1093, Apr. 2004.

[11] J.-Y. Yang, L. Zhang, Y. Yue, J. Jackel, A. Agarwal, L. Paraschis, and A. E. Willner, "Cd-insensitive pmd monitoring of a high-speed polarization-multiplexed data channel," *Opt. Express*, vol. 17, pp. 18171–18177, Sep. 2009.

[12] C. C. Chan, *Optical performance monitoring: advanced techniques for next-generation photonic networks*. Engineering, Academic Press, 2010.

[13] H. Takara, I. Shake, T. Ohara, and B. Kozicki, "Optical performance monitoring using asynchronous amplitude histogram," in *Optical Internet, 2007 and the 2007 32nd Australian Conference on Optical Fibre Technology. COIN-ACOFT 2007. Joint International Conference on*, pp. 1 –3, 2007.

[14] S. Dods and T. Anderson, "Optical performance monitoring technique using delay tap asynchronous waveform sampling," in *Optical Fiber Communication Conference, 2006 and the 2006 National Fiber Optic Engineers Conference. OFC 2006*, pp. 1 – 3, 2006.

[15] R. Luis, P. Andre, A. Teixeira, and P. Monteiro, "Performance monitoring in optical networks using asynchronously acquired samples with nonideal sampling systems and intersymbol interference," *Lightwave Technology, Journal of*, vol. 22, pp. 2452 – 2459, Nov. 2004.

[16] R. Luis, A. Teixeira, and P. Monteiro, "Optical signal-to-noise ratio estimation using reference asynchronous histograms," *Lightwave Technology, Journal of*, vol. 27, pp. 731 –743, Mar. 15 2009.

[17] B. Kozicki, O. Takuya, and T. Hidehiko, "Optical performance monitoring of phase-modulated signals using asynchronous amplitude histogram analysis," *Lightwave Technology, Journal of*, vol. 26, pp. 1353 –1361, May 15 2008.

[18] R. S. Luis, L. Costa, A. Teixeira, and P. Andrï¿½, "Chapter 6 - optical performance monitoring based on asynchronous amplitude histograms," in *Op-*

tical Performance Monitoring (C. C. Chan, ed.), pp. 145 – 174, Oxford: Academic Press, 2010.

[19] T. Shen, K. Meng, A. Lau, and Z. Y. Dong, "Optical performance monitoring using artificial neural network trained with asynchronous amplitude histograms," *Photonics Technology Letters, IEEE*, vol. 22, pp. 1665 –1667, Nov. 15 2010.

[20] J. Zhao, Z. Li, D. Liu, L. Cheng, C. Lu, and H. Y. Tam, "Nrz-dpsk and rz-dpsk signals signed chromatic dispersion monitoring using asynchronous delay-tap sampling," *Lightwave Technology, Journal of*, vol. 27, no. 23, pp. 5295–5301, 2009.

[21] J. Jargon, X. Wu, and A. Willner, "Optical performance monitoring by use of artificial neural networks trained with parameters derived from delay-tap asynchronous sampling," in *OFC 2009. Conference on*, pp. 1–3, Mar. 2009.

[22] B. Kozicki, A. Maruta, and K. ichi Kitayama, "Experimental demonstration of optical performance monitoring for rz-dpsk signals using delay-tap sampling method," *Opt. Express*, vol. 16, pp. 3566–3576, Mar. 2008.

[23] B. Kozicki, A. Maruta, and K.-I. Kitayama, "Experimental investigation of delay-tap sampling technique for online monitoring of rz-dqpsk signals," *Photonics Technology Letters, IEEE*, vol. 21, pp. 179 –181, Feb. 1 2009.

[24] T. Anderson, A. Kowalczyk, K. Clarke, S. Dods, D. Hewitt, and J. Li, "Multi impairment monitoring for optical networks," *Lightwave Technology, Journal of*, vol. 27, pp. 3729 –3736, Aug. 2009.

[25] S. D. Dods, T. B. Anderson, K. Clarke, M. Bakaul, and A. Kowalczyk, "Asynchronous sampling for optical performance monitoring," in *Optical Fiber Communication Conference and Exposition and The National Fiber Optic Engineers Conference*, p. OMM5, Optical Society of America, 2007.

[26] V. Ribeiro, L. Costa, M. Lima, and A. L. J. Teixeira, "Optical performance monitoring using the novel parametric asynchronous eye diagram," *Opt. Express*, vol. 20, pp. 9851–9861, Apr. 2012.

[27] T. T. Ng, J. L. Blows, M. Rochette, J. A. Bolger, I. Littler, and B. J. Eggleton, "In-band osnr and chromatic dispersion monitoring using a fibre optical parametric amplifier," *Opt. Express*, vol. 13, pp. 5542–5552, Jul. 2005.

[28] J.-Y. Yang, L. Zhang, X. Wu, O. Yilmaz, B. Zhang, and A. Willner, "All-optical chromatic dispersion monitoring for phase-modulated signals utilizing cross-phase modulation in a highly nonlinear fiber," *Photonics Technology Letters, IEEE*, vol. 20, pp. 1642 –1644, Oct. 2008.

[29] P. Westbrook, B. Eggleton, G. Raybon, S. Hunsche, and T. H. Her, "Measurement of residual chromatic dispersion of a 40-gb/s rz signal via spectral broadening," *Photonics Technology Letters, IEEE*, vol. 14, pp. 346 –348, Mar. 2002.

[30] M. G. Herrï¿½ez, L. Thï¿½venaz, and P. Robert, "Distributed measurement of chromatic dispersion by four-wavemixing and brillouin optical-time-domain analysis," *Opt. Lett.*, 2003.

[31] S. Li and D. Kuksenkov, "A novel dispersion monitoring technique based on four-wave mixing in optical fiber," *Photonics Technology Letters, IEEE*, vol. 16, pp. 942 –944, Mar. 2004.

[32] T. T. Ng, J. L. Blows, J. T. Mok, R. W. McKerracher, and B. J. Eggleton, "Cascaded four-wave mixing in fiber optical parametric amplifiers: application to residual dispersion monitoring," *Lightwave Technology, Journal of*, vol. 23, no. 2, pp. 818–826, 2005.

[33] R. Paschotta, "Cross-phase modulation," in *Encyclopedia of Laser Physics and Technology*, Willey-VCH, 2008.

[34] T. Luo, C. Yu, Z. Pan, Y. Wang, J. McGeehan, M. Adler, and A. Willner, "All-optical chromatic dispersion monitoring of a 40-gb/s rz signal by measuring the xpm-generated optical tone power in a highly nonlinear fiber," *Photonics Technology Letters, IEEE*, vol. 18, pp. 430 –432, Jan. 15 2006.

[35] T. Vo, M. Pelusi, J. Schroder, B. Corcoran, and B. Eggleton, "Multi-impairment monitoring at 320 gb/s based on cross-phase modulation radio-frequency spectrum analyzer," *Photonics Technology Letters, IEEE*, vol. 22, pp. 428 –430, Mar. 15 2010.

[36] T. Vo, J. Schroder, M. Pelusi, S. Madden, D.-Y. Choi, D. Bulla, B. Luther-Davies, and B. Eggleton, "Photonic chip-based simultaneous multi-impairment monitoring for phase-modulated optical signals," *Lightwave Technology, Journal of*, vol. 28, pp. 3176 –3183, Nov. 2010.

[37] R. Paschotta, "Self-phase modulation," in *Encyclopedia of Laser Physics and Technology*, Willey-VCH, 2008.

CHAPTER 3

CD monitoring scheme using RF analysis and Q-factor calculation

This chapter is based on the article [1]. This work is devoted to chromatic dispersion (CD) monitoring mainly for long-haul transmission links. The monitoring range can be adapted to monitor several thousands of ps/nm even at high bit rates such as 40 Gbit/s, with high sensitivity. It is only limited by the range of the variable dispersion compensator used. Since this type of devices take their time to adapt, this monitor is limited in its time response, although it shall be suited for dynamic point-to-point (PTP) transmission links.

3.1 Introduction

CD is one of the major limitations in optical communication systems, specially for bit rates of $10\,\text{Gbit/s}$ and beyond. CD monitoring techniques have been widely studied. These techniques are based on monitoring the magnitude of amplitude modulated (AM) pilot tones [2–5], non-linear effects in highly non-linear fiber [6, 7], phase-shift detection [8], two-photon absorption [9], analyzing the tap coefficients in electronic dispersion equalizers [12], among others. When evaluating a dispersion monitoring technique, two design parameters must be taken into account : the monitoring window and the monitoring sensitivity($\Delta P_{\text{AM}}/\Delta CD$), where ΔP_{AM} is the variation of the monitored power for a variation of CD, ΔCD. The larger this ratio is, the better. Long-haul transmission links have large accumulated dispersion. Therefore the dispersion monitoring window must be large in this case. Moreover monitoring sensitivity is also important, because for data rates equal or higher than $40\,\text{Gbit/s}$, a small change in CD, can cause a 1 dB power penalty [5] or more.

Previously it has been demonstrated, the ability to enhance the monitoring range and sensitivity by biasing the radio-frequency (RF) clock tone power [10], measuring the negative dispersion [11]. To the best of author knowledge the CD maximum monitoring range is 96 ps/nm at $40\,\text{Gbit/s}$, [10] taking into account only clock tone power monitoring techniques, which is well bellow the monitoring range provided by the proposed technique in this chapter (2040 ps/nm at $40\,\text{Gbit/s}$).

The author presents a technique based on [5] and [14], supported on an algorithm, Q-factor measuring and RF power tone monitoring. The objective is to increase the monitoring range to much higher values than the ones stated in the literature using several modulation formats at 40 Gbit/s. This method is more devoted to long-haul transmission links at high data rates, presenting a large monitoring range, with a monitoring sensitivity of 0.3363 dB/(ps/nm). This monitoring range can however be increased by increasing the compensation range of one variable dispersion compensator (VDC).

This chapter it is organized as follows. In section 3.2 the simulation setup is demonstrated. In section 3.3 and section 3.4, all the theory related to the calculation of the Q-factor and the operation principle of the RF power monitor,

respectively, is explained in detail. In section 3.5 and 3.6 the simulation results and the conclusions are presented, respectively.

3.2 Simulation Setup

The author presents a novel technique based on [5] and [14], with a novel monitoring philosophy, supported by an algorithm, Q-factor calculation, and RF power monitoring. The Q-factor is calculated by capturing opened eye diagrams with high-speed electro-optical sampling, following the technique proposed in [13, 14]. The schematic proposed allows accurate calculation of the CD by applying the VDC controller algorithm placed accordingly to the setup of Figure 3.1 and detailed in the flowchart of Figure 3.2. f_c is the clock frequency, λ is the wavelength and T is the period of CD variation against the power of the clock frequency component as shown in Figure 3.3.

In the RF Power Monitoring Block of Figure 3.1 the dispersion of VDC2 was set between $-T/2$ and $T/2$. Regardless of the amount of total accumulated dispersion at the output of VDC1, accordingly to Figure 3.3, a RF power minimum will be achieved, since many exist. As was mentioned before for that to happen, it is

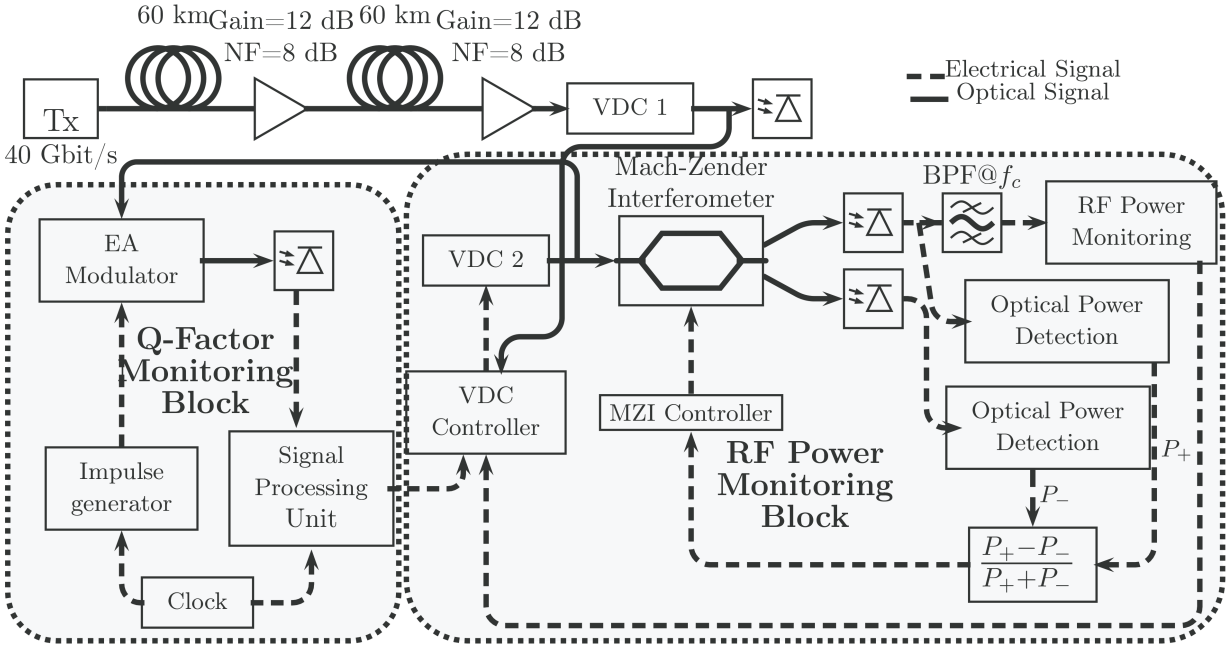

Figure 3.1: Simulation setup of the monitoring scheme using RF analysis and Q-factor monitoring.

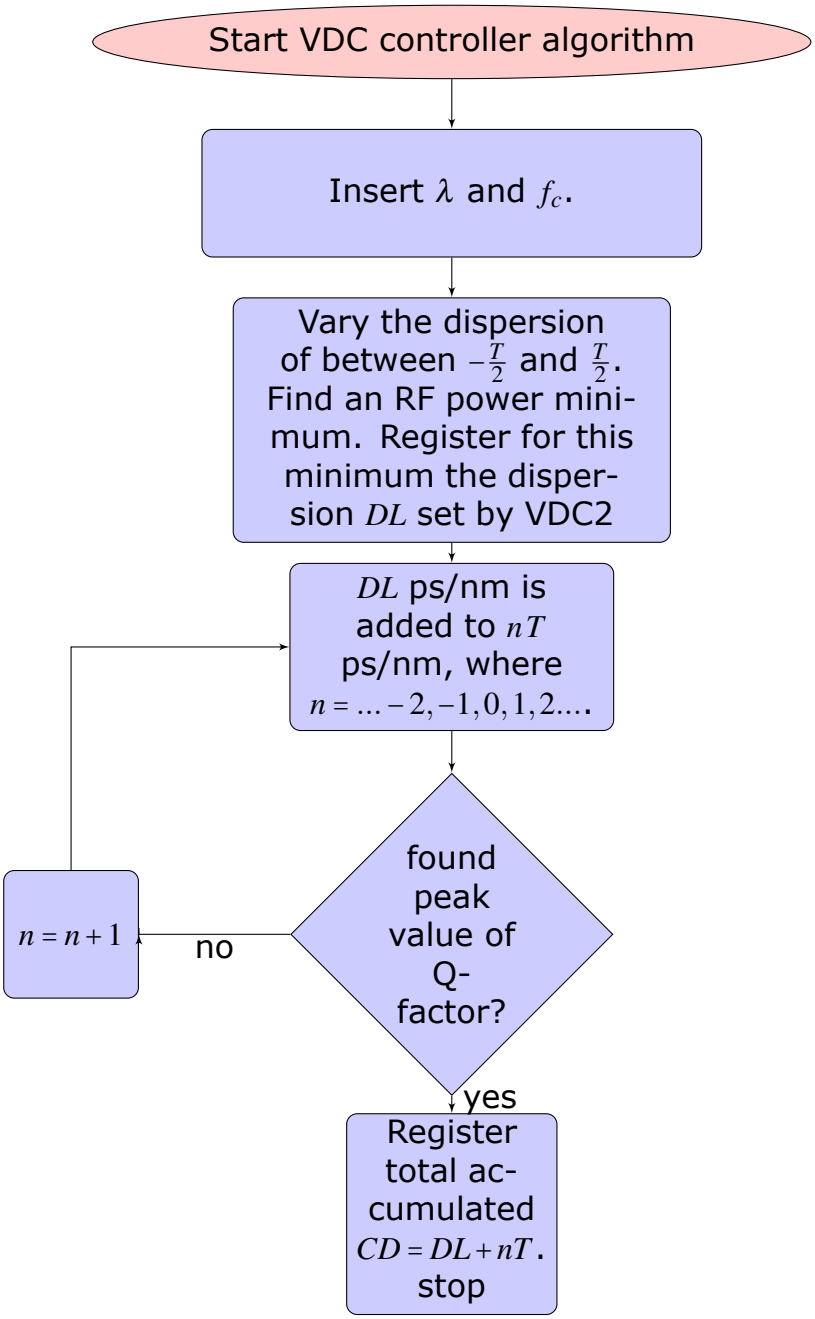

Figure 3.2: VDC controller flowchart

necessary to vary the dispersion in VDC2 between $-T/2$ and $T/2$, and take note of the dispersion in the mentioned range that sets a minimum in RF power. We may call it DL. The required next step is to find how far this minimum is from the 0 ps/nm dispersion value. If DL ps/nm is added with VDC2 to nT ps/nm,

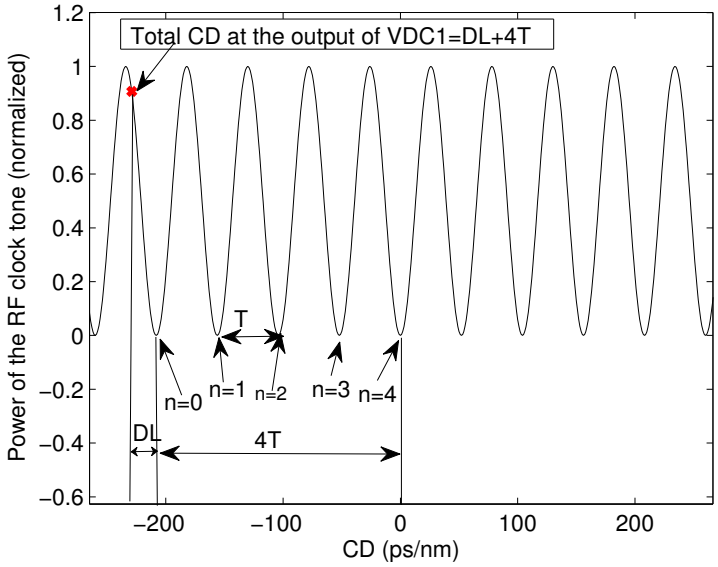

Figure 3.3: Variation of the RF power of the clock tone in respect to CD, for a 40 Gbit/s RZ signal.

---

where $n = \ldots -2, -1, 0, 1, 2 \ldots$, we may know that we will obtain a peak in the Q-factor value, only when the amount of dispersion set by VDC2 compensates completely the amount of dispersion at the output of VDC1. The monitoring window of this technique is therefore dependent of the compensation range of VDC2.

3.3 Q-factor calculation

In the proposed technique of this chapter, the calculation of the Q-factor is of most importance. Several techniques were proposed by the scientific community to calculate accurately the Q-factor, although some of them are computationally demanding [15, 16]. Some of these techniques are based in a exhaustive Gaussian approach, using the Moment Generating Function(MGF) through the saddle point approximation [15, 16]. Similar approach uses the same saddle point approximation, taking into account arbitrary signal pulse shape, chirping, filtering at the transmitter and at the receiver and CD [17]. Asynchronous amplitude histograms (AAH), has been already used, to produce asynchronous eye diagrams [14, 18–21]. The technique used in this chapter [13], for measuring the Q-Factor is also based on AAH, but instead of producing asynchronous eye diagrams, it generates opened eye diagrams. Asynchronous sampling, dispenses

timing extraction, and so it is transparent to the bit rate. This technique uses asynchronous under sampling, so the relationship between the clock frequency f_c and the sampling rate f_s is in the order of n/m, where n and m are natural numbers, and $n < m$ [13]. This work was done over a software simulator and due to memory limitations, the n/m relationship, had to be increased, to unrealistic values (should be much lower than 1, although in the computations 1 was used, otherwise very long patterns had to be computed). Although the validity of the results remains untouched, because what is really important is to demonstrate that is possible to generate opened eye diagrams following the equation [13]:

$$f_s = \frac{n}{m} f_c \pm a \tag{3.1}$$

and that was demonstrated, as shown in Figure 3.4. a is the offset frequency which enables the capture of the sampling points in different bit amplitudes. The eye diagram uses approximately m/n bits of the signal, to take one sampling point for the eye diagram. After k sampling points the waveform of one bit is produced. After approximately $jk\frac{m}{n}$ bits, the eye diagram is composed of a representation of j bit waveforms superposed from time zero over a specified interval. In the synchronous sampling technique, f_s is determined through hardware synchronization with f_c and by satisfying Eq. (3.2) [13]:

$$t_{step} = \frac{1}{f_s} - \frac{1}{\frac{n}{m} f_c} = \frac{1}{k f_c} \tag{3.2}$$

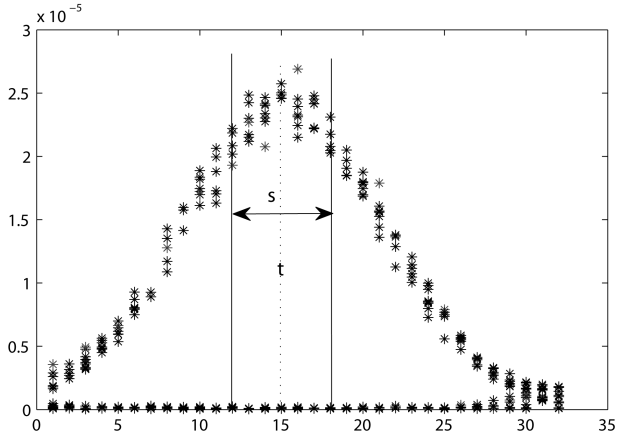

Figure 3.4: Simulation of an opened eye diagram, using the technique explained in Section 3.2. s is the time window centered at t used to take the sampling points that are within it to calculate the Q-factor

where t_{step} is the sampling time interval and k is the number of sampling points for each bit slot. If we solve Eq. (3.2) in order to f_s we obtain Eq. (3.3) [13]:

$$f_s = \frac{f_c}{\frac{1}{k} + \frac{m}{n}} \tag{3.3}$$

If we equalize Eq. (3.1) and Eq. (3.3), we get Eq. (3.4) [13]:

$$a = \frac{\left(\frac{n}{m}\right)^2}{k + \frac{n}{m}} f_c \tag{3.4}$$

We can see that $a < \frac{n}{m} f_c$ the first term of Eq. (3.1).

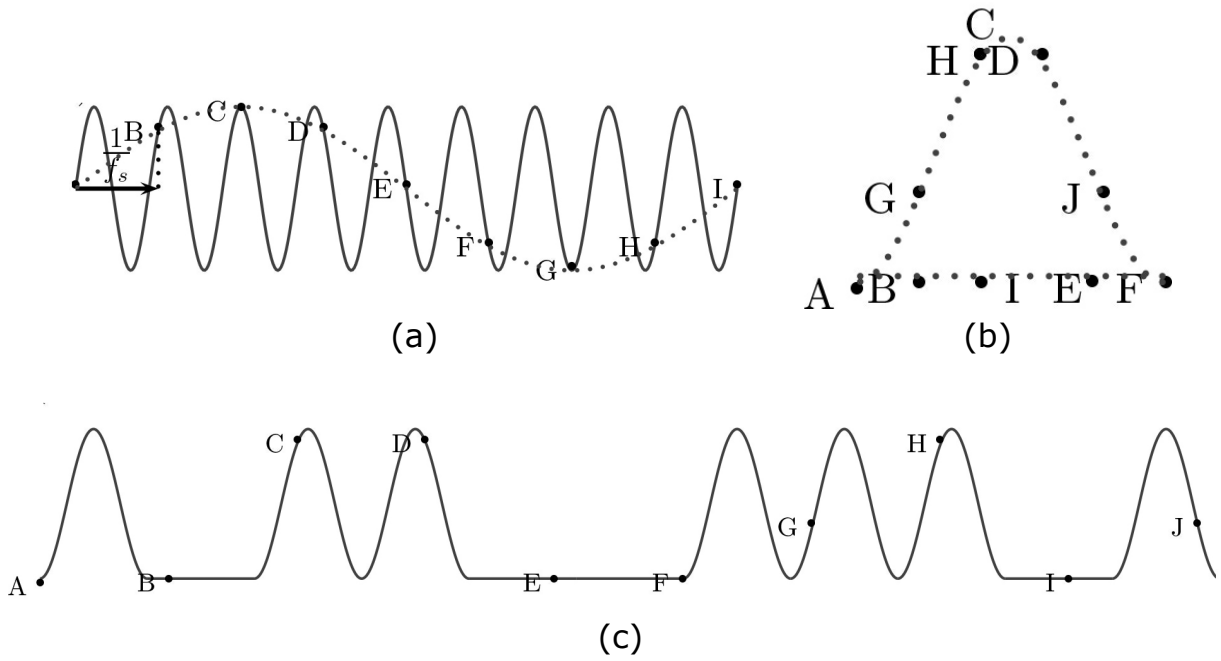

Figure 3.5: Illustrative figure of the technique for measuring the Q-factor and depicting opened eye diagrams. In (a) a sine wave is depicted(dot) taking just one sample of each period of the signal. In (c) a random signal is shown, and in (b) an opened eye diagram is depicted with the sampling points taken from (c).

In Figure 3.5 is shown how to obtain opened eye diagrams with this technique. In Figure 3.5(a) k=8, j=1 and n/m=1, so $a = \frac{1}{9} f_c$ and $f_s = \frac{8}{9} f_c$. f_s assures that the sampling points are taken at distinct amplitudes of the signal. In Figure 3.5(c) a random signal is depicted, representing zeros and ones. In this example k=5,

j=2, $a = \frac{1}{6} f_c$ and $f_s = \frac{5}{6} f_c$. This is sufficient to represent an opened eye diagram represented in Figure 3.5(b).

Parameter Q_t is estimated from the opened eye diagrams. Parameter Q_t is defined as:

$$Q_t = \frac{\mu_1 - \mu_0}{\sigma_1 + \sigma_0} \tag{3.5}$$

where μ_i and σ_i are the mean and standard deviations of the mark (i=1) and space (i=0), respectively. In Figure 3.4 an opened eye diagram is shown taken from simulation of an return-to-zero (RZ) signal format using the aforementioned technique. In this case k=32, n/m=1/5 and j=12, for a bit rate of $40\,\text{Gbit/s}$. It can be seen that this technique is able to produce fair opened eye diagrams. s shown in Figure 3.4 is the time window, centered at t. In Figure 3.6 is shown the Q-factor against CD. As expected the maximum Q-factor is achieved near 0 ps/nm CD.

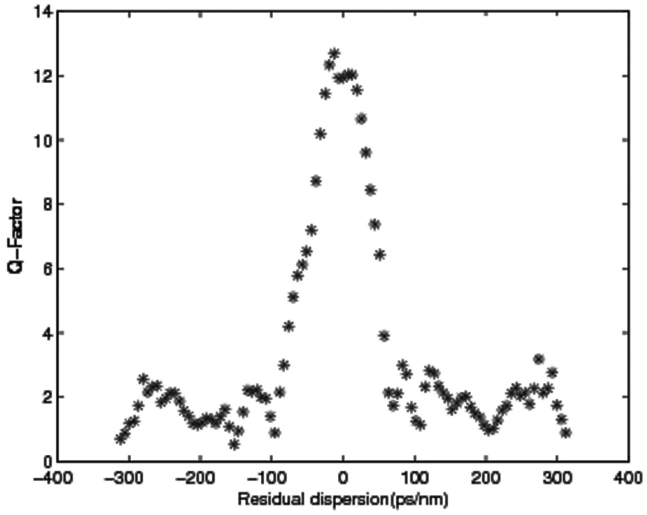

Figure 3.6: Q-factor versus calculated accumulated dispersion for an OSNR equal to 18.6 dB launch power equal to -3 dBm, using the simulation setup of Figure 3.1

3.4 RF power monitoring

It is well known that after a transmission link and a photo receiver, the magnitude of a clock component will fade with the increase of the total accumulated

CD of the optical link. Optical fiber dispersion causes a time delay between the upper and lower sideband clock components, since they travel at different velocities due to distinct refractive index for each one of them. The detected chromatic-dispersion-dependent RF power of an AM clock-power frequency can be expressed as [5]:

$$P_{AM} = \frac{1}{2}\left\{\Re P_o m \left| cos\left(\frac{\pi\lambda^2 DL}{c} f_c^2\right)\right|\right\}^2 R_L \tag{3.6}$$

where P_o is the averaged received optical power, before the photo receiver, $\Re$ is the responsivity, R_L is the resistive load of the optical receiver, m is the root mean square (rms) modulation index of the amplitude modulator, c is the speed of light in vacuum, λ is the operating wavelength, D is the fiber dispersion parameter, and DL is the total accumulated dispersion. Eq. (3.6) shows that the variation of the AM clock-power frequency, varies sinusoidally with the total accumulated dispersion. According to Eq. (3.6) it can be seen by the cosine argument, that the period of variation of the clock-power frequency with accumulated dispersion in ps/nm is:

$$T = \frac{c}{(f_c)^2\lambda^2} \tag{3.7}$$

λ in nm, c in nm/ps and f_c in ps^{-1}. Having a sinusoidal behaviour, Eq. (3.6), is not able to distinguish between maximums, so the monitoring window is limited to $-\frac{T}{2}$ and $\frac{T}{2}$. In the specified range using an Mach-Zehnder interferometer (MZI) the 0 ps/nm CD corresponds to a minimum in RF. The author used a Mach-Zehnder interferometer (MZI) before a photodetector, as shown in Figure 3.1, in order to increase the sensitivity of the technique. The frequency response of the constructive port of the MZI can be written as [5]:

$$H_+(f) = |H_+(f)|e^{j\Phi_+(f)} = \frac{j}{2}(e^{-j2\pi\tau f} + 1) \tag{3.8}$$

where $|H_+(f)|$ and $\Phi_+(f)$ are explicit in Figure 3.7. The detected RF power of the clock component after a dispersive fiber and a MZI is:

$$P_{AM} = \frac{1}{2}\left\{\Re P_o m K^2 \left| sin\left(\frac{\pi\lambda^2 DL}{c} f_c^2\right)\right|\right\}^2 R_L \tag{3.9}$$

where $K = 1/\sqrt{2}$ is the transmittance of the MZI at the wavelength of the clock component. If we compare Eq. (3.6) to Eq. (3.9), the first is related to a cosine

function and the second to a sine function. Therefore the monitoring resolution can be improved significantly, around zero dispersion, by using Eq. (3.9). Further considerations about the MZI controller may be found in [5].

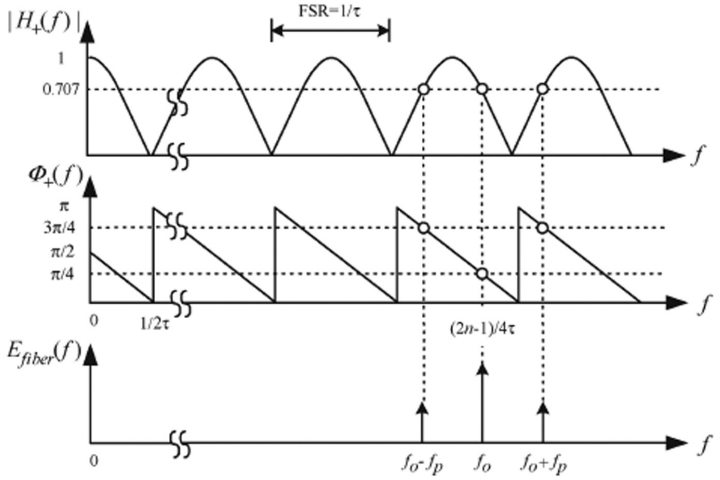

Figure 3.7: Optical amplitude and phase responses of the MZI at its constructive port. In the graphic below it is shown the electric field spectrum [5]

3.5 Simulation results and discussion

In the first simulation of Figure 3.8 the author varied the OSNR(dB) from almost 23 dB down to 7 dB. f_c is equal to 40 GHz, or equal to the bit rate frequency f_p, 40 Gbit/s. The author used the RZ(50%) modulation format and -3 dBm as the laser launch power. The accumulated dispersion is 2040 ps/nm. Monitoring errors start to appear at OSNR values lower than 9 dB. This monitoring errors occur because the amplitude of the noise is higher than the amplitude of the RF clock tone.

In Figure 3.9 we examine the impact of the delay variation in the calculation of the CD. Temperature changes can induce MZI delay variations, so it is relevant to discuss this topic here, since the author used a controller to control these variations. We see that after a delay variation of 50% the CD monitoring scheme starts to produce incorrect values of CD. This is due to the error signal generated by P_+ and P_- that controls the MZI which accepts a maximum normalized power difference of $\sqrt{(2)}/2$ for a delay variation of 50%. This is the maximum normalized power difference that produces correct values of CD.

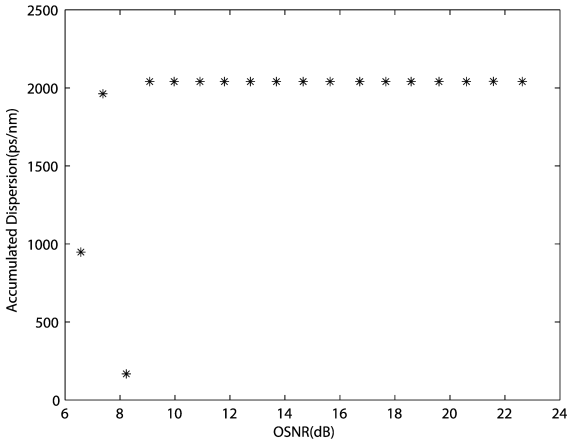

Figure 3.8: Simulated accumulated dispersion versus OSNR

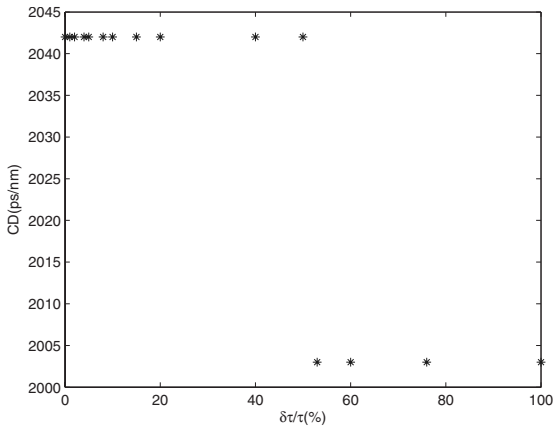

Figure 3.9: MZI delay variation versus calculated accumulated dispersion with RZ format.

In this simulation, the author examined three different modulation formats, RZ, NRZ and carrier-suppressed-return-to-zero (CSRZ). The author used -3 dBm as the launch power, 18.6 is the OSNR and varied the residual dispersion using VDC1 and VDC2, between -1000 ps/nm and 1000 ps/nm and monitor this CD variation. We can see that since the RZ format has a clear clock component, the results in Figure 3.10, show that this modulation format can be monitored with high accuracy. This is not the case of the NRZ results shown in Figure 3.11 which does not have a clock component and therefore results in an error that is close to $T \approx$ 100 ps/nm. In the case of CSRZ results shown in Figure 3.12 the

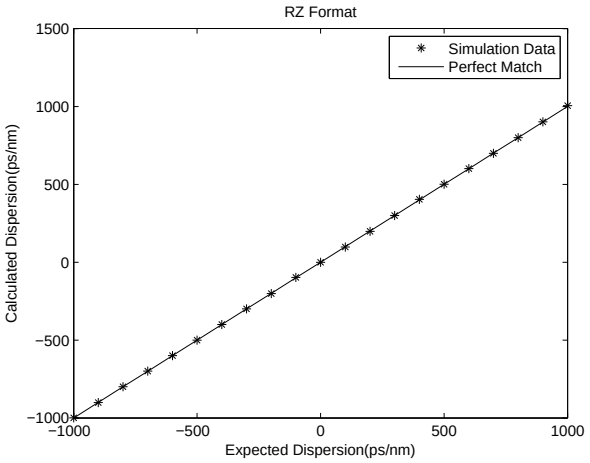

Figure 3.10: Simulation data obtained with the RZ format

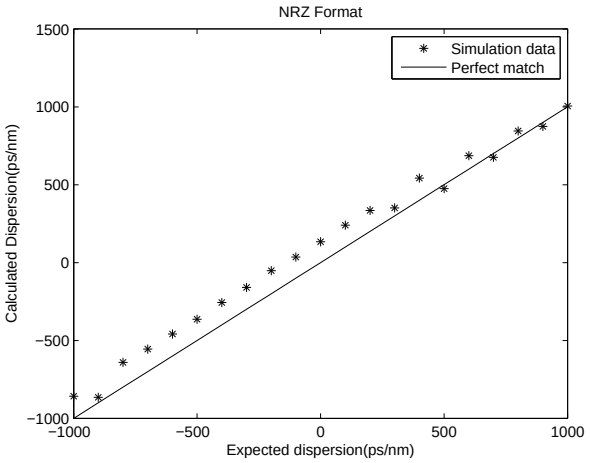

Figure 3.11: Simulation data obtained with the NRZ format

clock component is strong allowing to produce accurate results.

3.6 Conclusions

In this chapter the author proposed a technique that used RF power monitoring and Q-factor monitoring to enlarge the monitoring window. The technique was able to calculate accumulated dispersion up to 2040 ps/nm. This value is the limitation of the VDC envisioned in the simulation setup proposed, however if this value is increased larger monitoring ranges can be achieved. The technique shows very good behavior using RZ and CSRZ formats, although NRZ format

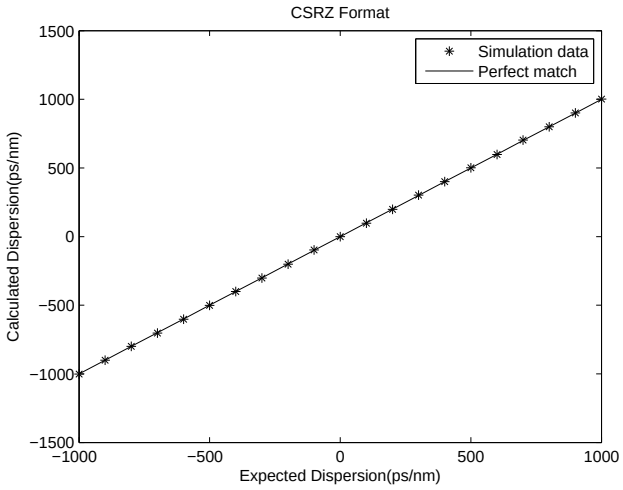

Figure 3.12: Simulation data obtained with the CSRZ format

demonstrate monitoring errors in the order of 100 ps/nm in the worst case.

Due to the moderate complexity, potential moderate cost, resilience to low OSNR and high sensitivity (0.3363 dB/(ps/nm)) for high values of chromatic dispersion, the author proposes this technique for long haul communication links at high data rates.

References

[1] V. Ribeiro, L. Costa, A. Teixeira, R. Nogueira and M. Lima,"Chromatic-dispersion-monitoring scheme using a mach-zehnder interferometer and q-factor calculation," J. Opt. Commun. Netw., IEEE/OSA, vol. 2, pp. 10-19, Jan. 2010.

[2] V. Ribeiro, M. Lima, A. Teixeira , R. Nogueira and D. Fidalgo, "Simulation of a chromatic dispersion monitoring scheme using an optical delay-and-add filter and a ber analyser," Revista do DETUA, Universidade de Aveiro, vol. 5, no. 2, Oct. 2008.

[3] L. B. Meflah, B. Thomsen, J. Mitchell and P. Bayvel, "Simultaneous chromatic dispersion, polarization mode-dispersion and osnr monitoring at 40gbit/s," Opt. Express, vol. 16, no. 20, Sep. 2008.

[4] Y. Wang, S. Hu, L. Yan, J. Y. Yang and A. E. Willner, "Chromatic dispersion

and polarization mode dispersion monitoring for multi-level intensity and phase modulation systems," Opt. Express, vol. 15, no. 21, Oct. 2007.

[5] K. T. Tsai and W. I. Way, "Chromatic-dispersion monitoring using an optical delay-and-add filter," Lightwave Technology, Journal of, vol. 23, no.11, Nov. 2005.

[6] J. Yang, L. Zhang, T. Wu, X. Wu, L. Christen, S. Nuccio, O. Yilmaz, W. Peng, and A. E. Willner, "Chromatic dispersion monitoring of 40-gb/s rz-dpsk and 80-gb/s rz-dqpsk data using cross-phase modulation in highly nonlinear fiber and a simple power monitor," in Optical Fiber Communication/National Fiber Optic Engineers, OSA Conference, Mar. 2008, paper OTuG5.

[7] P. S. Westbrook, B. J. Eggleton, G. Raybon, S. Hunsche and T. H. Her, "Measurement of residual chromatic dispersion of a 40-gbit/s rz signal via spectral broadening", Photonics Technology Letters, IEEE, vol. 14, no. 3, pp. 346-348, 2002.

[8] S. M. U. Motaghian Nezam, J. E. McCeehan, and A. E. Willner, "Chromatic dispersion monitoring using partial optical filtering and phase-shift detection of bit rate and doubled half bit rate frequency components," in Optical Fiber Communication, OSA Conference, 2004, paper ThU2.

[9] W. H. Guo, J. F. Donegan and L. P. Barry, "Expanding the range of chromatic dispersion monitoring with two-photon absorption in semiconductors," Lasers and Electro-Optics and the International Quantum Electronics Conference, Jun. 2007.

[10] S.M.R.M. Nezam, T. Luo, J.E. McGeehan and A.E. Willner, "Enhancing the monitoring range and sensitivity in csrz chromatic dispersion monitors using a dispersion-biased rf clock tone," Photonics Technology Letters, IEEE, vol. 16, no.5, pp. 1391-1393, May 2004.

[11] A. Liu, G. J. Pendock and R. S. Tucker, "Improved chromatic dispersion monitoring using single rf monitoring tone," Opt. Express, vol. 14, no. 11, pp. 4611-4616, May 2006.

[12] X. Yi, F. Buchali, W. Chen and W. Shieh, "Chromatic dispersion monitoring in electronic dispersion equalizers using tapped delay lines," Opt. Express, vol. 15, no. 2, Jan. 2007.

[13] I. Shake, H. Takara and S. Kawanishi, "Simple measurement of eye diagram and ber using high speed asynchronous sampling," Lightwave Technology, Journal of, vol. 22, no. 5, May 2004.

[14] I. Shake, H. Takara and S. Kawanishi, "Simple q-factor monitoring for ber estimation using opened eye diagrams captured by high-speed asynchronous electrooptical sampling," Photonics Technology letters, IEEE, vol. 15, no.4, Apr. 2003.

[15] J.L. Rebola and A.V.T. Cartaxo, "Gaussian approach for performance evaluation of optically preamplified receivers with arbitrary optical and electrical filters," IEE Proc.-Optoelectron. vol. 148, no. 3, Jun. 2001.

[16] M. Leiria, J.L. Rebola and A.V.T. Cartaxo, "Gaussian approach to the performance assessment of optical multiplexer/demultiplexer Concatenation in Tranparent Optical Networks," IEE Proc.- Optoelectron., vol. 151, No 3, Jun. 2004.

[17] E. Forestieri, "Evaluating the Error Probability in Lightwave Systems With Chromatic Dispersion, Arbitrary Pulse Shape and Pre-and post detection Filtering," Lightwave Tecnhology, Journal of, Vol 18, No 11, Nov. 2000.

[18] K. C. Jong, H. W. Tsao and S. L. Lee, "Novel Optical Performance Techniques Using Jittered Electro-Optical Sampling Pulses," Microwave and Optical Technology letters, vol.50, no.7, Jul. 2008.

[19] R. S. Luís, P. André, A. Teixeira, and P. Monteiro, "Performance Monitoring in Optical Networks Using Asynchronously Acquired Samples With Nonideal Sampling Systems and Intersymbol Interference," Lightwave Technology, Journal of, vol. 22, no. 11, Nov. 2004.

[20] P. André, A.L.J. Teixeira, M.J.N.Lima, J.L.Pinto and J.R.F. Da Rocha, "Optical Performance Monitor Based on Asynchronous Detection," in Lasers and Electro-Optics Society, The 14th Annual Meeting of the IEEE, 2001.

[21] N. Goder, M. Settembre, W. Laedke, F.Matera, M Tamburrini, I. Gabitov, H. Haunstein, J. Reid and S. Turitsyn: "Role of The Q Factor estimation in the field trial of 10 GBit/s transmission at 1300 nm with semiconductor optical amplifiers between Madrid and Merida," in Optical Fiber Communication, OSA Conference, Mar. 1999.

[22] J. X. Cai., "Modulation formats for undersea long-haul transmission," Digest of the IEEE/LEOS Summer Topical Meetings, pp. 21-23, Jul. 2008.

[23] N.S. Bergano, "Wavelength division multiplexing in long-haul transoceanic transmission systems," Lightwave Technology, Journal of, vol. 23, no. 12, pp. 4125 - 4139, Dec. 2005.

[24] A. Campillo, "Chromatic Dispersion-Monitoring Technique Based on Phase-Sensitive Detection," Photonics Technology Letters, IEEE, vol. 17, no. 6, Jun. 2005.

CHAPTER 4

Residual CD monitoring

This chapter is based on the articles [1, 2]. It presents a technique that substitutes an radio-frequency (RF) filter (common in RF tone power monitoring techniques [3, 4]) after the receiver, by an optical filter before the receiver. Additionally does not require the change of the transmitter, such as the RF pilot techniques presented in Chapter 2 Section 2, and allow low cost asynchronous sampling after the receiver. Moreover it allows the use of optical signal processing techniques before the receiver to sample the signal. Comparatively to the technique presented in the previous chapter this technique due to its moderate monitoring range, is suited to measure residual chromatic dispersion (CD) in the optical network. Figure 4.1 shows a comparison diagram about the main differences between the proposed technique in this chapter and the RF power monitoring technique reviewed in Chapter 2 Section 2 [5].

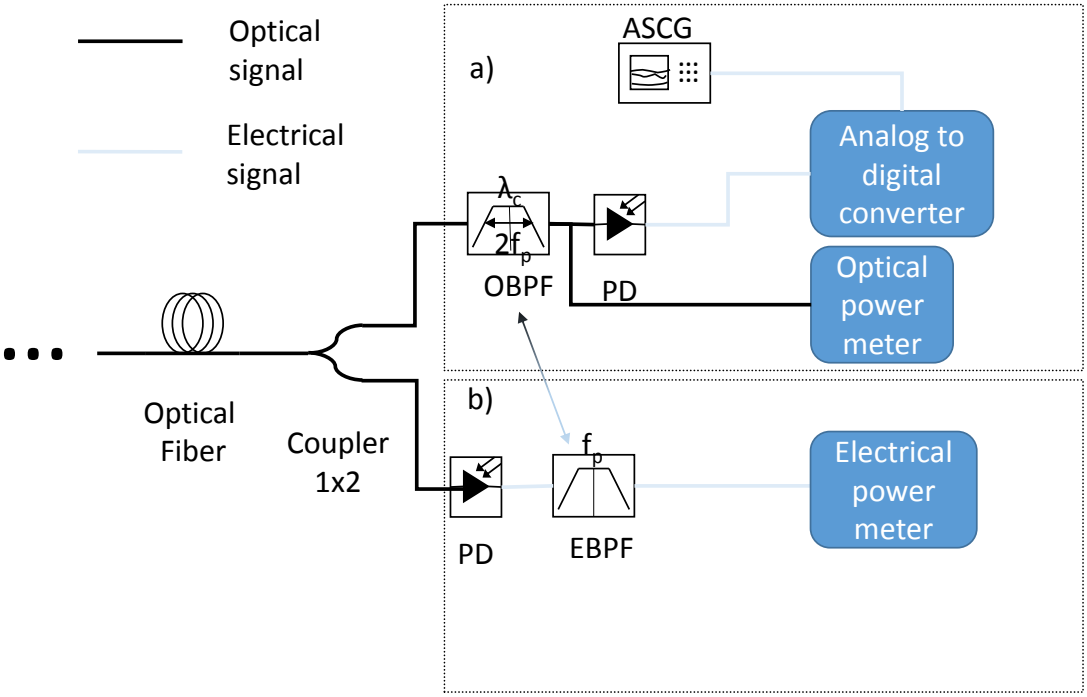

Figure 4.1: Showing the main differences between a)the proposed technique in this chapter and b) RF power monitoring technique [5]. There is a switch of one EBPF-Electrical band-pass filter by one OBPF optical bandpass filter. λ_c-center wavelength, f_p-bit rate frequency, ASCG-Asynchronous Sampling Clock Generator

4.1 Introduction

Prior work in the field of CD monitoring, implemented various schemes, including asynchronous delay tap sampling [6, 7], RF tone measurement [3, 4], self-phase modulation (SPM), four-wave mixing (FWM) and cross-phase modulation (XPM) [8–10], polarization scrambling [11], asynchronous chirp monitoring [12], two-photon absorption (TPA) with semiconductor micro-cavity [13], among others.

The well known RF tone measurement techniques is a technique with moderate dynamic range, cost, and acquisition time and also suitable to implement [15]. Monitoring CD by nonlinear effects (TPA, FWM, SPM, XPM) avoids high speed electrical domain signal processing, but requires normally high power, due to the low efficiency of the nonlinear process [8–10, 13].

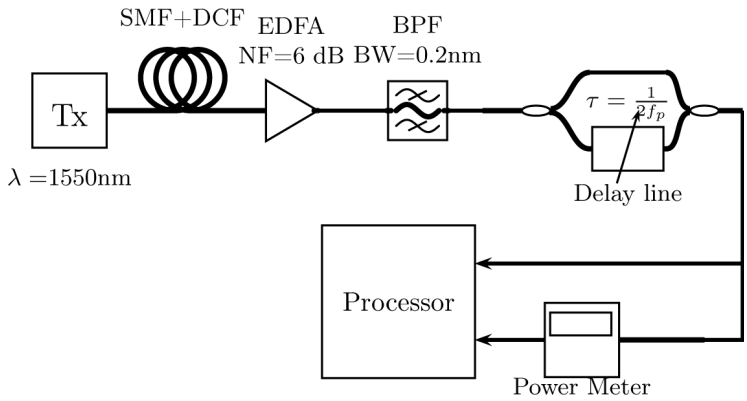

Figure 4.2: Simulation setup. At the receiver the signal is filtered by the BPF and sampled by the processor unit. Simultaneously the average power is measured by the optical power meter. BPF-Band Pass Filter, BW-Bandwidth, τ-time delay of the interferometer, EDFA-Erbium Doped Fiber Amplifier, SMF-Single Mode Fiber, DCF-Dispersion Compensating Fiber, NF-Noise Figure

The technique here presented, collects samples of data at asynchronous intervals, and determines the maximum amplitude of the optical signal in an appropriate time window. Figure 4.2 shows the simulation setup of the monitoring technique. The processor samples the signal asynchronously and determines the maximum amplitude among the collected samples. Then divides this value by the average power calculated by the optical power meter of Figure 4.2, yielding in a ratio, (known in telecommunications engineering to be the peak to average power ratio (PAPR)) transparent to the average power of the source laser.

The optical filter selects the two lower frequency sidebands of the signal, rejecting all the others. The Mach-Zehnder interferometer (MZI) with $\tau = 1/(2f_p)$, has the effect of increasing the monitoring sensitivity by 3 dB. The interferometer shifts the phase between the optical carrier and the two sidebands $+\pi/2$ and $-\pi/2$, so that these two sidebands have a π phase difference, and therefore, they could cancel each other. CD changes this phase difference, and the PAPR starts to increase when dispersion departs from 0 ps/nm. In Figure 4.3 it is shown the flowchart of the algorithm that supports this technique.

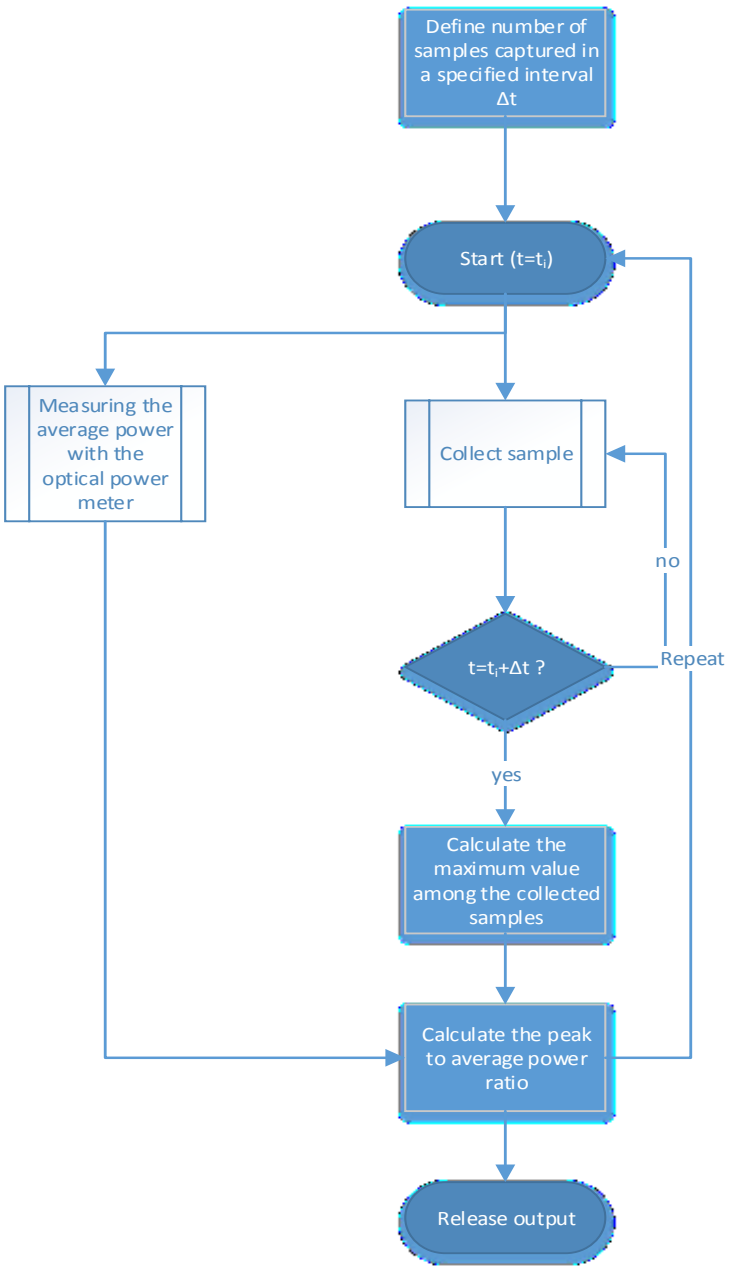

Figure 4.3: Flowchart of the proposed technique for residual dispersion monitoring.

4.2 Theory for residual CD monitoring using asynchronous sampling

The electric field equation of a sinusoidal input modulation, after passing through a dispersive fiber, an ideal filter and an interferometer is given by

Eq. (4.1) [5]:

$$r(t) = \sqrt{P_0} H_1 e^{i\phi_1 + 2i\pi t f_0} \left(1 + 1/4 \frac{m\,(H_2 + H_3)\, e^{i\left(q f_p{}^2 - \phi_1 + 1/2\,\phi_2 + 1/2\,\phi_3\right)}}{H_1} \cos\left(2\pi f_p t + 1/2\,\phi_2 - 1/2\,\phi_3\right) + \right.$$
$$\left. + 1/4i \frac{m\,(H_2 - H_3)\, e^{i\left(q f_p{}^2 - \phi_1 + 1/2\,\phi_2 + 1/2\,\phi_3\right)}}{H_1} \sin\left(2\pi f_p t + 1/2\,\phi_2 - 1/2\,\phi_3\right) \right) \otimes \mathbb{F}^{-1}\{rect(f_0, f_{BW})\}, \tag{4.1}$$

where f_p is the frequency of the sinusoid, f_0 is the carrier frequency, P_0 is the average laser launch power, m is the modulation index, $\mathbb{F}^{-1}\{rect(f_0, f_{BW})\}$ is the inverse Fourier transform of an ideal filter centered at f_0, with frequency bandwidth equal to f_{BW} and $\otimes$ is the convolution operator. The impact of the filter in a sinusoidal signal that only have two harmonics, at the the bit-rate frequency f_p, is null. However it is important for more complex signals such as return-to-zero (RZ) signals and therefore is included in the equation. The $H_1, H_2, H_3, \phi_1, \phi_2, \phi_3$ and q , parameters are defined as follows:

$$\begin{aligned}
H_1 &= \left|\cos(\pi\tau f_0)\right| \\
H_2 &= \left|\cos\left(\pi\tau\left(f_0 + f_p\right)\right)\right| \\
H_3 &= \left|\cos\left(\pi\tau\left(f_0 - f_p\right)\right)\right| \\
\phi_1 &= -\pi\tau f_0 + \tfrac{\pi}{2} + \angle\cos\left(\pi\tau f_0\right) \\
\phi_2 &= -\pi\tau f_0 + \tfrac{\pi}{2} + \angle\cos\left(\pi\tau\left(f_0 + f_p\right)\right) - \pi\tau f_p \\
\phi_3 &= -\pi\tau f_0 + \tfrac{\pi}{2} + \angle\cos\left(\pi\tau\left(f_0 - f_p\right)\right) + \pi\tau f_p
\end{aligned} \tag{4.2}$$

$$q = \frac{\pi\lambda_0^2 DL}{c}, \tag{4.3}$$

where λ_0 is the carrier central wavelength, D is the dispersion parameter, L is the fiber length, $\angle$ is the angle operator and τ is the delay time of the delay line of Figure 4.2 which is given by:

$$\tau = \frac{1}{2f_p}. \tag{4.4}$$

In such conditions we can write:

$$\begin{aligned}
H_1 &= \left|\cos\left(\pi\tau f_0\right)\right| \quad & H_2 &= \left|\cos\left(\pi\tau\left(f_0 + f_p\right)\right)\right| \\
H_3 &= H_2 & \phi_1 &= 2\pi n + \alpha \\
\phi_2 &= 2\pi n + \alpha + \tfrac{\pi}{2} & \phi_3 &= 2\pi n + \alpha + \tfrac{\pi}{2},
\end{aligned} \tag{4.5}$$

where α is an arbitrary angle dependent of f_0 . The optical power is given by:

$$
\begin{aligned}
P_{opt} = & |r(t)|^2 = \mathrm{Re}\,(r(t))^2 + \mathrm{Im}\,(r(t))^2 = \\
& \Big(1/4\sqrt{P_0}mH_2 \\
& \cos\left(2\pi t f_0 + q f_p{}^2 + \phi_2 + 2\pi f_p t\right) + \\
& 1/4\sqrt{P_0}mH_3 \\
& \cos\left(2\pi t f_0 + q f_p{}^2 - 2\pi f_p t + \phi_3\right) + \\
& \sqrt{P_0}H_1 \cos\left(2\pi t f_0 + \phi_1\right)\Big)^2 + \\
& \Big(1/4\sqrt{P_0}mH_2 \\
& \sin\left(2\pi t f_0 + q f_p{}^2 + \phi_2 + 2\pi f_p t\right) + \\
& 1/4\sqrt{P_0}mH_3 \\
& \sin\left(2\pi t f_0 + q f_p{}^2 - 2\pi f_p t + \phi_3\right) + \\
& \sqrt{P_0}H_1 \sin\left(2\pi t f_0 + \phi_1\right)\Big)^2 \\
= & \frac{1}{16}P_0(m^2H_2{}^2 + \\
& + 2m^2H_2H_3\cos(\phi_2 + 4\pi f_p t - \phi_3) + \\
& + 8mH_1H_2\cos(qf_p{}^2 + \phi_2 + 2\pi f_p t - \phi_1) + \\
& m^2H_3{}^2 + \\
& 8mH_3H_1\cos(qf_p{}^2 + \phi_3 - 2\pi f_p t - \phi_1) \\
& + 16H_1{}^2).
\end{aligned}
\tag{4.6}
$$

Using Eq. (4.5) into Eq. (4.6) we obtain:

$$
\begin{aligned}
P_{opt} = & \frac{1}{16}P_0\left(H_2{}^2m^2 + 2m^2H_2H_3\cos\left(4\pi f_p t\right) - \right. \\
& 8mH_2H_1\sin\left(qf_p{}^2 + 2\pi f_p t\right) + m^2H_3{}^2 \\
& \left. -8mH_3H_1\sin\left(qf_p{}^2 - 2\pi f_p t\right) + 16H_1{}^2\right).
\end{aligned}
\tag{4.7}
$$

To calculate the maximum amplitude of the signal we must calculate the

derivative of Eq. (4.7) in order to t and equal it to zero:

$$\begin{aligned}\frac{dP_{opt}}{dt} = {} & P_0 m H_3 H_1 \cos\left(q {f_p}^2 - 2\pi f_p t\right) f_p \pi - \\ & 1/2 P_0 m^2 H_3 H_2 \sin\left(4\pi f_p t\right) f_p \pi - \\ & P_0 H_1 m H_2 \cos\left(q {f_p}^2 + 2\pi f_p t\right) f_p \pi = 0.\end{aligned} \tag{4.8}$$

Then we must find the solutions of this equation. We conclude that the solutions are:

$$t = \begin{cases} (2i+1)/(2f_p) & if, \begin{array}{l} DL \geq 2nD_{Talbot} \\ DL < (2n+1) D_{Talbot} \end{array} \\ (2i+1)/(f_p) & if, \begin{array}{l} DL \geq (2n+1) D_{Talbot} \\ DL < (2n+2) D_{Talbot} \end{array} \end{cases} \tag{4.9}$$

where $n = \ldots, -2, -1, 0, 1, 2, \ldots$ and $i = 0, 1, 2, \ldots$. D_{Talbot} is defined as [16]:

$$D_{Talbot} = \frac{c}{{f_p}^2 {\lambda_0}^2}. \tag{4.10}$$

D_{Talbot} is due to the Talbot effect, which describes the apparent re-emergence of a periodic sequence of pulses, propagating in the dispersive medium. Talbot studied the re-emergence of a repeated sequence of images in a periodic spatial diffraction grating. Chromatic dispersion plays the role of the spatial diffraction, where the minimums in the measured power are repeated at $2nD_{Talbot}$, where $n = \ldots, -2, -1, 0, 1, 2, \ldots$

Substituting the solutions given by Eq. (4.9) into Eq. (4.7), for instance for $i = 1$, leads to Eq. (4.11*a*) and Eq. (4.11*b*), which is a relationship between the maximum amplitude of the signal and CD, similar to the obtained in 3.9:

$$\begin{aligned}P_{opt}(q) = \frac{1}{16} P_0 \left(m^2 {H_2}^2 + 16 m H_2 H_1 \sin(q {f_p}^2)\right. \\ \left. 2m^2 H_2 H_3 + m^2 {H_3}^2 + 16 {H_1}^2\right),\end{aligned} \tag{4.11a}$$

if $2nD_{Talbot} \leq DL < (2n+1) D_{Talbot}$ and:

$$\begin{aligned}P_{opt}(q) = \frac{1}{16} P_0 \left(m^2 {H_2}^2 - 16 m H_2 H_1 \sin(q {f_p}^2)\right. \\ \left. 2m^2 H_2 H_3 + m^2 {H_3}^2 + 16 {H_1}^2\right),\end{aligned} \tag{4.11b}$$

if $(2n+1) D_{Talbot} \leq DL < (2n+2) D_{Talbot}$.

The ratio between the optical power and the average power is given by:

$$ratio = \frac{P_{opt}(q)}{\frac{1}{16}P_0\left(H_2{}^2m^2 + m^2H_3{}^2 + 16H_1{}^2\right)} = \\ = 1 + \frac{2m^2H_2H_3}{\left(H_2{}^2m^2 + m^2H_3{}^2 + 16H_1{}^2\right)} + \\ \left|\frac{16mH_2H_1}{\left(H_2{}^2m^2 + m^2H_3{}^2 + 16H_1{}^2\right)}\sin\left(qf_p{}^2\right)\right| \tag{4.12}$$

which leads to an equation that is independent from the launch power P_0.

4.3 Simulation Results and discussion

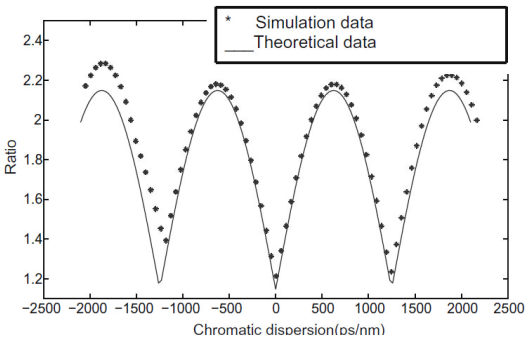

Figure 4.4: Dispersion monitoring for a 10 GHz sinusoidal input modulation. Simulation and theoretical data are plotted. Theoretical data is plotted accordingly to Eq. (4.12). Ratio is the PAPR.

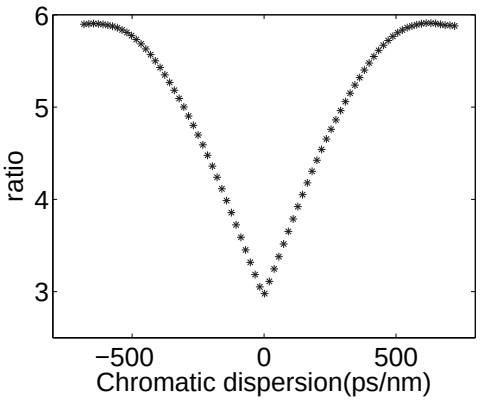

Figure 4.5: Dispersion monitoring for a 10 Gbit/s RZ modulation. Ratio is the PAPR. Simulation data is plotted.

Figure 4.4 shows the theoretical plot versus the simulation data, in terms of the ratio value, for $P_0 = 1mW$, $\lambda_0 = 1550nm$, $f_p = 10GHz$ and $m = 1$ using a sinusoidal format. We see a very close relationship between the theoretical curve obtained from Eq. (4.12) and simulation data, obtained using OptiSystem 7.0. We do not have a clear explanation about the differences between the simulated values and the theoretical ones at higher values of chromatic dispersion within the scope presented in Figure 4.4. Although we want to compare the theoretical values with a more closed-to-reality model such as the one provided by the simulation, which leads us to not shut down from the simulation, parameters such as the

nonlinear parameter and the differential group delay (DGD) parameter, that are not included in the theoretical curve. Although we may confirm the validity of the model in a certain monitoring range between -1200 ps/nm and 1200 ps/nm.

Figure 4.5 shows the simulation results for the RZ format. The curve is similar to the one of Figure 4.4. This indicates that the theoretical approach is also similar to the one used in the sinusoidal format, indicating that the curve follows the form $|\sin(qf_p^2)|$.

4.4 Experimental results and discussion

The experimental setup is presented in Figure 4.6. The transmitter generates RZ Gaussian pulses, at $40\,\mathrm{Gbit/s}$. CD is emulated combining SMF and dispersion compensating fiber (DCF). The optical filter used in this experiment was the x-tract tunable optical filter from Netest, with rectangular shape and 0.64 nm bandwidth. The filter was centered at fc=1549.94 nm, which is the central wavelength of the transmitter laser and has 10 dB attenuation at fc. The MZI consists of a polarization maintaining fiber (PMF) with one half bit DGD between the two axis of polarization, a polarization controller which regulates polarization for 45^o, a polarization beam splitter, which separates the two state of polarization (SOP)s and an acrylic box, that isolates the MZI from variations in polarization, induced by temperature changes. An extra 9.4 dB of attenuation is inserted by the MZI. The SOP locker isolates the MZI from polarization changes before it. Polarization shall be stabilized, and the output optical spectrum must be observed, to avoid some drift in it. The PMF with a DGD of one half-bit, acts like two signals, each one in one axis of polarization, interfering with each other. The polarization beam splitter could be substituted by a polarizer. It only guarantees that we get the maximum power when the polarization controller aligns one of the axis of the polarization beam splitter to the 45^o of the PMF.

In the receiver the author used an Agilent 86100A oscilloscope to collect the maximum power and the average power in a time window. In fact the author used synchronous sampling in the experiment (not in simulation), although it is not required. The author expects that if a proper time window, depending on the sample rate, is given the monitoring errors caused by imperfect sampling will be minor. The time window must be large enough in order to ensure that at least one power maximum is found. However it may occur that due to imperfect

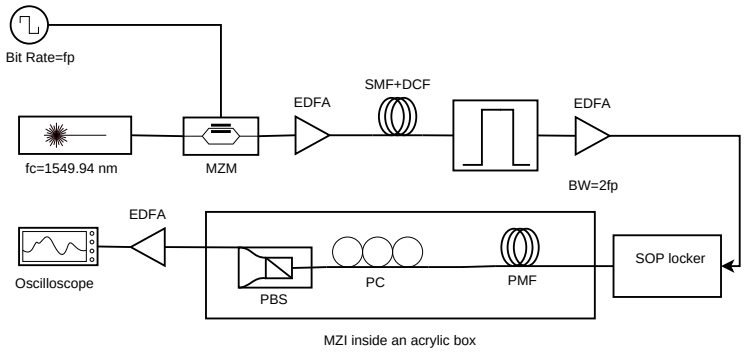

Figure 4.6: Experimental setup of the proposed monitoring technique. PMF-Polarization Mantaining Fiber, EDFA-Erbium Doped Fiber Amplifier, MZM-Mach Zehnder Modulator, MZI-Mach-Zehnder Interferometer, SOP-State of Polarization, PBS-Polarization Beam Splitter, SMF-Single Mode Fiber, DCF-Dispersion Compensating Fiber, BW-Bandwidth, PC-Polarization Controller, fc-central frequency

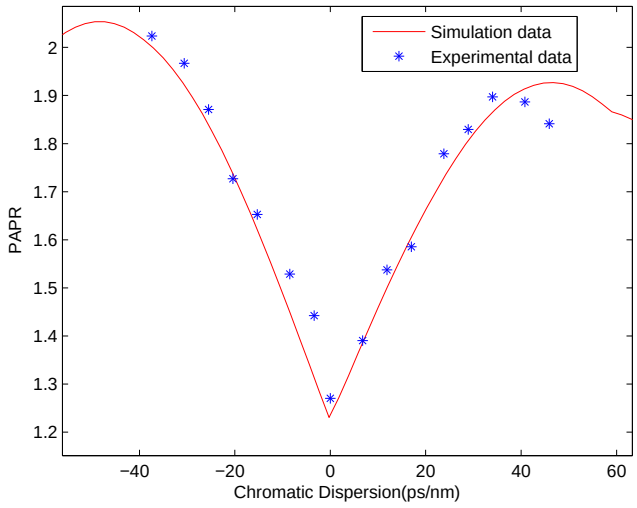

Figure 4.7: PAPR as a function of CD.

sampling an approximation of this power sampling is found causing monitoring errors.

The main results are shown in Figure 4.7. We see a good agreement between the simulated results, and the experimental ones, inside the monitoring window. We may also see, in the experimental results a very distinct peak, at 0 ps/nm. This agrees with the simulation results, as expected. Only when dispersion reaches +40 ps/nm the agreement between the simulated data and

experimental data start to diverge. Also the monitoring sensitivity for negative CD is slightly greater than for positive one. The author believe that this is due to the difference between the ideal delay of the MZI, and the one used in the experiment. The one measured by an optical network analyzer, used in the experiment, is 12.72 ps and the ideal delay is 12.5 ps, equal to half-bit delay time. Simulations tried to emulate the experimental conditions, although due to model limitations, it was not possible to fully emulate the MZI (with the same components of the one shown in Figure 4.6). This may explain the differences between the experimental and simulation results when the CD reaches 40 ps/nm. The MZI used was the one provided by the simulator, and it comes as one single component. The simulator used was Optisystem 7.0 .

4.5 Conclusions

The author shows a CD monitoring technique based in asynchronous sampling, that eliminates ambiguity at 0 ps/nm, and also have high sensitivity at this region of the monitoring window. It also has an acceptable monitoring resolution and monitoring window. This technique allows to use optical domain processing techniques and electro-optical sampling before the receiver reducing the required bandwidth of the photo-detector. This enables that this technique can be used at 100 Gbit/s and beyond. The author also elaborates the theory that led to a new equation that relates the maximum optical power, with CD. Simulation results agree with the theoretical results. Experimental results demonstrate the practical implementation of the proposed technique to monitor the chromatic dispersion of RZ modulation formats. In this chapter it was demonstrated a low cost chromatic dispersion monitoring technique, that is suitable to be implemented at very high data rates.

References

[1] V. Ribeiro , A. Teixeira and M. Lima, "Chromatic dispersion monitoring technique using optical asynchronous sampling and double sideband filtering," Optical Fiber Technology, Elsevier, vol. 16, pp. 124 - 127, 2010

[2] V. Ribeiro , A. Teixeira and M. Lima, "Experimental validation of a chromatic

dispersion monitoring technique using optical asynchronous sampling and double sideband filtering," Optical Fiber Technology, Elsevier, vol. 17, 135 - 137, 2011

[3] Y. K. Lize, L. Christen, J. Y. Yang, P. Saghari, S. Nuccio, A. E. Willnera and R. Kashyap, "Independent and simultaneous monitoring of chromatic and polarization-mode dispersion in ook and dpsk transmission," Photonics Technology Letters, IEEE, vol. 19, no.1, 2007

[4] Z. Pan, Y. Xie, S. A. Havstad, Q. Yu, A. E. Willner, V. Grubsky, D. S. Starodubov and J. Feinberg, "Real-time group-velocity dispersion monitoring and automated compensation without modifications of the transmitter," Optics Communications, Elsevier, vol. 230, 145-149, 2004

[5] K. T. Tsai and Winston I. Way; 'Chromatic dispersion monitoring using an optical delay-and-add filter',Lightwave Technology, Journal of, vol. 23, no.11, 2005

[6] B. Kozicki , A. Maruta and K. I. Kitayama, "Experimental investigation of delay-tap sampling technique for online monitoring of rz-dqpsk signals," Photonics Technology Letters, IEEE, vol. 21, no.3, 2009.

[7] S.D. Dods and T.B. Anderson, ' Optical performance monitoring technique using delay tap asynchronous waveform sampling' in Optical Fiber Communication, OSA conference, 2006, paper OThP5.

[8] P.S. Westbrook, B.J. Eggleton, G. Raybon, S. Hunsche and T. H. Her, "Measurement of residual chromatic dispersion of a 40-Gbit/s RZ signal via spectral broadening," Photonics Technology Letters, IEEE, vol. 14, no. 3, 2002

[9] S. Li and D.V. Kuksenkov:' A novel dispersion monitoring technique based on four-wave mixing in optical fiber' Photonics Technology Letters, IEEE, vol. 16, no. 3, 2004

[10] T. Luo, C. Yu, Z. Pan, Y. Wang, J.E. Mcgeehan, M. Adler and A.E. Willner, "All-optical chromatic dispersion monitoring of a 40-Gbit/s RZ signal by measuring the XPM-generated optical tone power in a highly nonlinear fiber," Photonics Technology Letters, IEEE, Vol. 18, No. 2, 2006.

[11] K.J. Park, J.H. Lee, C.J.Youn and Y.C. Chung, "A simultaneous monitoring technique for polarization-mode dispersion and group-velocity dispersion," in Optical Fiber Communication, OSA Conference, 2002, paper WE4.

[12] T. Inui, T. Komukai, K. Mori and T. Morioka, "160-gb/s adaptive dispersion equalization using an asynchronous dispersion-induced chirp monitor," Lightwave Technology, Journal of, vol. 23, no.6, Jun. 2005.

[13] K. Bondarczuk, P. J. Maguire, L. P. Barry, J. O'Dowd, W. H. Guo, M. Lynch, A. L. Bradley, J. F. Donegan and H. Folliot, 'Chromatic Dispersion Monitoring of 80-Gbit/s OTDM Data Signal via Two-Photon Absorption in a Semiconductor Microcavity',Photonics Technology Letters, IEEE, vol.19, no.1, Jan. 2007.

[14] Z. Pan, C. Yu and A. E. Willner, "Optical Performance monitoring for the next generation optical communication networks," Optical Fiber Technology, Elsevier, vol. 16, no.1, pp. 20 - 45, Jan. 2010.

[15] A.Teixeira, L.Costa, G. Frantzl, S. Azodolmolky, I.Tomkos, K. Vlachos, S Zsigmond, T. Cinkler , G. Tosi Beleffi, P. Gravey, T Loukina, J.A.LÃizaro, C.Vasquez, J.Montalvo and E. Le Rouzic, "An integrated view on monitoring and compensation for dynamic optical networks from management to physical layer," Photonics Network Communications, vol. 18, pp. 191-210, 2009

[16] Stephan Wielandy, Michael Fishteyn and Benyuan Zhu,"Optical performance monitoring unsing nonlinear detection," Lightwave Technology, Journal of, vol.22, no.3, 2004

[17] Govind P. Agrawal,"Nonlinear Fiber Optics," 4^{th} edition, Academic Press, Elsevier, pp. 89-102, 2006

CHAPTER 5

Multi-impairment optical performance monitoring

This chapter is dedicated to multi-impairment optical performance monitoring. The author details an optical performance monitoring technique with significant level of transparency. The technique is based on a novel performance diagram and artificial neural networks (ANNs). The technique is able to demonstrate comprehensive performance diagrams even for quadrature phase-shift keying (QPSK) modulation formats. This enables to monitor signals with this modulation format. This specific work resulted in 3 publications [1–3] and one patent (see Appendix A). In this chapter the author approaches [1, 2] and in Chapter 6 [3] is approached, due to the fact that it also includes all-optical signal processing (AOSP).

5.1 Introduction

Optical performance monitoring (OPM) has been a widespread research topic in the field of optical fiber communications. Several solutions have been proposed to evaluate the performance of optical networks. Performance parameters include chromatic dispersion (CD) [4–6], 1^{st} order polarization mode dispersion (PMD) [7, 8], or optical signal to noise ratio (OSNR) [8, 9], among other. One or more of these techniques are based in at least one of the following methods: radio-frequency (RF) spectrum analysis, nonlinear optical effects detection and statistical signal processing using synchronous or asynchronous sampling. Despite the usefulness of these techniques for specific applications, the demand for a low cost, multi-impairment Optical Performance Monitor is significant.

The methods addressed above may be classified by the capability to monitor simultaneously all the parameters with one single device. Statistical signal processing by synchronous or asynchronous sampling, seems to be the best candidate [10–13]. RF spectrum analysis and nonlinear optical effects detection collides with the interdependence between different impairments [14], which requires additional techniques to solve this issue [15].

Recently, techniques using machine learning and ANNs have been proposed in conjunction with very well known optical performance diagrams [16, 17]. These optical performance diagrams are based on asynchronous amplitude histograms [18], delay-tap asynchronous diagrams [10–12] or synchronous eye diagram (SED)s [13].

Jargon et al. [11] have reported an optical performance technique using ANNs, which monitors simultaneously CD, PMD and OSNR for an non-return-to-zero (NRZ)-on-off keying (OOK) modulation format at $10\,\mathrm{Gbit/s}$. The monitoring window ranges from 0 to 700 ps/nm, 0 to 35 ps and 18 to 30 dB respectively. The authors do not report the errors obtained in these computations [11–13].

Machine learning with asynchronous time-delay diagrams (ATDD) histograms has also been used to compute OSNR, CD and PMD [12]. The monitoring windows reported, range from 0 to 1600 ps/nm, 0 to 50 ps and 15 to 27 dB, for CD, PMD and OSNR, respectively, using $10\,\mathrm{Gbit/s}$ NRZ-OOK modulation format. The patent application [12] uses several algorithms to predict CD, PMD and OSNR, including a linear and a nonlinear kernel algorithm, for pattern recognition. It

demonstrates good estimates for CD and PMD, although the monitoring accuracy for OSNR is mentioned "as poor" [12].

A novel technique has been developed in [13] using parameters extracted from SEDs, presenting a monitoring range of 18 to 30 dB, 0 to 700 ps/nm and 0 to 35 ps for OSNR, CD and PMD, respectively. This results are shown for a 10 Gbit/s NRZ-OOK modulation format.

In [19] delay tap asynchronous sampling is used to monitor a 100 Gbit/s QPSK modulation format signal. Two different direct detection receivers have been tested (i.e single ended detection and balanced detection). Superior accuracy is achieved with balanced detection.

In [20] SEDs with ANN, have been used to compute several impairments using 40 Gbit/s return-to-zero (RZ)-OOK and 40 Gbit/s RZ-Differential Phase Shift Keying (DPSK). The errors reported are 2.53 ps/nm for CD and 0.58 dB for OSNR, when using 40 Gbit/s RZ-OOK signal. The OSNR is 1.85 dB and CD is 3.18 ps/nm for 40 Gbit/s RZ-DPSK. The errors reported for CD using RZ-OOK modulation format are about 5 % of the maximum range of the monitoring window used (50 ps/nm).

A novel technique so called parametric asynchronous eye diagram (PAED) [1] in conjunction with ANNs is presented to monitor simultaneously several impairments. The PAED uses samples of the signal (y) and of the differentiated signal (x), to form the diagram (where $x = \frac{\partial y(t)}{\partial t}$ and y=y(t), hence the name Parametric). The technique is completely transparent to modulation format and bit rate, in terms of hardware and signal processing. This means that no change in hardware or processing algorithm is required when the bit rate and modulation format change. Results demonstrate the effectiveness of this technique when dealing with NRZ, RZ and QPSK modulation formats and bit rates of 10 Gbit/s, 20 Gbit/s and 40 Gbit/s. The author reports results showing that with a simple receiver comprising only single ended detection, the optical performance technique presented in this technique is capable to monitor a signal modulated with 40 Gbit/s QPSK.

The PAED captures the information of the first order derivative, which is strongly affected by CD and PMD, due to the pulse broadening caused by those effects. The differentiator increases the sensitivity of the monitor at high frequency components of the signal, which for instance may be beneficial for CD,

where the components with higher frequency, have higher delay, and suffer higher fading due to CD. When dispersion is too high the fading at high frequencies increases to a point where it is not possible to distinguish between one level of dispersion and the other. The differentiator allows to increase the range of the monitoring window. PAED is focused on rise and fall edges and treats them separately, while ATDD is focused on transitions, from binary levels.

The impact of dispersion in PAED effects occurs mainly on rise and fall edges, while the impact of noise is mainly concentrated in the center of PAED. These three regions are represented on PAED in an easy and understandable manner as can be seen in Figure 5.1. The visual analysis of ATDD depends on the delay used, modulation format and bit rate. The visual and processing analysis of PAED is completely independent of these parameters (ie. no need to change the OPM algorithm). Asynchronous amplitude histograms fall in a different category. They are based in the evaluation of histograms, which gives an averaged measurement of Q-factor, which is affected by middle level samples.

5.2 Artificial neural networks

"ANNs are neuroscience inspired computational tools that are trained by the use of input-output data to generate a desired mapping from an input stimulus

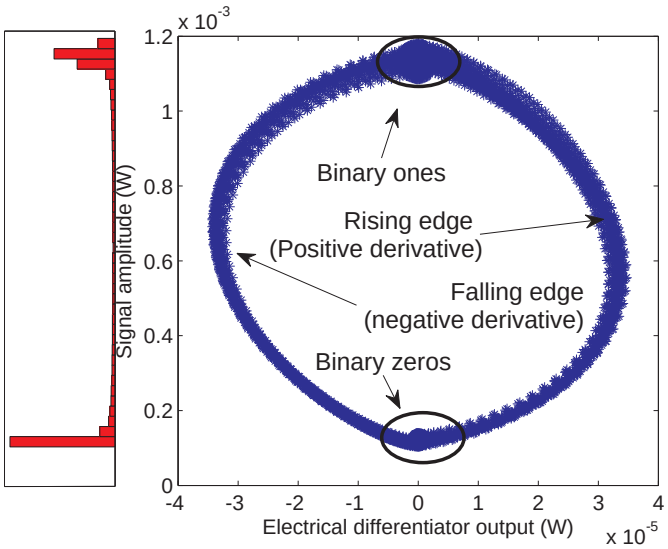

Figure 5.1: Histogram and PAED referencing the rising, falling edges and the binary ones and zeros.

to the targeted output" [13]. The input-output pairs are grouped in two different sets, the training set and the test set, both are taken from the input and output of a physical device or physical model. They are different in the sense that they have different input-output combinations, being this essential to test the validity of the model. The training set and the test set are composed by $n+m$ columns, where *n* is the number of inputs and *m* is the number of outputs. Each row represents one training or test data example.

In a first phase the ANN is trained with the training set. The training set is the input-output combinations taken from a physical device or model that adjust the structure of the ANN, in order to make it behave as the aforementioned physical device or model, with the minimum possible error. The training applies to adjust the weights of the ANN in each training epoch (iteration), until a specified Mean Square Error, between the *m* outputs of the training set and the *m* output values obtained during the training process, has been met, or a defined number of epochs has been achieved. In Figure 5.2, the weights of the ANN are illustrated by the arrow lines, where the mathematical operation executed by them is multiplication. The neurons in the hidden and output layer, first sum all

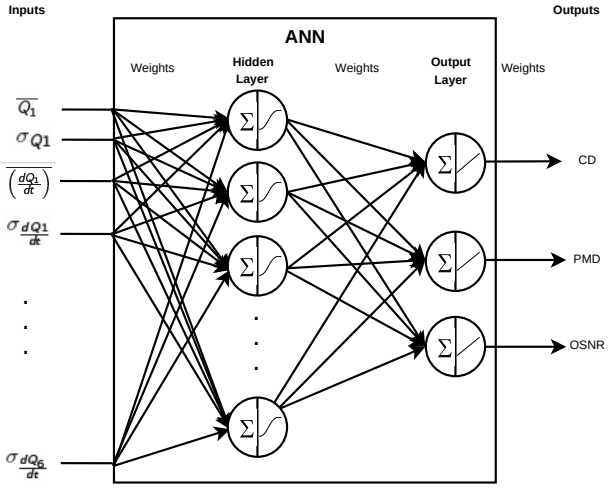

Figure 5.2: ANN. Q_n represents the n^{th} subset of the diagram of PAED (see 5.6), σ the standard deviation, $\overline{Q_n}$ and $\overline{\frac{dQ_n}{dt}}$, represents the mean of the amplitude and derivative of the subset of the diagram, respectively

its inputs, and then pick the result of this sum, as the coordinate x of a sigmoid (hidden layer), or linear (output layer) function. The output of each neuron is the ordinate $y = f(x)$ of such functions. It may occur that low errors are achieved

with the training sets, due to the effect known as overtraining in ANNs, but that does not mean that the ANN is well modeled. To test if the ANN is well modeled it must be validated with the test set. If the errors between the test values and the ones predicted by the ANN are sufficiently low, the ANN is well modeled, and the training process is completed. The results shown in figures presented in this technique, when related with ANNs output, are always based on the test data.

Neural networks allow nonlinear modeling, although it is useful to inspect the requirement for a nonlinear approach, which from the best of our knowledge has not been done yet, in the literature. The author has used linear partial least squares (PLS) regression as a term of comparison. The setup used to capture the results is demonstrated in Figure 5.3, and the transmitter sends a NRZ modulated signal at 10 Gbit/s.

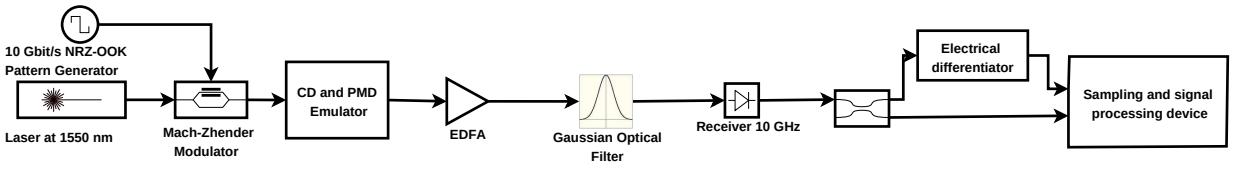

Figure 5.3: Setup of the technique using an electrical differentiator.

In Figures 5.4 and 5.5, the author demonstrates the results using PLS and ANN, respectively, for modeling CD, PMD and OSNR, splitting PAED in 4 and 6 subsets for pattern recognition, methodologically similar to Figure 5.6. The mean and standard deviations for each subset, and for each axis of the diagram, were calculated and inserted as inputs in the two models. The inputs are scaled, and the principal components are made orthogonal using principal component analysis. The ANN model uses 40 neurons in the hidden layer, which yields a relatively large network. Although the accuracy, through the range of CD, PMD and OSNR, justify this approach. Further in this Chapter we will see a comparison between 10 and 40 neurons accuracy, in the hidden layer and is clear, that higher accuracy is achieved in the 40 neurons approach. Increasing this number lead to lower error with the training set examples, while will lead also to higher error in the test set examples, which has no interest in this case.

Comparing the results of Figures 5.4 and 5.5, we may achieve to the conclusion that the approach using PLS is less accurate than the approach using ANN. The author stresses out that PLS is almost insensitive to the number of

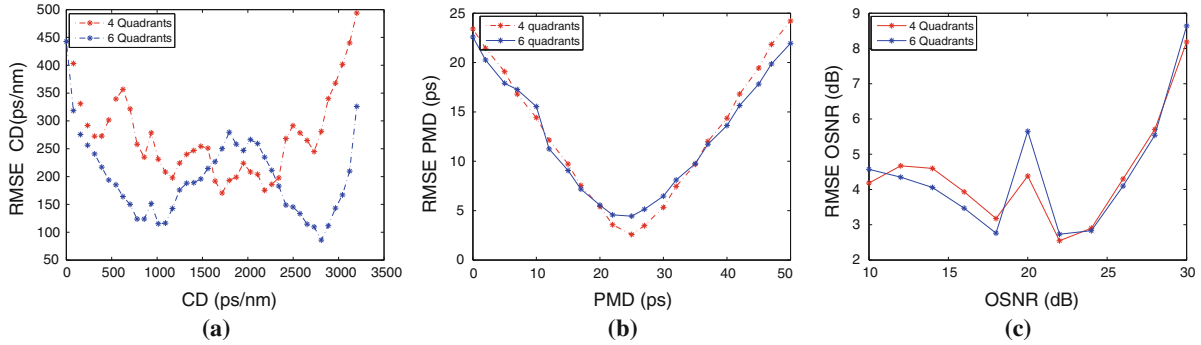

Figure 5.4: Linear PLS regression results using a 10 Gbit/s NRZ signal. PAED is split in 4 and 6 subsets of the diagram. For each subset, the mean and the variance for the X and Y axis are calculated. Results for a) CD, b) PMD and c) OSNR

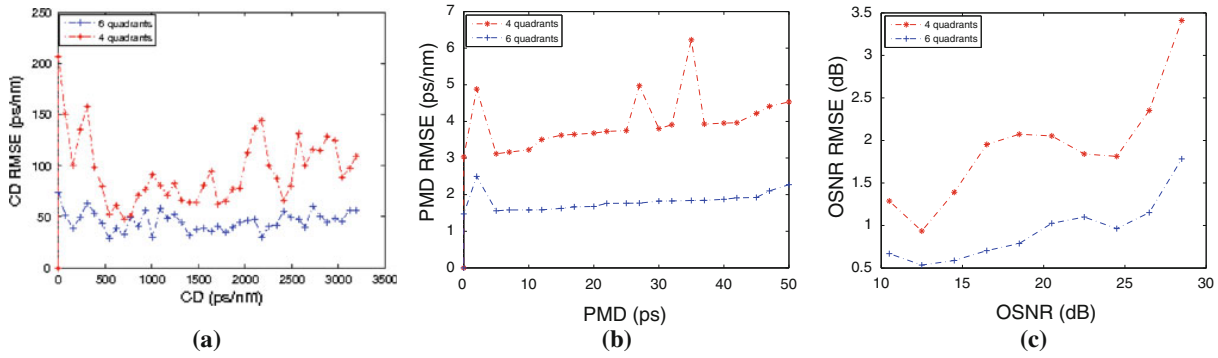

Figure 5.5: ANN results using a 10 Gbit/s NRZ signal. PAED is split in 4 and 6 subsets of the diagram. For each subset, the mean and the variance for the X and Y axis are calculated. Results for a) CD, b) PMD, c) OSNR

---

subsets used to split the diagram, while ANN clearly shows better results when splitting PAED in 6 subsets. This may indicate that since PLS cannot learn well the relationships between the input and the output, it does not matter how much information is added to the model. So, we may conclude that a nonlinear approach, such as ANN, is necessary for multi-impairment modeling in fiber, when using PAED.

5.3 Simulation setup

In Figure 5.3 the setup of the novel technique using an electrical differentiator is shown. The technique captures samples from the signal and from the differ-

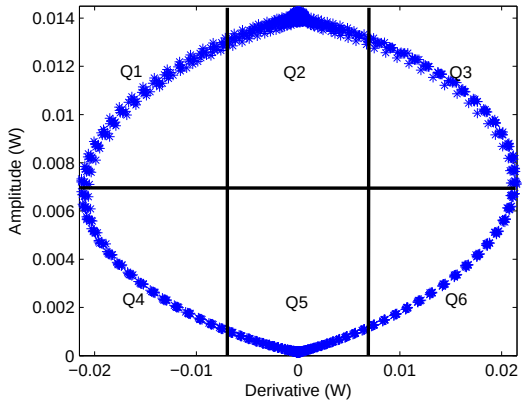

Figure 5.6: PAED split in 6 subsets of the diagram for training procedure

entiated signal, and plots them, one against the other, in X-Y mode, as shown in Figure 5.8. The power of the signal is split in two equal (not mandatory) parts. One part is sent to the differentiator and the other is sent directly to a signal processor.

The setup of Figure 5.3 comprises a laser centered at 1550 nm, one pattern generator, providing $10\,\mathrm{Gbit/s}$ NRZ-OOK modulation format, transmitting pulses with 35% of the bit duration spent in the rise time and 35 % in the fall time (ITU recommendation G.957), a Mach-Zehnder modulator, a CD and a PMD emulator. Shorter rise and fall times, produce less accurate results, due to the spreading of dispersion to higher frequencies, which are not available for monitoring purposes due to the limited bandwidth of the photo-detector. The PMD emulator has a depolarization rate of 10.8 degrees/GHz. This takes into account the rotation of the principal states of polarization (PSP).

The erbium-doped fiber amplifier (EDFA) emulates the effect of OSNR by tuning the noise figure. An optical gaussian filter centered at 1550 nm and bandwidth higher than 20 GHz, filters the optical signal. Higher bandwidths are possible without significant decrease in the monitor performance. Although the bandwidth of the filter and the photodetector should not be much higher than the bandwidth of the signal. High frequency noise will degrade PAED, since this noise is discriminated by the high pass filter profile of the differentiator, creating an additional jitter in the rising and falling edges of the diagram. The OSNR was measured after the optical gaussian filter. One 1^{st} order Gaussian electrical filter, included in the receiver, simulates the PIN photo-diode passband

of 10 GHz bandwidth. The propagation delay of the electrical differentiator shall be compensated in the simulation, to synchronize the electrical differentiated signal, and the modulated signal.

The differentiator is intended to be an analog filter with proper bandwidth. A digital differentiator may also be used, although it would require the Nyquist sample rate to work properly. Therefore in essence if we would like to take advantage of asynchronous undersampling we shall not use a digital differentiator at least for OPM applications. It would be contradictory in terms of cost and philosophy of this work. The author runs the simulations using different pseudo-random bit sequence (PRBS) and with random sample offset, relatively to the beginning of the PRBS, for each combination of impairments .

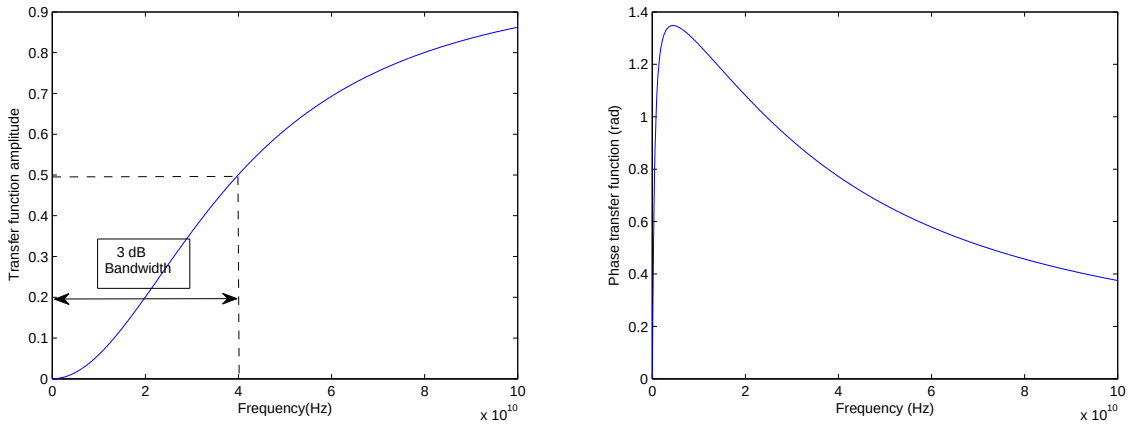

(a) (b)

Figure 5.7: (a) Amplitude transfer function of the differentiator and (b) Phase transfer function of the differentiator.

In Figure 5.7 the amplitude and phase transfer function of the differentiator is shown. It was implemented in the frequency domain with one zero at $-3.14\,\mathrm{Grad/s}$ and one pole at $-251\,\mathrm{Grad/s}$. The differentiator is a high pass filter, rising the amplitude transfer function by 20 dB/decade, between 500 MHz and the cut-off frequency of 40 GHz. Millimeter-wave monolithic microwave integrated circuits technology can go up to 100 GHZ frequencies [21], and there are already companies in the market that are producing high pass filters at 40 GHz bandwidths and beyond (for example Millitech).

The alternative to the electrical differentiator is one optical differentiator. The

purpose of using an optical differentiator is that it gives the possibility to optically sample the signal, after the differentiator, enabling superior bandwidths. The author tested successfully in the simulator the optical differentiator proposed by Velanas et al. [22]. It has high transparency to the wavelength, and so it is suitable for Optical Sampling Oscilloscopes. In [3] the author presented an experimental demonstration of PAED using a similar scheme, however instead of a dispersion-shifted fiber (DSF) as in [22] the author has used a semiconductor optical amplifier (SOA) for modulated signals up to 40 GHz bandwidth. The author did not use one amplitude optical differentiator to compute the OPM results, because we will have to deal with strong nonlinearities, which consume high processing time, specially when several combinations of PMD, CD and OSNR are to be computed. Computer memory and reasonable time to compute the results in this situation can be overcome. From Figure 5.8 one can see that despite using two OOK modulation formats and two different bit rates, the PAED remains with similar shape, across Figures 5.8a, 5.8b, 5.8d and 5.8e. Figures 5.8c and 5.8f show a NRZ and RZ signal degraded with the same value of CD, PMD and OSNR. The value of CD and PMD of the diagrams of 5.8c and 5.8f is higher than in the Figures 5.8a, 5.8b, 5.8d and 5.8e while the inverse occurs with OSNR. The effect of CD is evident, it tends to decrease the derivative in the lower part of the diagram, due to pulse brodening. The decrease of OSNR tends to spread the samples along the contour of PAED due to the increase of added noise. PMD tends to distort PAED, turning it antisymmetrical due to different rising and falling edges caused by the impact of PMD. One can see that the PAED tends to close when facing signal degradation, having a behavior similar to the SED as can be seen in Figure 5.9. Figure 5.9 shows the eye diagram impacted by CD for several modulation formats including QPSK.

5.4 Simulation results and discussion

The software used to train the ANN was the software package neuromodeler 1.5 by Zhang et al. [23], also used in [13] and [19] .

The center subsets of the diagram are better, evaluating OSNR, because is there where the noise is mainly concentrated. The outer subsets of the diagram are better evaluating dispersion effects such as PMD and CD, because dispersion enlarges the bit duration, reducing the derivative at the rising and falling edges.

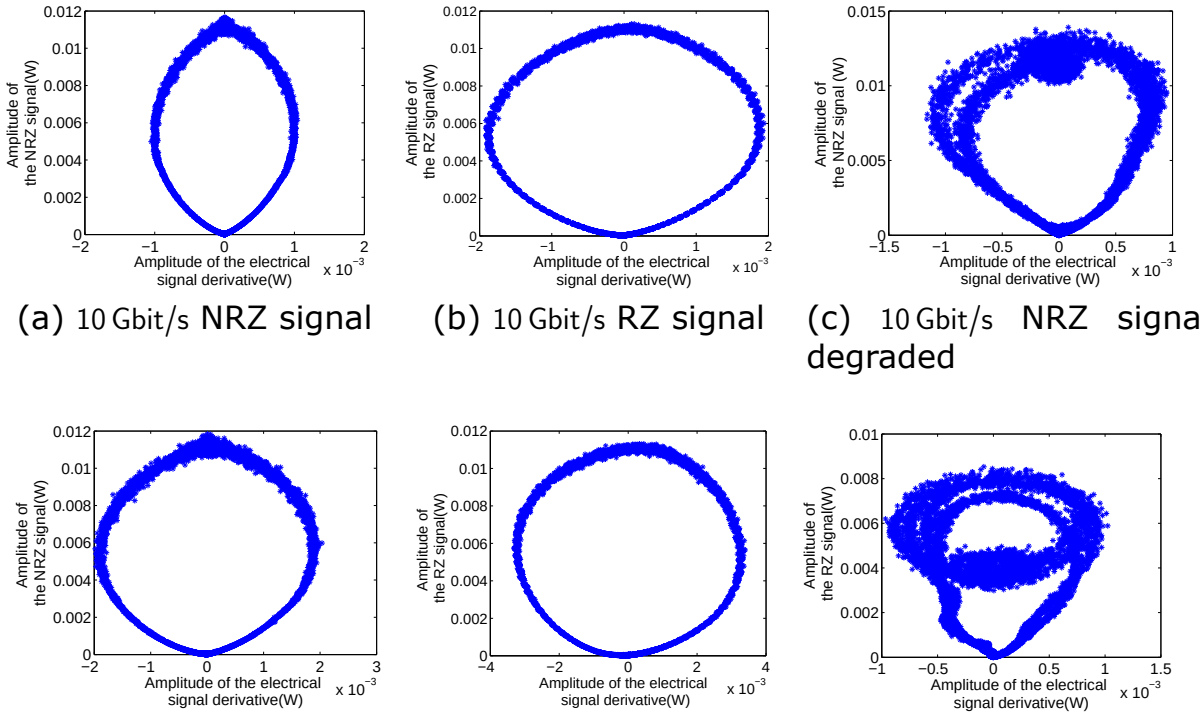

(a) 10 Gbit/s NRZ signal (b) 10 Gbit/s RZ signal (c) 10 Gbit/s NRZ signal degraded

(d) 20 Gbit/s NRZ signal (e) 20 Gbit/s RZ signal (f) 10 Gbit/s RZ signal degraded

Figure 5.8: Diagrams generated by the novel technique, using different modulation formats and bit rates. Figures 5.8a, 5.8b, 5.8d and 5.8e with CD=0 ps/nm, PMD=0 ps, OSNR=30 dB. Figures 5.8c and 5.8f with with CD=500 ps/nm, PMD=7 ps, OSNR=20 dB

The author runs the simulation setup with Optisystem 10.0, and simultaneously, Matlab® code also ran with the simulation. The ANN was tested with 40 and 10 hidden neurons (NRZ only), 24 inputs and 3 outputs. The ANN was trained, with the Quasi-Newton(MLP) method. The inputs are preprocessed using the *mapstd* and *processpca* Matlab® functions. This is a simulation example for the best performance possible, in terms of the minimal root mean squared error, that can be achieved. Increasing the number of hidden neurons , above 40, will not provide better performance, although in practice the number of hidden neurons can be decreased if speed is the demanding factor. A decrease in performance may occur when we set the number of hidden neurons from 40 to 10 as shown in Figure 5.10.

There are some hardware implementations of ANNs that can implement them,

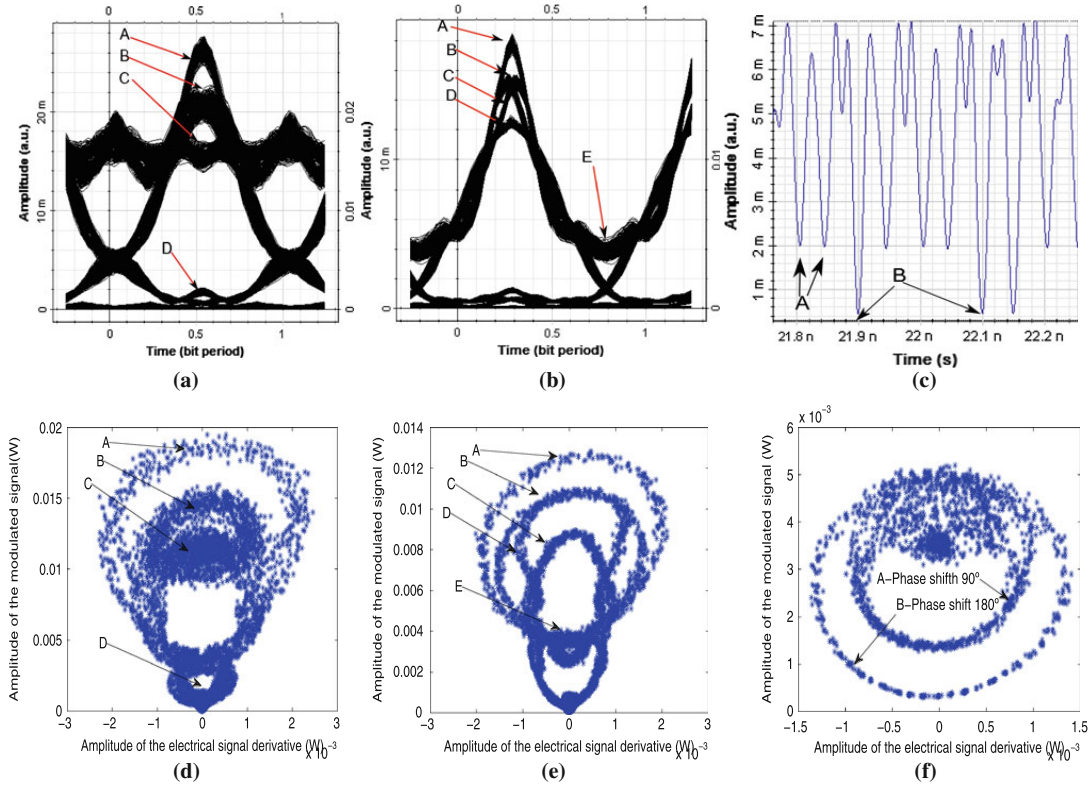

Figure 5.9: Comparison between SED and PAED. a), d) 10 Gbit/s NRZ modulated signal, b), e) 10 Gbit/s RZ modulated signal c), f) 40 Gbit/s QPSK modulated signal. a), d) CD = 500, ps/nm PMD = 0 ps, OSNR=18 dB, b),e) CD = 400 ps/nm, PMD = 0 ps, OSNR = 27 dB, c), f) CD = 60 ps/nm, PMD = 0 ps, OSNR = 30 dB

even using optical components. An extensive review of hardware implementations of ANN can be found in [24]. Field programmable gate arrays, give a relatively cost effective, reconfigurable implementation of an ANN [24].

5.4.1 NRZ-OOK 10 Gbit/s

The results plotted in Figures 5.10a to 5.10c, show the CD, PMD and OSNR obtained (CD out, PMD out, OSNR out) against the desired values (CD in, PMD in, OSNR in). The root-mean-square-error (RMSE) is calculated for each value of CD, PMD and OSNR and the error bars shown are based on this calculation. In the case that the ANN has 40 neurons CD RMSE remains bellow 60 ps/nm until about 3000 ps/nm, above that it starts to increase. PMD RMSE is higher at the borders of the monitoring window, remaining steady, with small fluctua-

tions, along the center of the monitoring window. The RMSE of OSNR increases gradually with the increase of the value of OSNR. Better results are achieved for the ANN with 40 neurons.

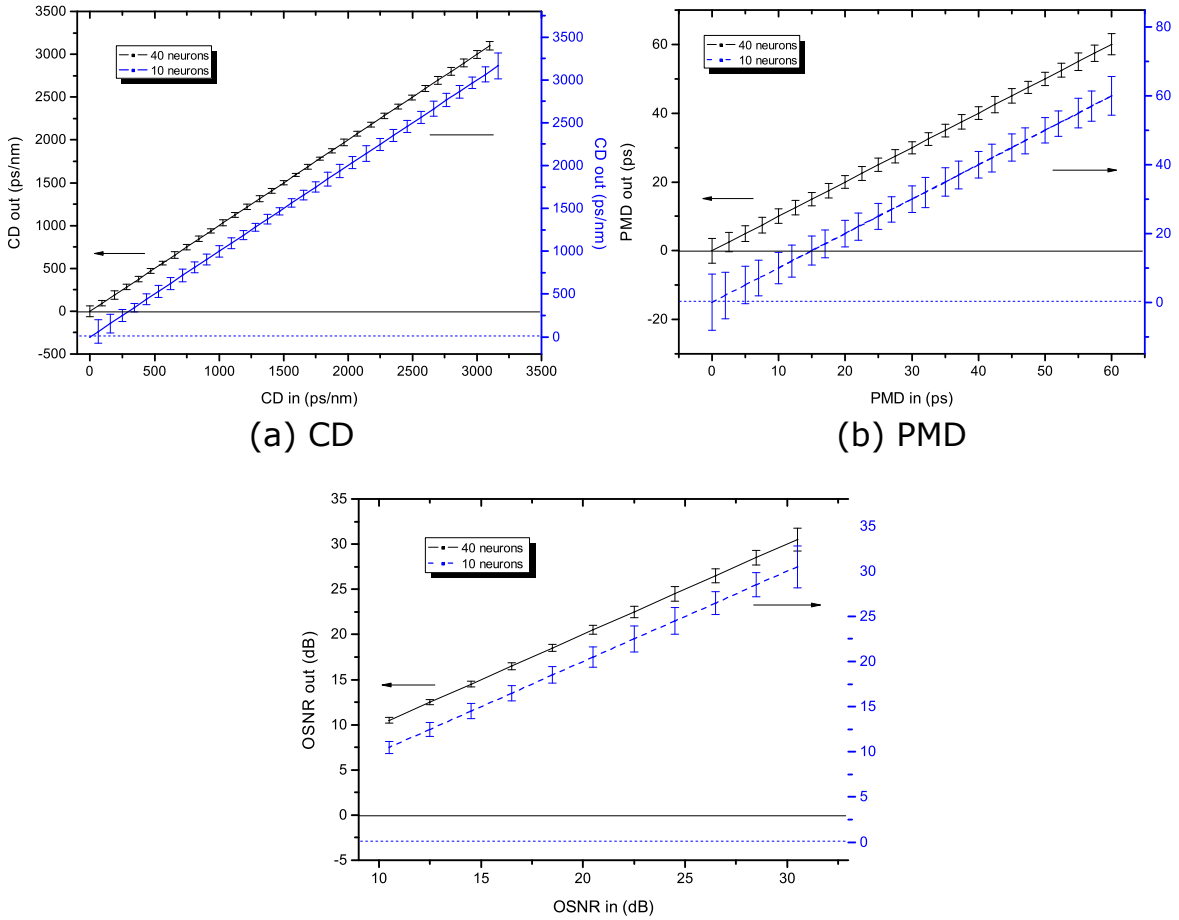

(a) CD (b) PMD

(c) OSNR

Figure 5.10: 10 Gbit/s NRZ. Error bars of CD PMD and OSNR test data

5.4.2 QPSK 40 Gbit/s

In Figure 5.11, the results for a signal modulated with 40 Gbit/s QPSK are shown. The setup used is the same as in Figure 5.3, except that the transmitter must be a QPSK transmitter and the photodetector has a bandwidth of 40 GHz, which is related with the bandwidth of the signal by a factor of 2. Lower values of bandwidth were tested for the direct detection receiver, although the RMSE obtained was not satisfactory. The number of neurons used in the ANN hidden

layer was 40, and the training process is the same as the one used before. The author tried several options for the receiver, although a 20 GHz receiver does not allow sufficient accuracy, despite the bandwidth of a QPSK modulated signal is 20 GHz. An alternative to this scheme with increased complexity was tested using a coherent receiver. However it does not provide a significant increase in accuracy, when compared with the former option. Therefore the author only show the results, when it is considered a receiver comprising a 40 GHz photodetector. Although costs may justify one option or the other. The coherent receiver (alternative solution) uses two 20 GHz receivers and requires 4 analog-digital converters and two differentiators. The quadrature and in-phase signals are handled as two intensity modulated signals and therefore, the signal can be represented in similar diagrams as the ones shown in Figure 5.8, which is not possible with the former option. The quadrature and phase samples are superimposed, generating a PAED.

The results in Figure5.11, show RMSE as a function of the values of each impairment. CD RMSE and PMD RMSE are below 20 ps/nm and 1.3 ps. OSNR RMSE is near 1.5 dB at about 11 dB, but decreases rapidly and then starts to increase gradually, with a small fluctuation at 25 dB.

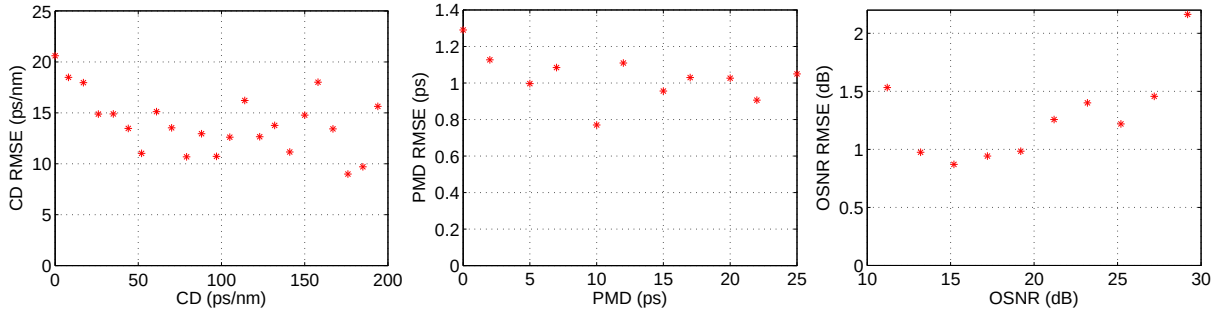

(a) CD (b) PMD (c) OSNR

Figure 5.11: 40 Gbit/s QPSK results trained by choosing 6 subsets of PAED. RMSE as a function of CD, PMD and OSNR test data

5.4.3 Mixed traffic RZ and NRZ 10 Gbit/s and 20 Gbit/s

To the best of our knowledge, so far the performance monitoring in optical networks, showed no technique that have had the capability to monitor, mixed

traffic, with a single monitor. The author calls mixed traffic, when the networks support traffic with several modulation formats and bit rates, traveling in the network (optical burst switching (OBS) networks for example). In Figure 5.12, the author presents results that demonstrate the potential of this optical performance technique, to make the output of the ANN follow the test data examples, by making use of RZ and NRZ modulation formats at 10 and 20 Gbit/s, mixed in a training data set. Due to the relative complexity of the problem, the number of neurons in the hidden layer were increased from 40 to 50. The training process is identical to that used previously. The ANN comprises 24 inputs and 5 outputs. The outputs give the predictions of CD, PMD, OSNR, bit rate and modulation format. Table 5.1, summarizes the results obtained. Different monitoring windows were used for each modulation format and bit rate, due to the intrinsic nature, of each one of these types of traffic. The RMSE values for CD, PMD and OSNR are presented in the same table. PAED in conjunction with ANNs give the possibility to integrate all these types of traffic, due to the intrinsic nature of PAED, which gives similar diagrams for all kinds of OOK traffic. This eases considerably the learning of ANNs.

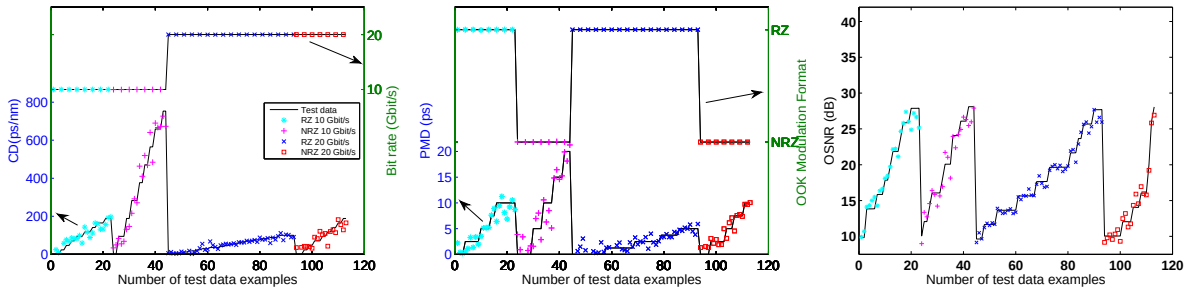

(a) CD (b) PMD (c) OSNR

Figure 5.12: CD, PMD, OSNR, bit rate and modulation format predictions as a function of number of test data examples, when mixed traffic is in the network

The predictions for bit rate and modulation format, correspond to an almost perfect match. The derivative is higher for higher bit rates, due to faster rise and fall times. This allows to distinguish between bit rates and OOK modulation formats. Information about bit rate and modulation format will be important in future optical networks in the scope of OPM.

Table 5.1: Monitoring windows for each impairment - RMSE-Root Mean Square Error

	10 Gbit/s				20 Gbit/s			
	RZ-OOK		NRZ-OOK		RZ-OOK		NRZ-OOK	
	Range	RMSE	Range	RMSE	Range	RMSE	Range	RMSE
CD (ps/nm)	0-200	24.95	0-800	47.44	0-100	10.46	0-200	24.65
PMD (ps)	0-10	1.75	0-20	2.30	0-5	0.82	0-10	1.11
OSNR (dB)	10-28	1.19	10-28	1.38	10-28	0.75	10-28	0.73

5.4.4 Discussion of results

Our results for 40 Gbit/s QPSK, show better accuracy than [19], for a single ended detection scheme, which decrease cost relatively to the balanced detection scheme proposed by that technique. The 10 Gbit/s NRZ results show higher monitoring window for CD, PMD and OSNR than [11–13]. The technique presented in [11] presented a correlation coefficient of 0.97, between the test data examples and the output of the ANN. The author obtained a correlation coefficient of 0.99. The results using mixed traffic present lower accuracy and also lower monitoring range for 10 Gbit/s NRZ signal, mixed with other modulated signals, than the results presented in sections 4.1. This is due to the fact that above a certain level of impairments the ANN cannot give accurate predictions for the bit rate and modulation format, turning out difficult the learning of ANN.

5.5 Conclusions

Parametric asynchronous eye diagram is a straightforward and cost-effective alternative to SED, when the purpose is to visually evaluate the quality of the signal. Parametric asynchronous eye diagram, together with ANNs showed to be a valid solution in the monitoring of different types of traffic with different modulation formats and bit rates, including 10 Gbit/s NRZ, 40 Gbit/s QPSK and mixed traffic with different OOK modulation formats and bit rates traveling through the network, such as 10 Gbit/s NRZ, 10 Gbit/s RZ, 20 Gbit/s RZ and 20 Gbit/s NRZ. In comparison to ATDD it can be mathematically verified by comparing the cross-correlation between the derivative and the signal and the cross-correlation between the signal and its delayed copy, that in the former case the

cross-correlation is always near to zero, when there is no delay between the signal and the derivative, while in the later case, the cross-correlation is always higher than the former case. If one compares the phase portraits generated by PAED and ATDD, it can be assumed that ATDD can only gives detailed information about what happens in the low frequency components, while PAED can discriminate not only the low frequency components of the signal in the zeros and the ones, but also the high frequency components in the transitions. In this transitions, i.e, in the high frequency components is where dispersion, either caused by CD or PMD, is more severe. This characteristics allowed to double the CD monitoring window provided by ATDD [12]. Therefore one can conclude that PAED is richer in terms of information that it gives to the user. Besides PAED is not bit rate dependent as ATDD. It can also generate comprehensible phase-portraits when using QPSK modulation format enabling to monitor several impairments in this case.

References

[1] V. Ribeiro, L. Costa, M. Lima, and A. L. J. Teixeira, "Optical performance monitoring using the novel parametric asynchronous eye diagram," *Opt. Express*, vol. 20, pp. 9851–9861, Apr. 2012.

[2] V. Ribeiro, M. Lima, and A. Teixeira, "Comparison of optical performance monitoring techniques using artificial neural networks," *Neural Computing and Applications*, vol. 23, no. 3-4, pp. 583–589, 2013.

[3] V. Ribeiro, M. Lima, and A. Teixeira, "Parametric asynchronous eye diagram for optical performance monitoring," in *Optical Fiber Communication Conference and Exposition (OFC/NFOEC), 2012 and the National Fiber Optic Engineers Conference*, pp. 1–3, Mar. 2012.

[4] V. Ribeiro, L. Costa, A. Teixeira, R. Nogueira, and M. Lima, "Chromatic-dispersion-monitoring scheme using a mach-zehnder interferometer and q-factor calculation," *J. Opt. Commun. Netw.*, vol. 2, pp. 10–19, Jan. 2010.

[5] A. L. Campillo, "Chromatic dispersion-monitoring technique based on phase-sensitive detection," *Lightwave Technology, Journal of*, vol. 17, no. 6, pp. 1241–1243, 2005.

[6] P. Westbrook, B. Eggleton, G. Raybon, S. Hunsche, and T. H. Her, "Measurement of residual chromatic dispersion of a 40-gb/s rz signal via spectral broadening," *Photonics Technology Letters, IEEE*, vol. 14, pp. 346 –348, Mar. 2002.

[7] S. Nezam, Y.-W. Song, C. Yu, J. McGeehan, A. Sahin, and A. Willner, "First-order pmd monitoring for nrz data using rf clock regeneration techniques," *Lightwave Technology, Journal of*, vol. 22, pp. 1086 – 1093, Apr. 2004.

[8] F. Khan, A. Lau, Z. Li, C. Lu, and P. Wai, "Osnr monitoring for rz-dqpsk systems using half-symbol delay-tap sampling technique," *Photonics Technology Letters, IEEE*, vol. 22, pp. 823 –825, Jun. 1 2010.

[9] R. Luis, A. Teixeira, and P. Monteiro, "Optical signal-to-noise ratio estimation using reference asynchronous histograms," *Lightwave Technology, Journal of*, vol. 27, pp. 731 –743, Mar. 15 2009.

[10] T. Anderson, A. Kowalczyk, K. Clarke, S. Dods, D. Hewitt, and J. Li, "Multi impairment monitoring for optical networks," *Lightwave Technology, Journal of*, vol. 27, pp. 3729 –3736, Aug. 2009.

[11] J. Jargon, X. Wu, and A. Willner, "Optical performance monitoring by use of artificial neural networks trained with parameters derived from delay-tap asynchronous sampling," in *OFC 2009. Conference on*, pp. 1–3, Mar. 2009.

[12] T. Anderson, S. Dods, A. Kowalczyk, J. Bedo, and K. P. Clarke, "Method and apparatus for sampled optical signal monitoring, patent application," Jan. 2009.

[13] J. A. Jargon, X. Wu, and A. E. Willner, "Optical performance monitoring using artificial neural networks trained with eye-diagram parameters," *Lightwave Technology, Journal of*, vol. 21, no. 1, pp. 54–56, 2009.

[14] S. Wielandy, M. Fishteyn, and B. Zhu, "Optical performance monitoring using nonlinear detection," *Lightwave Technology, Journal of*, vol. 22, pp. 784 – 793, Mar. 2004.

[15] J.-Y. Yang, L. Zhang, Y. Yue, J. Jackel, A. Agarwal, L. Paraschis, and A. E. Willner, "Cd-insensitive pmd monitoring of a high-speed polarization-multiplexed data channel," *Opt. Express*, vol. 17, pp. 18171–18177, Sep. 2009.

[16] H. Takara, I. Shake, T. Ohara, and B. Kozicki, "Optical performance monitoring using asynchronous amplitude histogram," in *Optical Internet, 2007 and the 2007 32nd Australian Conference on Optical Fibre Technology. COIN-ACOFT 2007. Joint International Conference on*, pp. 1 –3, 2007.

[17] S. Dods and T. Anderson, "Optical performance monitoring technique using delay tap asynchronous waveform sampling," in *Optical Fiber Communication Conference, 2006 and the 2006 National Fiber Optic Engineers Conference. OFC 2006*, pp. 1 – 3, 2006.

[18] T. Shen, K. Meng, A. Lau, and Z. Y. Dong, "Optical performance monitoring using artificial neural network trained with asynchronous amplitude histograms," *Photonics Technology Letters, IEEE*, vol. 22, pp. 1665 –1667, Nov. 15 2010.

[19] X. Wu, J. Jargon, L. Paraschis, and A. Willner, "Ann-based optical performance monitoring of qpsk signals using parameters derived from balanced-detected asynchronous diagrams," *Photonics Technology Letters, IEEE*, vol. 23, pp. 248 –250, Feb. 15 2011.

[20] X. Wu, J. Jargon, R. Skoog, L. Paraschis, and A. Willner, "Applications of artificial neural networks in optical performance monitoring," *Lightwave Technology, Journal of*, vol. 27, pp. 3580–3589, Aug. 2009.

[21] H. Wang, K.-Y. Lin, Z.-M. Tsai, L.-H. Lu, H.-C. Lu, C.-H. Wang, J.-H. Tsai, T.-W. Huang, and Y.-C. Lin, "Mmics in the millimeter-wave regime," *Microwave Magazine, IEEE*, vol. 10, pp. 99–117, Feb. 2009.

[22] P. Velanas, A. Bogris, A. Argyris, and D. Syvridis, "High-speed all-optical first- and second-order differentiators based on cross-phase modulation in fibers," *Lightwave Technology, Journal of*, vol. 26, pp. 3269 –3276, Sep. 15 2008.

[23] Q.-J. Zhang, K. Gupta, and V. Devabhaktuni, "Artificial neural networks for rf and microwave design - from theory to practice," *Microwave Theory and Techniques, IEEE Transactions on*, vol. 51, pp. 1339 – 1350, Apr. 2003.

[24] J. Misra and I. Saha, "Artificial neural networks in hardware: A survey of two decades of progress," *Neurocomputing*, vol. 74, no. 1-3, pp. 239 – 255, 2010.

CHAPTER 6

All-optical signal processing

The emergence of novel all-optical signal processing (AOSP) techniques is fundamental, for the deployment of optical networks with high levels of transparency. AOSP is historically competing with electrical signal processing (ESP). Although nowadays they are seen more like complementary than competitive [1]. When one wants to justify the investment of time and resources in the research of AOSP solutions, one has to remember the success of erbium-doped fiber amplifier (EDFA), that substituted electronic repeaters. The later were set in parallel to process each wavelength division multiplexing (WDM) channel [2], while the former is able to provide massive parallelism in one single optical device. This has enabled a drastic reduction of costs. Moreover AOSP solutions such as EDFA, provides larger bandwidth devices [2], which enables the emergence of novel applications to come into the field. Besides massive parallelism, low levels of crosstalk and potential to consume less energy are appointed as

some of the advantages of AOSP over ESP [1, 3]. Will this be sufficient to move some of the current functionalities performed in the electrical domain to the optical domain? The aforementioned advantages suggest that the answer may be yes [1].

In this chapter the author makes a general review of some of the functionalities proposed in the literature to be performed by AOSP, namely, all-optical regeneration (AOR) and all-optical polarization control (AOPC). This last functionality is based on [4]. If it is appropriate it will be considered ESP techniques with the same functionality to weigh both approaches. Finally we will demonstrate an experimental application of AOSP in optical performance monitoring (OPM) based on [5].

6.1 Regeneration

One of the main topics of research has been optical signal regeneration. One can divide this topic according to the extension for which the optical signal is regenerated:

- 1R-retransmission or re-amplification
- 2R-reshaping and re-amplification
- 3R-re-timing, reshaping and re-amplification

therefore several levels of regeneration can be set. It will only be addressed 1R and 2R regeneration levels.

6.1.1 1R regeneration

Since 1R regeneration deals with re-amplification and retransmission the author will firstly focus on its basic element: the optical amplifier.

The basic idea of travelling wave amplifier (called maser at that time) was first introduced by Geusic and Scovil [6, 7]. Rapidly the idea of an optical fiber amplifier started to grow and in 1964 it was invented by E. Snitzer using fiber lasers of neodymium-doped glass fiber [8]. Interestingly this work was 20 years "dormant" before it emerged as an exceedingly technological improvement with the advent of silica glass fiber for telecommunications [7]. The development of

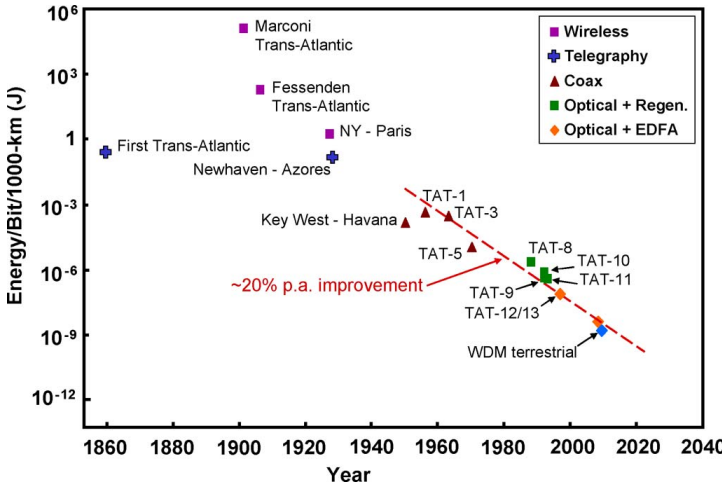

Figure 6.1: Energy consumption during the evolution of telecommunications for several transoceanic transmission systems. After [11].

the EDFA in 1987 for travelling wave amplification at $1.55\ \mu$m, was led by two independent groups in AT&T Bell Laboratories and at the University of Southampton [9, 10]. Although the first installment of EDFA has been in 1996 by AT&T and its european partners [7]. Prior to that, the standard way to amplify an optical signal was by placing periodically, electrical regenerators. In Figure 6.1 it can be seen the energy per bit per 1000 km during the evolution of telecommunications for several transoceanic transmission systems [11]. Electronic regenerators with optical fiber cables were dominant during the mid-late 80's and in the beginning of the 90's. EDFA plus optical fiber cable allowed in the following years a steady decrease of energy consumption, which indicates higher energy efficiency for the all-optical solution.

Raman amplification has also been explored since it was demonstrated in the 70's by a group of researchers from Bell labs [12, 13]. It has been deployed in long-haul and ultralong-haul optical fiber transmission systems in the earlier 2000s [13]. Raman amplification in comparison to EDFA, provides gain in a wider wavelength range, higher energy efficiency at high pump powers (see Figure 6.2), potential to provide lower noise figure, among other. Recently Raman amplifiers have been used for other AOSP functionalities such as polarization control [14], as we will see later in this chapter.

Finally fiber optical parametric phase insensitive or phase sensitive ampli-

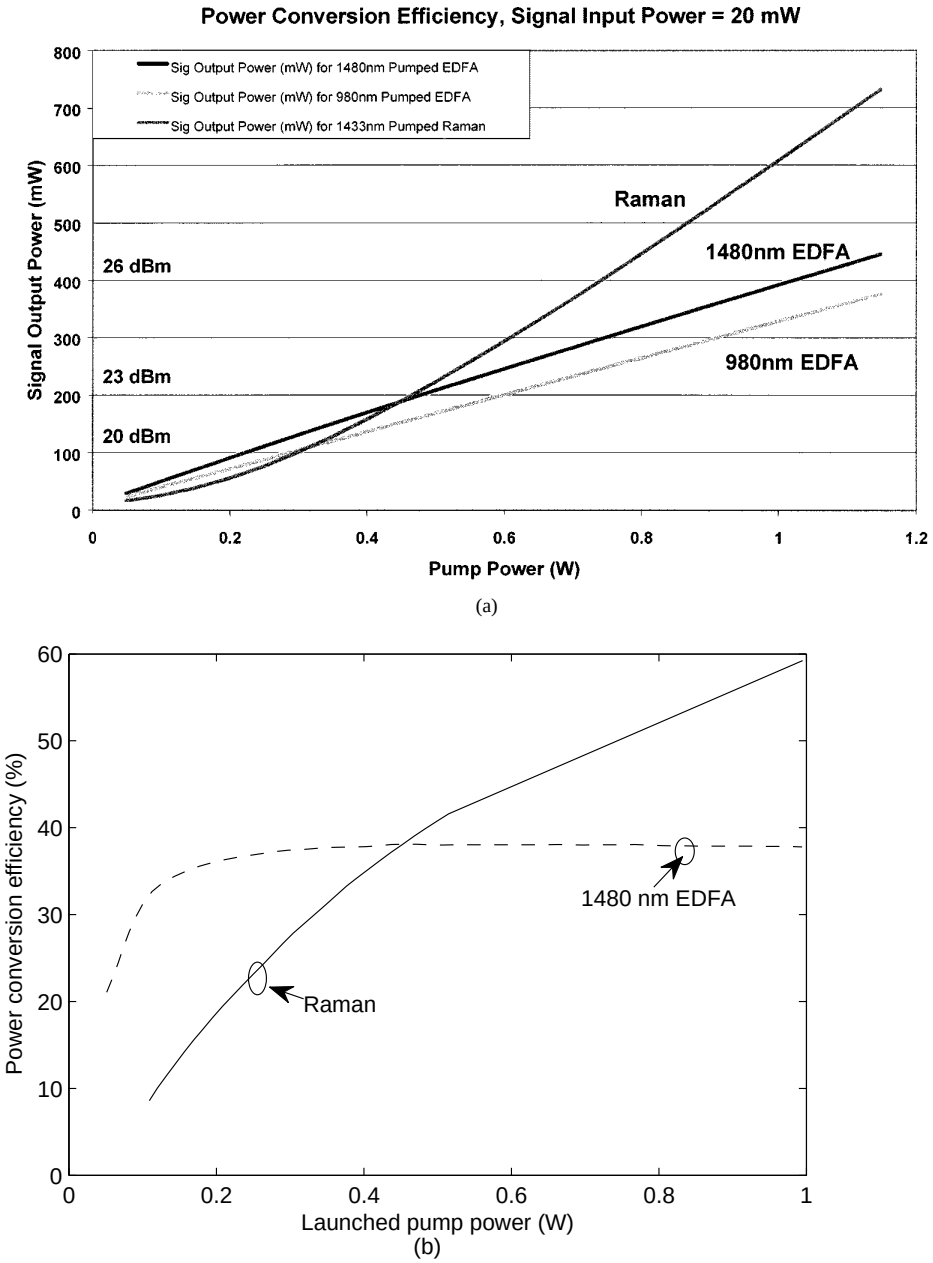

Figure 6.2: Converted signal output power and power conversion efficiency for a signal input power of 20 mW as a function of the pump power. After [13].

fiers have also been proposed, based on the four-wave mixing (FWM) effect. Theoretically a 3dB quantum-limit noise figure can be reached in a phase insensitive amplifiers such as fiber optical parametric amplifier (FOPA) [15] or EDFA ,

while an intriguing 0 dB quantum-limit noise figure can be achieved in a phase sensitive FOPA [16]. Phase sensitive FOPAs have been used for other AOSP functionalities such as phase noise mitigation. It will be addressed later.

6.1.2 2R regeneration

2R regeneration deals with re-amplification and reshaping. This is not an exhaustive review, but a summary of the most prominent techniques for 2R regeneration. For an exhaustive review about this topic the reader can find a recent review in [17].

One prominent scheme is the Mamyshev regenerator [18]. Mamyshev regenerator is based on the self-phase modulation (SPM) effect and it addresses amplitude modulation formats. This simply consists of a bandpass filter and a spool of highly non-linear fiber (HNLF) preceded by an amplifier. Self-phase modulation (SPM) broads the spectrum of the signal and a bandpass filter detuned from the central frequency of the signal, slices a portion of the spectrum. Since the broadening of the spectrum is related with digital 1's, this scheme is opaque to low-power noise [17].

FWM effect can also be used in order to perform 2R regeneration. If a signal at frequency f_s is launched into the fiber with a pump at frequency f_p an idler is generated at frequency $f_i = 2f_p - f_s$, and the power of the signal is amplified. Moreover other higher order FWM products are also generated with the idler. This can be used as amplitude limiter due to parametric amplifier saturation. The transfer function of the output signal in order to the input signal is somewhat similar to a hyperbolic tangent. Also higher order FWM products can be used in order to suppress the noise with lower power. This is due to the proportionality of the field of the nth order FWM product $E_n \propto E_{in}^n$, where E_{in} is the input signal field.

Other class of FWM 2R regenerators are the phase sensitive FOPA, which have the ability to reshape the amplitude and phase of the signal by mitigating the phase noise in binary phase-shift keying (BPSK) signals [16]. This type of phase sensitive amplifiers can in theory provide an intriguing 0 dB noise figure [16, 19]. In Figure 6.3 is presented a conceptual diagram of the technique published in Nature Photonics [16]. Developments of this technique have led to proposals to deal with higher order modulation formats such as quadrature

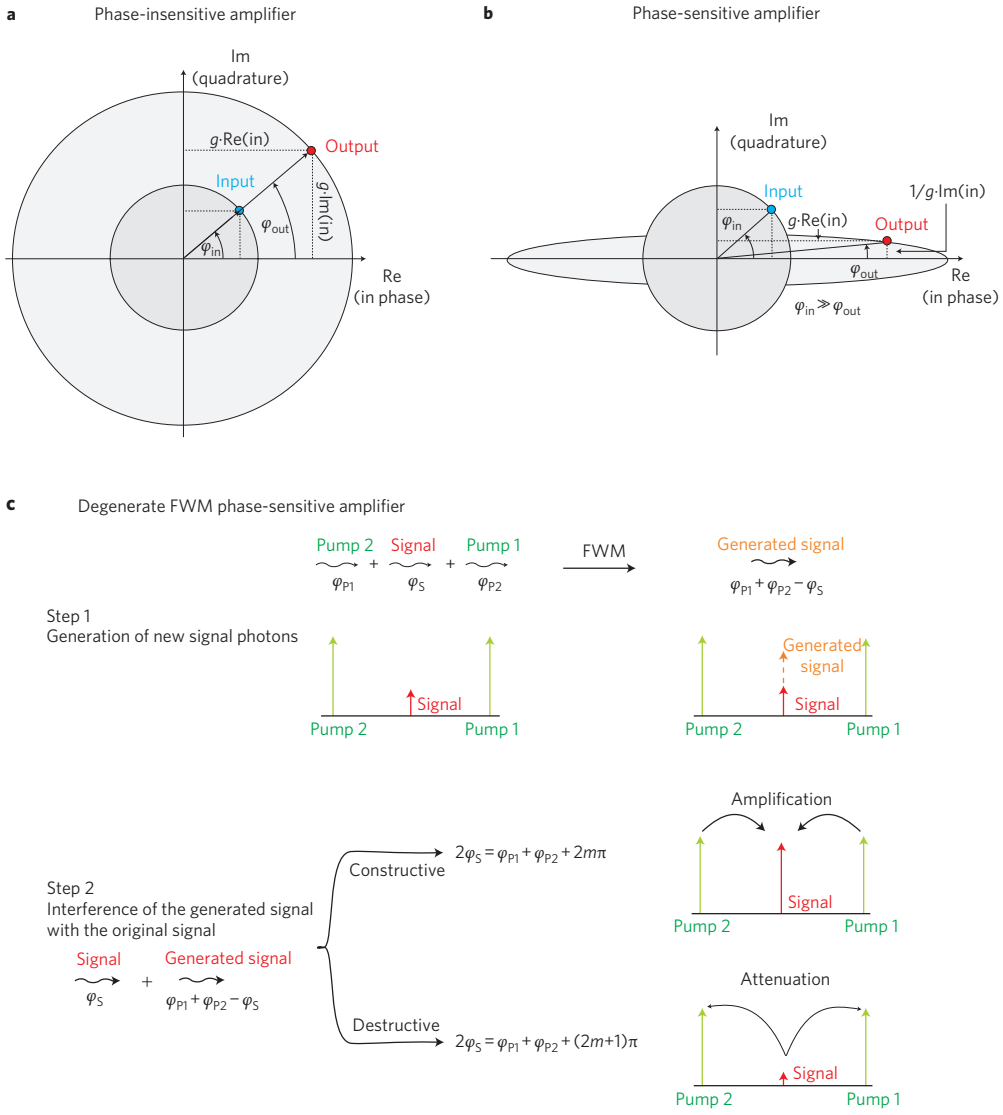

Figure 6.3: Operation of phase sensitive amplifier and a phase insensitive amplifier. After [16]

phase-shift keying (QPSK) [20, 21].

Another useful way to regenerate phase encoded signals is by converting them to amplitude modulation and use an 2R amplitude regenerator to mitigate the phase noise together with the amplitude noise [17]. Afterwards to this the signal is remodulated again into phase modulation.

6.2 Polarization control

6.2.1 Introduction

All-optical packet processing in optical packet-switched (OPS) networks is currently based on a range of non-linear devices such as semiconductor optical amplifiers (SOAs) or nonlinear waveguides which require specific input polarization states for optimum performance [22]. Consequently, careful adjustment of the state of polarization (SOP) of the incoming optical signal in such systems is required for successful processing of the optical packets. However, since the SOP of each packet arriving to each processing node varies arbitrarily, depending on its source node and the traversed optical path, all-optical, fast adjustment of the SOP on a packet-by-packet basis is a key technology to enable all-optical processing of optical packets in future OPS networks [23].

Previously, the electro-optic effect in LiNbO3 (lithium niobate) crystals coupled with an automatic digital feedback algorithm has been used to transform a random SOP at the input of the polarization controller device into a specified output SOP [24–26]. However, such schemes are limited by the speed of the automatic digital feedback algorithm and the electronic response time which is currently limited to a range of microseconds. Moreover, they are not fast enough to annihilate strong polarization variations [27].

Recently, a number of all-optical polarization stabilization strategies utilizing the quasi-instantaneous response of nonlinear optical effects have been proposed either numerically [14, 28, 29] or experimentally [27, 29**?** , 30]. These nonlinear effects include the Raman effect [14, 29], stimulated brillouin scattering (SBS) [**?**] and FWM[27, 30]. However, these works have not addressed the problem of fast polarization alignment of optical packets. In this work, the principles of [27] were used. They are depicted in Figure 6.4 and use a low polarization mode dispersion (PMD)-dispersion-shifted fiber (DSF) to align the SOP of adjacent optical packets having different and distinct SOP. In Figure 6.4 the signal is attracted to the polarization of the pump during the length of the fiber. Therefore the depolarized signal at z=0 becomes polarized at z=L.

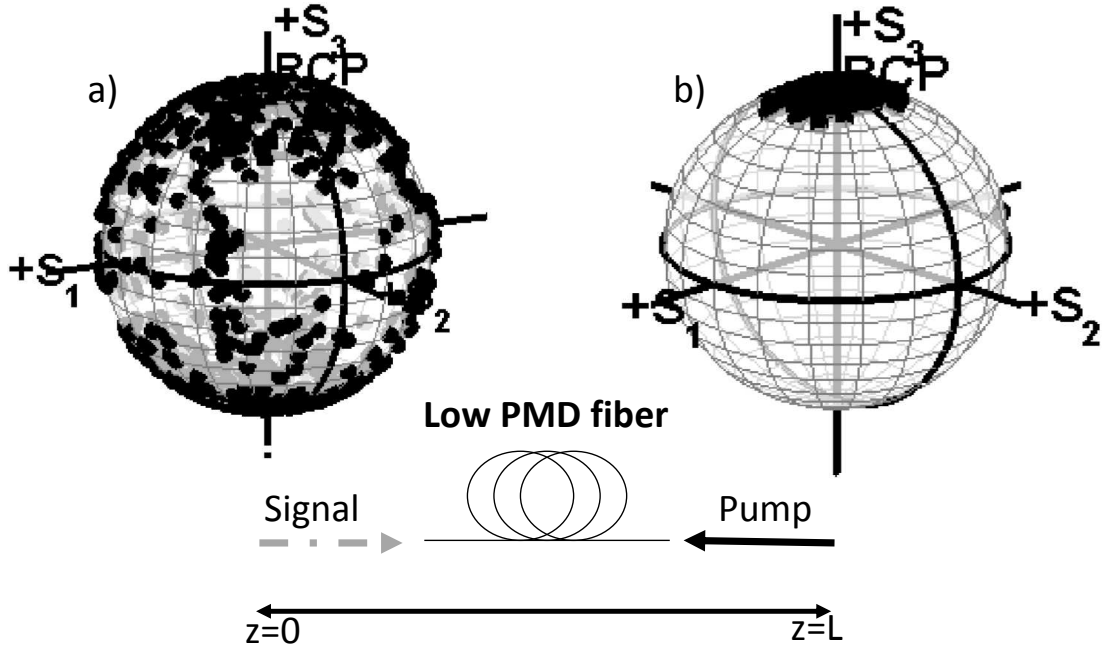

Figure 6.4: Simplified concept demonstration of polarization attraction effect in a counter-propagation scheme a) Poincaré sphere diagram of the signal SOP at the input (z = 0) of the fiber, b) Poincaré sphere diagram of the signal SOP at the output (z = L) of the fiber.

6.2.2 Experimental Setup

Figure 6.5 shows the experimental setup and in Figure 6.6 the experimental setup realization in the laboratory is shown. Light at 1572 nm from an external cavity laser (ECL) was modulated with a Mach-Zehnder modulator (MZM), driven by a pulse-pattern generator (PPG) to generate optical packets comprising a 10 Gbit/s non-return-to-zero (NRZ) $2^{11}-1$ pseudo-random bit sequence (PRBS) payload. Packet durations of 409 ns (shown in inset 1 of Figure 6.5), and 205 ns were used in experiments with two network loads of $\rho = 25\%$ and $\rho = 50\%$, respectively. ρ is defined as:

$$\rho = \frac{2\delta}{2\delta + \Delta} \tag{6.1}$$

where δ is the duration of the packet and Δ is the sum of the two guard-times between three consecutive packets. In the cases studied in this paper, the two previously mentioned guard-times are different and are used to distinguish be-

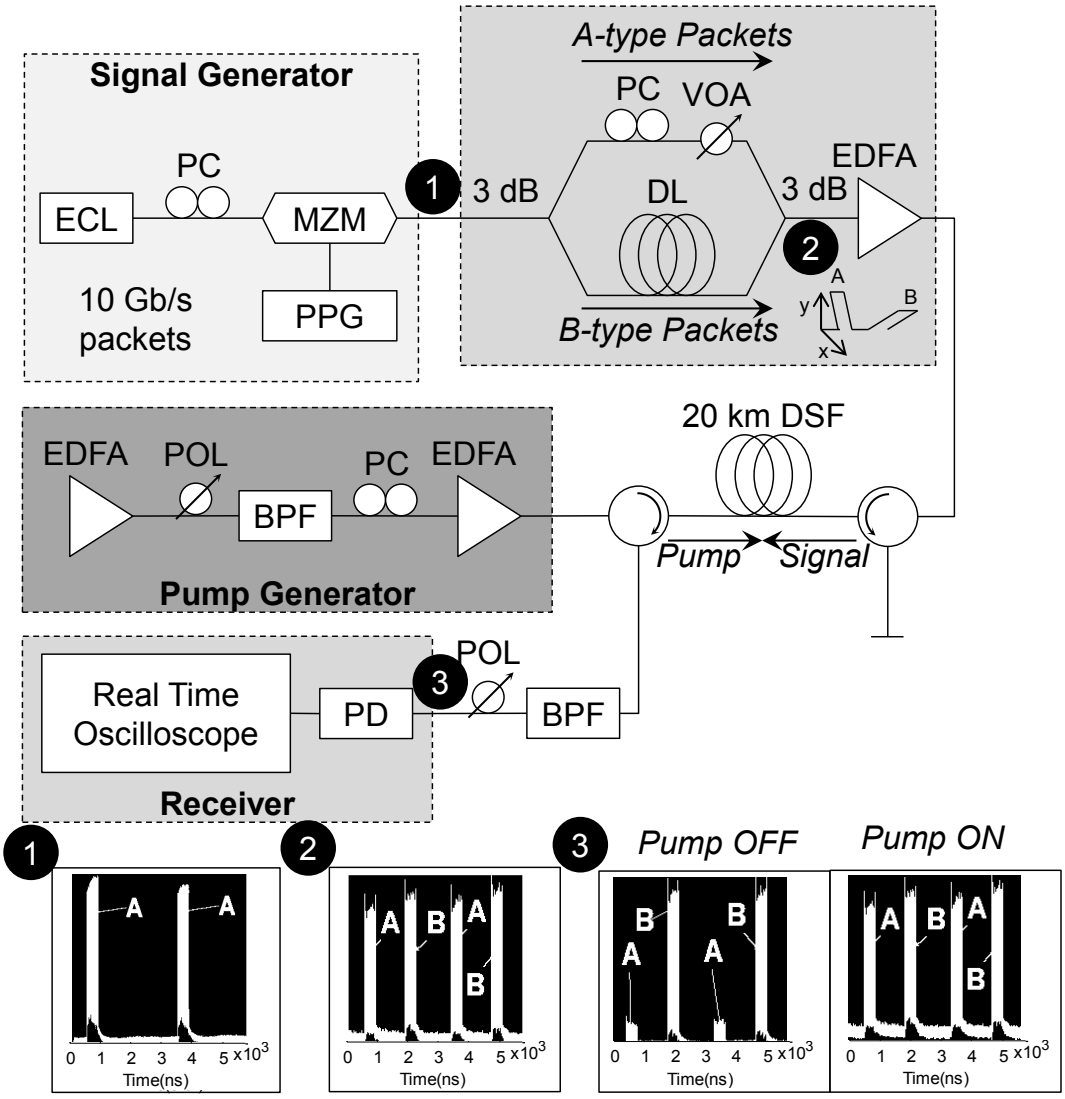

Figure 6.5: Simplified experimental setup. DSF: dispersion shifted fiber, MZM: mach-Zehnder modulator, PPG: pulse pattern generator, EDFA: erbium doped fiber amplifier, VOA: variable optical attenuator, PC: polarization controller, POL: polarizer, BPF: band pass filter, DL: optical delay line. A-type packets are coupled with B-type packets, having different polarization alignments as shown in point 2 of the experimental setup.

tween two consecutive packets, designated A and B. The time response and efficiency of the polarization attraction process is conditioned by the packet duration and the network load ρ. Shorter packet durations allow less time for the polarization attraction process to stabilize while higher ρ yields less time between packets. Therefore this requires very fast response of the polarization

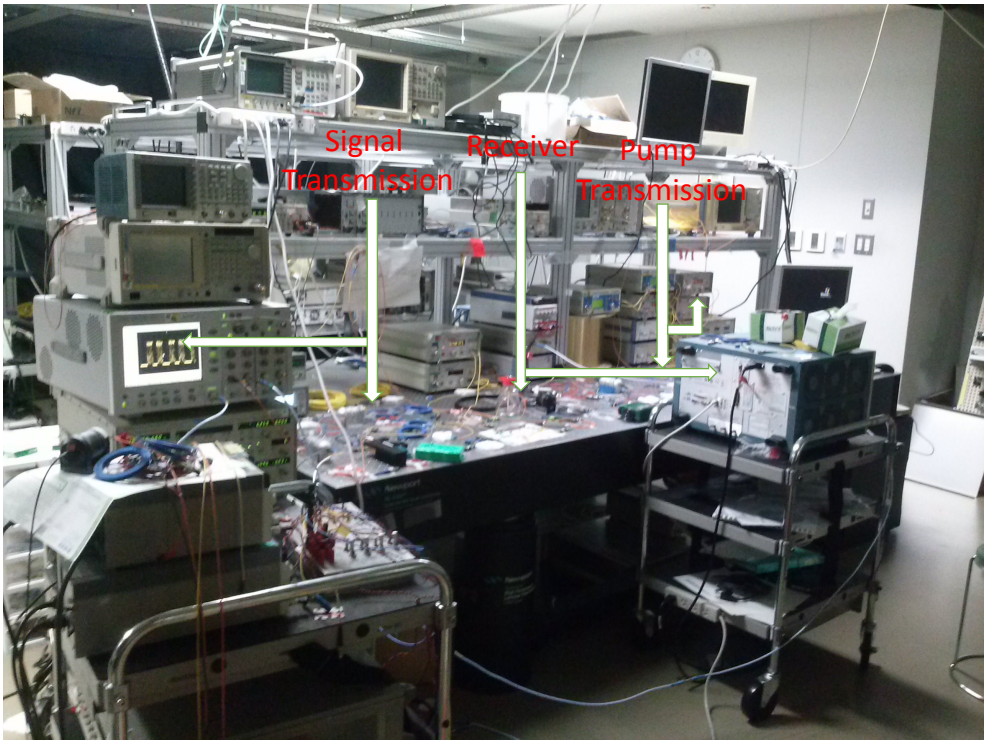

Figure 6.6: Experimental setup in the laboratory of National Institute of Information and Communications Technology (NICT), Japan, 2013

attraction process to accommodate fast switching of the SOP.

Once the packets are generated, a 3 dB coupler was used to split the packet signal in to 2 paths, labeled A and B. A polarization controller (PC) and a variable optical attenuator (VOA) were used to control the power and the SOP of the signal in path A. The signal on path B was delayed by a 300 m fiber delay line when using 409 ns packet duration and 80 m when using 205 ns packet duration, to time interleave the 2 packet streams before being re-combined. The output optical

Table 6.1: Experiments parameters

	bit-error rate (BER) evaluation	Stability evaluation	
Packet duration	409 ns	409 ns	205 ns
DL length	300 m	300 m	80 m
ρ (%)	25	25	50

signal was a packet signal with a network load of $\rho = 25\%$ for 409 ns packets, as shown in inset 2 of Figure 6.5 and $\rho = 50\%$ for packet durations of 205 ns with different polarization states for adjacent packets. The different packet durations and ρ were used in two different experiments denominated BER evaluation and stability evaluation, with experimental parameters shown in Table 6.1.

The combined packet signal was then amplified to an average power of 19.5 dBm in an EDFA before being launched into a 20 km span of low PMD-DSF, with the zero dispersion wavelength located at 1560 nm. Prior to fiber transmission, an optical circulator was used to prevent the counter propagating pump signal of reaching the transmitter.

In order to reduce the impact of SBS, a broad linewidth pump signal was generated by an amplified spontaneous emission (ASE) noise generator (EDFA) polarized (POL) and filtered with a 30 GHz band-pass filter (BPF), centered at 1565 nm. The ASE noise signal was then polarized to a well-defined SOP with a PC used to control the input polarization to the DSF span. An additional high-power EDFA was used to set an average power of 23 dBm to enable the polarization attraction effect. The pump was combined with the signal using an additional optical circulator which was also used to separate the packet signal after DSF transmission.

On the receiver side, the separated signal was filtered by a BPF to limit its noise bandwidth and a variable polarization filter (POL) was used to emulate a polarization dependent device before reception. For BER estimation the signal was sampled at 50 GS/s in a real-time oscilloscope. Traces of 0.4 ms of the detected signal were captured for offline processing. The offline processing algorithm used a packet detector which distinguishes A and B-type packets for the aforementioned guard-times between packets, allowing BER estimates for A and B-type packets independently. To assess the performance of the system in the presence of nonlinearities, the author also performed BER measurements using a continuous signal, blocking path A and setting the PPG to generate a continuous 10 Gbit/s NRZ signal.

6.2.3 Experimental Results

First it was evaluated the back-to-back (BTB) performance of the system using a 10 Gbit/s NRZ continuous signal with the receiver polarization filter re-

moved. The measured receiver sensitivity curve for this case is shown in Figure 6.7, presenting a value of -17 dBm for a BER of 10^{-3}. With the pump off and after transmission through the fiber, a penalty of less than 0.2 dB was observed. With the pump on, it was observed a 0.5 dB penalty for a BER of 10^{-3}, associated to fiber reflections and insufficient isolation of signals in circulators and optical filters.

6.2.3.1 BER evaluation

In Figure 6.8 it is shown the performance of the system when using a packet duration of 409 ns and network load of $\rho = 25\%$ as shown in Figure 6.5 inset 3, for both cases, with and without the pump. It can be observed in Figure 6.8 that the sensitivity when the pump is off at 10^{-3} BER is around -21 dBm for the B-type packets whilst the A-type packets are undetectable and unrecoverable by any forward error correction mechanism. With the pump on it was possible to recover the A-type packets for BERs in the order of 10^{-3} and a sensitivity of around -18 dBm is observed. The penalty is around 2.9 dB at 10^{-3} BER, compared to the pump off case B-type packets. This penalty is also believed to be partly due to reflections and to poor isolation in optical circulators and optical filters. It can also be attributed to the degree of polarization (DOP) of packets A, which

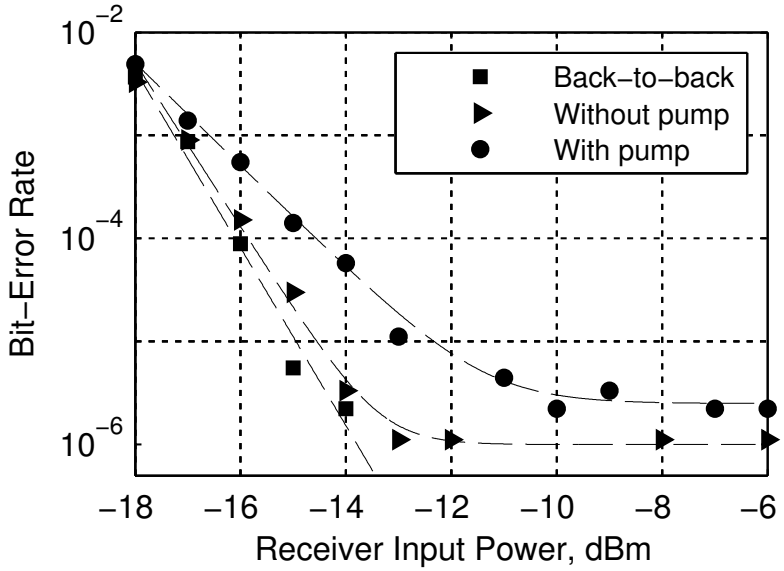

Figure 6.7: Receiver sensitivity for a continuous signal transmission of a 10 Gbit/s NRZ 2^{11} PRBS.

may suffer a decrease due to very fast polarization fluctuations over time (much shorter than the packet duration). This may cause additional errors and the decrease of the DOP. In order to evaluate the BER for each section of the packet as shown in Figure 6.9, the packet was divided in 4 sections, each with 1024 bits out of 4096, which is the length of the packet. A certain number of packets was captured and for each section of each packet the number of errors was measured and summed, e.g. $E_s = \sum_{i=1}^{n} e_{s,i}$, where E_s is the total number of errors in the section s and $e_{s,i}$ is the number of errors in the section s of the packet i. The BER is therefore $E_s/(nbits/4)$ where $nbits$ is the total number of bits taking into account n packets. This methodology was used for packets A and B. Figure 6.9 shows that the BER is higher in the beginning and in the end sections of the packet for receiver powers of -19 and -20 dBm. This is mainly due to amplifier transients. However, as expected this behavior is not so evident in the BTB case for the A and B-type packets. This trend is followed by both received power cases which are related with the receiver input power of Figure 6.8. Nevertheless, the pump off and pump on cases get their BER decreased in the 2^{nd} and 3^{th} center sections of the packet. In the BTB case this reduction is not so evident as it was mentioned before, although a significant decrease of

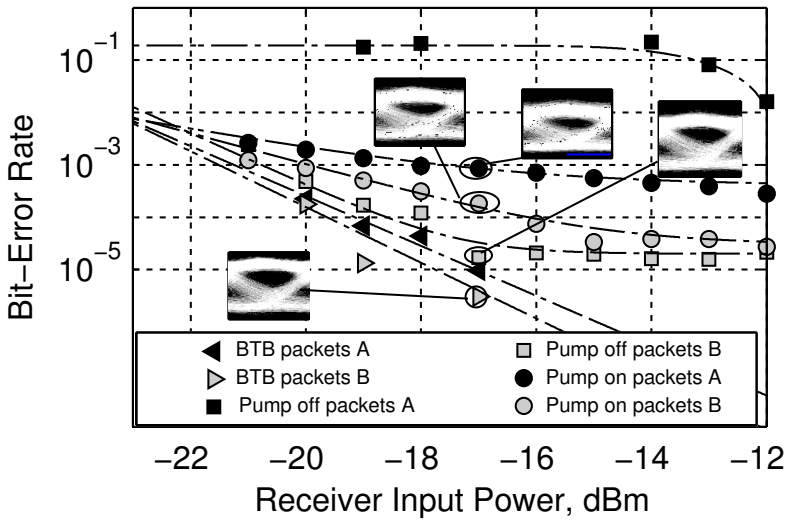

Figure 6.8: Measured receiver sensitivity for packets with duration of 409 ns duration. Receiver sensitivity for A and B-type packets in BTB, pump off and pump on cases.

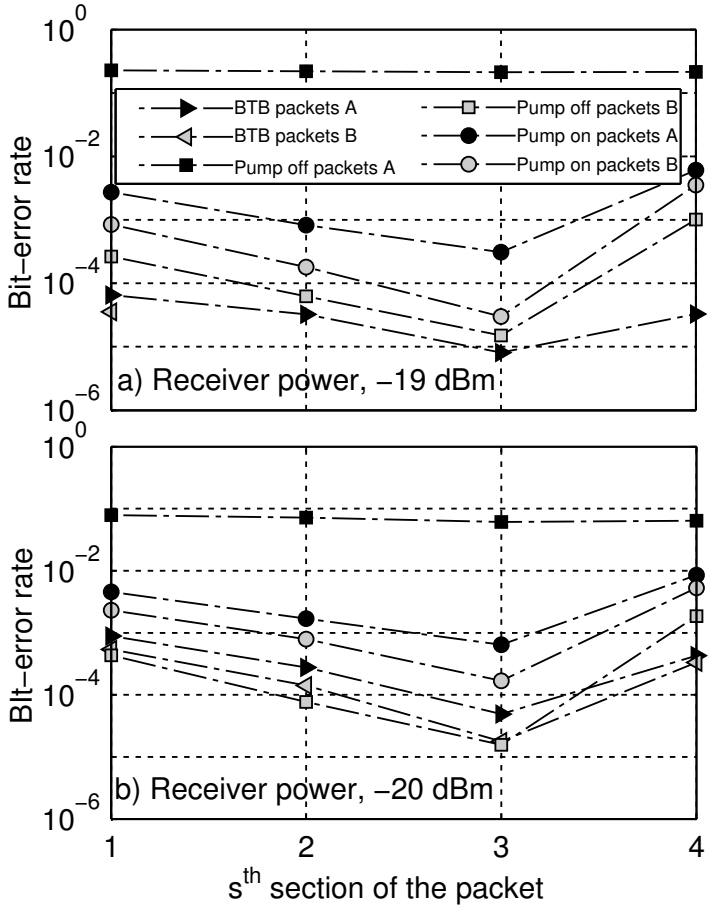

Figure 6.9: Measured BER for the s^{th} section of the packet. The BER is measured for each section evaluating for a) -19 dBm and b) -20 dBm receiver power.

BER occurs in Figure 6.9 b). At the end of the packet, i.e., in the 4^{th} section, the pump off packets B case had a significant degradation relatively to the BTB case for both received powers, of -19 and -20 dBm. As evolving along the packet the relative degradation between the cases B-pump off and B-pump on gets slightly improved. This may indicate that the attraction process becomes more efficient towards the end of the packets.

6.2.3.2 Stability evaluation

Finally, it was evaluated the potential of this scheme for long term operation measuring the polarization stability over a period of 30 minutes, for packets

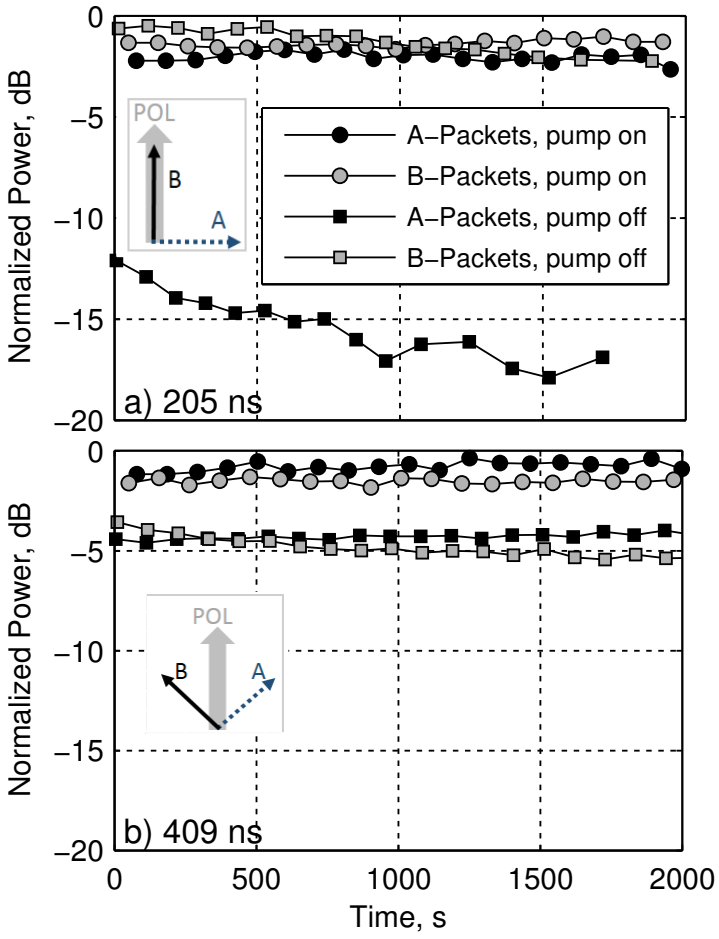

Figure 6.10: Polarization stability test a) 205 ns b) 409 ns. Insets with arrow lines showing schematically the initial (pump off) relative polarization of packets A (blue dashed arrow line) and B (black continuous arrow line), relatively to the alignment of the receiver polarization filter (grey thicker arrow line).

---

with duration of 205 and 409 ns, as shown in Figure 6.10. In the case of the 205 ns packets, the two types of packets have distinct SOP when the pump is off. However at $t = 0$ where t is time, B-type packets are more aligned with the receiver and hence have more detected normalized power, as shown in Figure 6.10 a). Over time the normalized power of both types of packets decreases and shows to be unstable. After the 30 minutes the A-type packets became undetectable by the packet detector algorithm and that is the reason why it was only shown 30 minutes, although the results were collected for a longer time.

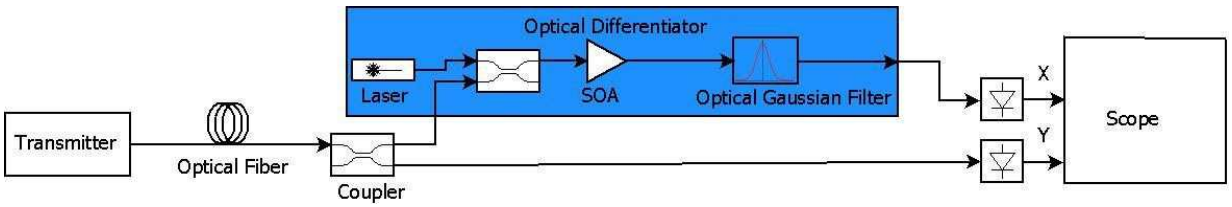

Figure 6.11: Experimental setup for the generation of performance diagrams using an all-optical signal differentiator. SOA- C band semiconductor optical amplifier

With the pump turned on both A and B-type packets show to stabilize their power over time. Moreover the A-type packets recover all its power by aligning its polarization with the receiver, as shown in Figure 6.10 a) and its inset.

For the 409 ns packets the SOP of both packets was misaligned by approximately 45 degrees with respect to the alignment of the receiver polarization filter as shown schematically in inset of Figure 6.10 b). In this case, it can be observed a power fluctuation of the B-type packets of about 1.5 dB during the 30 minutes period but little fluctuation is noticed for the A-type packets over time. When the pump is on, both types of packets remain with stable normalized power over time as shown in Figure 6.10 b). Moreover, when the pump is on the normalized power of the A and B-type packets is equalized to a value close to 0 dB.

6.3 All-optical signal processing in optical performance monitoring

In this section it is reported an application of AOSP in OPM. This demonstration was part of the work done in OPM demonstrated in Chapter 5 and published in optical fiber conference (OFC) 2012 [5]. All-optical differentiators were studied as part of the proposed experimental setup to generate OPM diagrams. With this experimental setup it was demonstrated an alternative to synchronous eye diagram (SED) by using AOSP techniques in the generation of parametric asynchronous eye diagram (PAED). In Figure 6.11 the experimental setup is shown.

The derivative of the signal is calculated by an optical differentiator and the samples of the signal (Y) are sampled against the samples of the derivative of the signal (X), in X-Y mode. The parametric equations that rule the process of

representing the PAED are:

$$X = \frac{dv(t)}{dt}$$
$$Y = v(t) \tag{6.2}$$

where v(t) is the modulated signal, which travels through the transmission channel. The main component of the setup is the differentiator. It was used the optical differentiator proposed in [31], however for lower bandwidths an electrical differentiator can be used to create the derivative of the signal. The papers [31, 32] are based on a phase modulator and an optical filter. Phase modulation is achieved through cross-phase modulation (XPM) in a highly nonlinear device. A probe laser centered in a wavelength distinct from the wavelength of the transmission channel transmits through a SOA which serves as a phase modulator. One optical gaussian filter (OGF) serves as a frequency discriminator to extract the chirp variation of the modulated probe light. The center of the OGF must be shifted a few hundreds of picometers above or below (direct or inverse derivative, i.e., inverse derivative=$\overline{direct}$-direct, where $\overline{direct}$ is the average power of the direct derivative, respectively) the central wavelength of the probe laser. Key aspects of this optical differentiator are that except the wavelength of the probe laser, all other wavelengths, within a certain bandwidth, are available for the transmission channel.

In Figure 6.12 the experimental results are shown, using the setup of Figure 6.11. The PAED is at the right of the SED. The derivative samples are in the horizontal axis and the amplitude of the signal is in the vertical axis. In this case the inverse derivative was used, which means that lower derivative is achieved in the rise edge of the bit and higher derivative is achieved in the fall edge of the bit. This is useful to have the rise and fall edges of the bit represented in PAED left and right of the diagram as a normal SED does. We can see that the PAED shows an eye aperture similar to the SED. In Figure 6.12 (c) we can also see that the bit has a small inflection at the bottom of the bit, represented both in the SED and PAED. Most of the samples appear with higher concentration in two specific spots of the PAED, related with the high and lower levels of the bit. Simulation results demonstrate that they should have the same derivative (in the horizontal axis), although due to some impact of cross-gain modulation (XGM) in the SOA, this two spots are displaced. This can be solved with a highly nonlinear

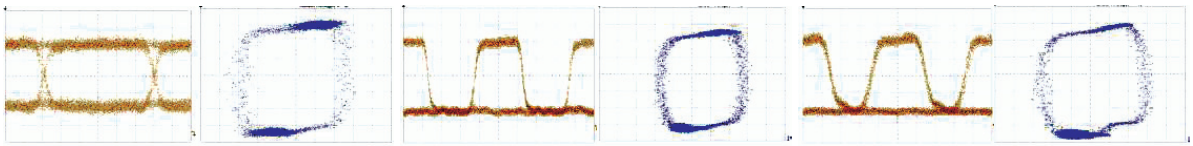

(a) 10 Gbit/s NRZ (b) 10 Gbit/s RZ Signal (c) 20 Gbit/s RZ Signal

Figure 6.12: Experimental results showing the diagrams generated by the experimental setup of Figure 6.11. PAED for several bit rates and modulation formats.

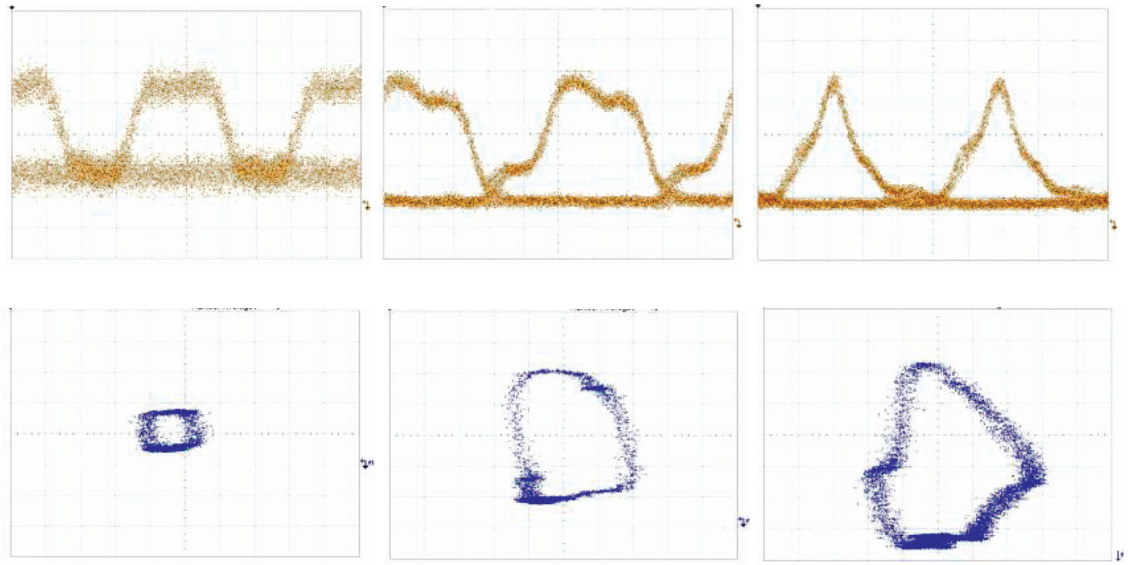

(a) OSNR 12 dB (b) DGD 30 ps (c) CD 170ps/nm

Figure 6.13: Experimental results for a 20 Gbit/s RZ signal. (a) Low OSNR CD=0 ps/nm DGD=0 ps, (b) OSNR=24 dB CD=0 ps/nm DGD =30 ps and (c) OSNR=24 dB, CD=170 ps/nm, DGD= 0 ps

fiber (chalcogenide fibers), where XGM has no impact.

In Figure 6.13 the impact of optical signal to noise ratio (OSNR), differential group delay (DGD) and chromatic dispersion (CD) on PAED is tested, separately. In Figure 6.13 (a) we can see that both SED and PAED tends to close, however PAED maintains its shape. When DGD and CD, impact on the waveform, PAED gets distorted in a similar manner as a SED does.

6.4 Conclusion

In this chapter, some of the functionalities of all-optical signal processing were overviewed. It was presented the investigation about all-optical polarization alignment of optical packets in the sub-microsecond regime scale using the polarization attraction effect from a counter-propagating pump signal in a low polarization-mode dispersion-shifted fiber. The potential of such a scheme to provide rapid polarization alignment required for critical response-time applications such as optical packet switched networks, where polarization alignment may be required on a packet-by-packet basis, was demonstrated. It has been investigated two packet durations 205 and 409 ns, with distinct network load 50% and 25%, respectively. Both have shown to have stable state of polarization at the output of the fiber, during a period of 30 minutes, when distinct state of polarization is applied at the input of the fiber.

It was also demonstrated an example of how AOSP can be useful for OPM, by introducing an all-optical differentiator to create OPM diagrams. This demonstrate the usefulness of OPM and AOSP to work either in separate or together to enable transparent optical applications.

References

[1] H. J. Caulfield and S. Dolev, "Why future supercomputing requires optics," *Nature Photonics*, vol. 4, pp. 261–263, May 2010.

[2] J. Dakin and R. G. Brown, *Handbook of optoelectronics (two-volume set)*. Taylor & Francis, Apr. 2006.

[3] R. Tucker and K. Hinton, "Energy consumption and energy density in optical and electronic signal processing," *Photonics Journal, IEEE*, vol. 3, pp. 821–833, Oct. 2011.

[4] V. Ribeiro, R. S. Luï¿½s, J. M. D. Mendinueta, B. Puttnam, A. Shahpari, N. Muga, M. Lima, S. Shinada, N. Wada, and A. Teixeira, "Sub-microsecond packet polarization alignment using all-optical polarization attraction," in *Proc Optoelectronics and Communications Conf. - OECC Melbourne, Australia;*, July 2014.

[5] V. Ribeiro, M. Lima, and A. Teixeira, "Parametric asynchronous eye diagram for optical performance monitoring," in *Optical Fiber Communication Conference and Exposition (OFC/NFOEC), 2012 and the National Fiber Optic Engineers Conference*, pp. 1–3, Mar. 2012.

[6] J. E. Geusic and H. E. D. Scovil, "A unidirectional traveling-wave optical maser," *Bell System Technical Journal*, vol. 41, no. 4, pp. 1371–1397, 1962.

[7] P. Becker, N. Olsson, and J. Simpson, "Chapter 1 - introduction," in *Erbium-Doped Fiber Amplifiers* (P. B. O. Simpson, ed.), Optics and Photonics, pp. 1 – 11, San Diego: Academic Press, 1999.

[8] C. J. Koester and E. Snitzer, "Amplification in a fiber laser," *Appl. Opt.*, vol. 3, pp. 1182–1186, Oct. 1964.

[9] R. Mears, L. Reekie, I. Jauncey, and D. Payne, "Low-noise erbium-doped fibre amplifier operating at 1.54 μm," *Electronics Letters*, vol. 23, pp. 1026–1028, Sep. 1987.

[10] E. Desurvire, J. R. Simpson, and P. C. Becker, "High-gain erbium-doped traveling-wave fiber amplifier," *Opt. Lett.*, vol. 12, pp. 888–890, Nov. 1987.

[11] R. Tucker, "Green optical communications;part i: Energy limitations in transport," *Selected Topics in Quantum Electronics, IEEE Journal of*, vol. 17, pp. 245–260, Mar. 2011.

[12] R. H. Stolen and E. P. Ippen, "Raman gain in glass optical waveguides," *Appl. Phys. Lett.*, vol. 22, no. 6, pp. 276–278, 1973.

[13] M. Islam, "Raman amplifiers for telecommunications," *Selected Topics in Quantum Electronics, IEEE Journal of*, vol. 8, pp. 548–559, May 2002.

[14] N. J. Muga, M. F. S. Ferreira, and A. N. Pinto, "Broadband polarization pulling using raman amplification," *Opt. Express*, vol. 19, pp. 18707–18712, Sep. 2011.

[15] Z. Tong, A. Bogris, M. Karlsson, and P. A. Andrekson, "Full characterization of the signal and idler noise figure spectra in single-pumped fiber optical parametric amplifiers," *Opt. Express*, vol. 18, pp. 2884–2893, Feb. 2010.

[16] R. Slavik, R.k, F. Parmigiani, J. Kakande, C. Lundstrï¿½m, M. Sjï¿½din, P. Andrekson, R. Weerasuriya, S. Sygletos, A. D. Ellis, L. Grï¿½ner-Nielsen, D. Jakobsen, S. Herstrom, R. Phelan, J. Gorman, A. Bogris, D. Syvridis, S. Dasgupta, P. Petropoulos, and D. J. Richardson, "All-optical phase and amplitude regenerator for next-generation telecommunications systems," *Nature Photonics*, vol. 4, pp. 690–695, 2010.

[17] M. Matsumoto, "Fiber-based all-optical signal regeneration," *Selected Topics in Quantum Electronics, IEEE Journal of*, vol. 18, pp. 738–752, Mar. 2012.

[18] P. Mamyshev, "All-optical data regeneration based on self-phase modulation effect," in *Optical Communication, 1998. 24th European Conference on*, vol. 1, pp. 475–476 vol.1, Sep. 1998.

[19] Z. Tong, C. Lundstrï¿½m, P. A. Andrekson, C. J. McKinstrie, M. Karlsson, D. J. Blessing, E. Tipsuwannakul, B. J. Puttnam, H. Toda, and L. Grï¿½ner-Nielsen, "Towards ultrasensitive optical links enabled by low-noise phase-sensitive amplifiers," *Nature Photonics*, vol. 5, no. 7, pp. 430 – 436, 2011.

[20] J. Kakande, A. Bogris, R. Slavik, F. Parmigiani, D. Syvridis, P. Petropoulos, and D. Richardson, "First demonstration of all-optical qpsk signal regeneration in a novel multi-format phase sensitive amplifier," in *Optical Communication (ECOC), 2010 36th European Conference and Exhibition on*, pp. 1–3, Sept 2010.

[21] J. Kakande, A. Bogris, R. Slavik, F. Parmigiani, D. Syvridis, P. Petropoulos, D. Richardson, M. Westlund, and M. Sköld, "Qpsk phase and amplitude regeneration at 56 gbaud in a novel idler-free non-degenerate phase sensitive amplifier," in *Optical Fiber Communication Conference/National Fiber Optic Engineers Conference 2011*, p. OMT4, Optical Society of America, 2011.

[22] S. J. B. Yoo, "Optical packet and burst switching technologies for the future photonic internet," *Lightwave Technology, Journal of*, vol. 24, pp. 4468–4492, Dec. 2006.

[23] D. Blumenthal, J. Bowers, L. Rau, H. F. Chou, S. Rangarajan, W. Wang, and H. Poulsen, "Optical signal processing for optical packet switching networks," *Communications Magazine, IEEE*, vol. 41, pp. S23–S29, Feb. 2003.

[24] A. Hidayat, B. Koch, H. Zhang, V. Mirvoda, M. Lichtinger, D. Sandel, and R. Noé, "High-speed endless optical polarization stabilization using calibrated waveplates and field-programmable gate array-based digital controller," *Opt. Express*, vol. 16, pp. 18984–18991, Nov. 2008.

[25] M. Martinelli, P. Martelli, and S. M. Pietralunga, "Polarization stabilization in optical communications systems," *Lightwave Technology, Journal of*, vol. 24, pp. 4172–4183, Nov. 2006.

[26] B. Koch, A. Hidayat, H. Zhang, V. Mirvoda, M. Lichtinger, D. Sandel, and R. Noe, "Optical endless polarization stabilization at 9 krad/s with fpga-based controller," *Photonics Technology Letters, IEEE*, vol. 20, no. 12, pp. 961–963, 2008.

[27] J. Fatome, S. Pitois, P. Morin, and G. Millot, "Observation of light-by-light polarization control and stabilization in optical fibre for telecommunication applications," *Opt. Express*, vol. 18, pp. 15311–15317, Jul. 2010.

[28] F. Chiarello, L. Ursini, L. Palmieri, and M. Santagiustina, "Polarization attraction in counterpropagating fiber raman amplifiers," *Photonics Technology Letters, IEEE*, vol. 23, no. 20, pp. 1457–1459, 2011.

[29] M. Martinelli, M. Cirigliano, M. Ferrario, L. Marazzi, and P. Martelli, "Evidence of raman-induced polarization pulling," *Opt. Express*, vol. 17, pp. 947–955, Jan. 2009.

[30] J. Fatome, P. Morin, S. Pitois, and G. Millot, "Light-by-light polarization control of 10-gb/s rz and nrz telecommunication signals," *Selected Topics in Quantum Electronics, IEEE Journal of*, vol. 18, no. 2, pp. 621–628, 2012.

[31] J. Xu, X. Zhang, J. Dong, D. Liu, and D. Huang, "All-optical differentiator based on cross-gain modulation in semiconductor optical amplifier," *Opt. Lett.*, vol. 32, pp. 3029–3031, Oct. 2007.

[32] P. Velanas, A. Bogris, A. Argyris, and D. Syvridis, "High-speed all-optical first- and second-order differentiators based on cross-phase modulation in fibers," *Lightwave Technology, Journal of*, vol. 26, pp. 3269 –3276, Sep. 15 2008.

CHAPTER 7

Conclusions

Optical networks development lead to a more transparent signal transmission. Therefore for that to happen is required that a number of devices be available to accommodate different types of traffic. It is desirable that these types of traffic be accommodated by one single device, although with the current available technologies this is very difficult to achieve. Thus transparency has been categorized by levels: opaque, translucent and fully transparent. Generally nowadays networks are translucent and inside this level we can find other sub-levels of transparency. In this thesis we have presented several models and experiments that pretend to be applied in transparent/translucent optical networks. Each has is own specifications and can be applied in different contexts and distinct types of optical networks,i.e, static point-to-point network (Chapter 3 and 4), optical burst switched networks (Chapter 5) and optical packet switched networks (Chapter 6). The author has addressed optical performance monitoring and all-optical signal processing, mainly polarization control. This are important functions in future transparent optical networks. The former brings to the network smartness and adaptive behaviour, the second brings signal pro-

cessing without optical-electrical-optical conversion.

7.1 Concluding remarks

1. Optical performance monitoring is an important function in dynamic transparent networks. It brings adaptivity and intelligence to the optical network. We should evaluate the type of network in which we want to apply optical performance monitoring. Translucent static point to point optical networks may not have strict requirements in terms of modulation format and data rate, since they do not change so often. Next we must evaluate if this type of links are long-haul or short-haul. For example for long-haul transmission links, chromatic dispersion is compensated with digital signal processing, although the digital signal processing algorithm must estimate accumulated chromatic dispersion and residual chromatic dispersion. Basically if we could assure that the network operator will never change the fiber in one or more spans we could guarantee at least that the value of accumulated chromatic dispersion is fixed and a dynamic optical performance monitor for this case will not be required. Although this is not what happens and therefore a dynamic optical performance monitor is required to measure accumulated chromatic dispersion. One can use a digital optical performance monitor although if a significant change in the value of chromatic dispersion occurs, the time of convergence of the digital signal processing algorithm may be too long. Therefore it is desirable to have a chromatic dispersion monitor with large monitoring window and if possible with good sensitivity even for large values of chromatic dispersion. This will probably reduce the convergence time of the digital signal compensator. In Chapter 3 the author proposed such a chromatic dispersion monitor. It can work with modulation formats with a protruding clock tone component.

2. Due to temperature changes, stress in the fiber, among other the value of the accumulated dispersion monitored by the previous device may be not strictly exact. Therefore after digital compensation based on the value of the accumulated dispersion monitored by the device proposed in Chapter 3, it may exist a residual dispersion that also requires monitoring. The author has proposed the technique of chapter 4 that has a limited monitoring

window for high data rates. Besides being suited for other contexts this technique may be applied in this context.

3. To reduce cost and achieve a more elegant optical performance monitoring scheme it would be desired, that we can dispose multi-impairment optical performance monitoring. In Chapter 5, we present a technique that does multi-impairment optical performance monitoring. It has the ability to monitor simultaneously optical signal to noise ratio, differential group delay and chromatic dispersion with considerable monitoring ranges. We presented results for non-return-to-zero modulation format and quadrature-phase shift keying in 10 Gbit/s and 40 Gbit/s respectively. We also presented results for simultaneous monitoring of multiple modulation formats and data rates. Since we use a differentiator with proper bandwidth it gives a different value of electrical derivative for different data rates so it is possible to distinguish between them. Modulation formats gives distinct phase portrait for similar values of chromatic dispersion so it is possible to distinguish it by pattern recognition in artificial neural networks. This ability may be suited for optical burst switched networks if the response time of the monitor is appropriate.

4. All-optical signal processing is also an important function in future transparent optical networks. Therefore the author presented in Chapter 6 an all-optical polarization controller that has demonstrated stability during a certain period of time and suitable performance in terms of bit error rate measurements. We finally demonstrated experimentally how all-optical signal processing can interact with optical performance monitoring by using an all-optical differentiator to generate performance diagrams demonstrated in Chapter 5.

7.2 Future work

The work developed in Chapter 3 may have future developments in terms of practical implementations. The setup may be simplified by removing the Mach-Zehnder interferometer (MZI), at the price of loosing 3 dB sensitivity, but this reduces cost and complexity of the proposed technique, significantly. The Q-factor monitoring block can be simplified, by using a simple asynchronous

amplitude histograms (AAH)s. Therefore it will have a loss in terms of accuracy of the method, but the whole setup becomes much more simpler. The work in Chapter 4 requires further investigation. In fact comparing Eqs. 3.9 and 4.11*a*, 4.11*b*, we found them very similar. While Eq. 3.9 relates the average radio-frequency (RF) power of the clock tone or pilot tone with the chromatic dispersion (CD), the two last mentioned equations related the highest optical power of an optically filtered signal with CD. For this highest power to be a monotonic function of CD the signal must be filtered with a rectangular filter, with a bandwidth that is equal to the bandwidth of the signal. Further investigations must study the impact of optical signal to noise ratio (OSNR) and polarization mode dispersion (PMD) on the monitoring results.

The optical performance monitor developed in Chapter 5, due to its elasticity may have future developments in future projects proposed by the author. One can propose the performance monitor developed in Chapter 5 to dynamically adapt the network in a software defined scenario, in order to accomplish the quality of service, by changing the modulation format or/and data rate. In order to accomplish this objective several developments have to be made, by separating the calculation of the data rate and the modulation format from the calculation of the impairments by itself, accordingly to Figure 1.1. As a researcher the author things to continue his work in all-optical signal processing. The author things to extend to multi-mode fiber the work done in Chapter 6 related with polarization control. Recently there was developments in that way by a research group in France, that the author plans to explore in future work.

Appendices

Appendix A

Patent application

(11) Número de Publicação: **PT 105360 A**

(51) Classificação Internacional:
G01R 13/00 (2006.01)

(12) **FASCÍCULO DE PATENTE DE INVENÇÃO**

(22) Data de pedido: **2010.10.29**

(30) Prioridade(s):

(43) Data de publicação do pedido: **2012.04.30**

(45) Data e BPI da concessão: /

(73) Titular(es):
UNIVERSIDADE DE AVEIRO
UATEC, ED. DA REITORIA 3º PISO, CAMPUS UNIVERSITÁRIO DE SANTIAGO 3810-193 AVEIRO **PT**
INSTITUTO DE TELECOMUNICAÇÕES **PT**

(72) Inventor(es):
ANTÓNIO LUÍS JESUS TEIXEIRA **PT**
MÁRIO JOSÉ NEVES DE LIMA **PT**
VITOR MANUEL COSTA RIBEIRO **PT**

(74) Mandatário:
LUÍS MANUEL DE ALMADA DA SILVA CARVALHO
RUA VÍCTOR CORDON, 14 1249-103 LISBOA **PT**

(54) Epígrafe: **MÉTODO DE GERAÇÃO DE DIAGRAMAS DE OLHO PARAMÉTRICOS EM MODO ASSÍNCRONO**

(57) Resumo:
A PRESENTE INVENÇÃO DIZ RESPEITO À ÁREA DAS TELECOMUNICAÇÕES, MAIS CONCRETAMENTE À ÁREA DOS SISTEMAS DE COMUNICAÇÃO DIGITAIS, DESCREVENDO-SE UM NOVO MÉTODO DE GERAÇÃO DE DIAGRAMAS DE OLHO EM MODO ASSÍNCRONO. ESTE PROCEDIMENTO PERMITE QUE, SEM O USO DE TÉCNICAS DE RECUPERAÇÃO E SINCRONIZAÇÃO COM O SINAL DE RELÓGIO QUE NORMALMENTE REQUEREM ELECTRÓNICA DE ALTA VELOCIDADE E COMPLEXOS MECANISMOS DE SINCRONISMO, FAZER A MONITORIA DA QUALIDADE DO SINAL (RELACIONADA COM AS MEDIÇÕES DO FACTOR DE QUALIDADE Q) OU DO DESEMPENHO (RELACIONADO COM O GRAU DE IMPACTO QUE OS IMPEDIMENTOS À TRANSMISSÃO DE SINAL, COMO A DIAFONIA ENTRE CANAIS, A DISPERSÃO E OUTROS, TÊM NO SISTEMA DE COMUNICAÇÃO) DO CANAL DE COMUNICAÇÃO, INDEPENDENTEMENTE DO RITMO DE TRANSMISSÃO OU DO FORMATO DE MODULAÇÃO E SEM O CONHECIMENTO PRÉVIO DE NENHUM DOS DOIS PARÂMETROS REFERIDOS. ESTE MÉTODO EMPREGA UM DIVISOR DE POTÊNCIA QUE DIVIDE A POTÊNCIA DO SINAL DE DADOS EM DUAS PARTES, ENVIANDO CADA UMA DAS DUAS PARTES PARA DUAS RAMIFICAÇÕES, ESTANDO A PRIMEIRA LIGADA A UM DISPOSITIVO DE AMOSTRAGEM E REPRESENTAÇÃO NO ECRÃ (EXEMPLO OSCILOSCÓPIO) E A SEGUNDA A UM DIFERENCIADOR QUE DIFERENCIA O SINAL NO TEMPO E O ENVIA TAMBÉM PARA O DISPOSITIVO DE AMOSTRAGEM E REPRESENTAÇÃO NO ECRÃ. AS AMOSTRAS CAPTURADAS DA PRIMEIRA SÃO REPRESENTADAS, PREFERENCIALMENTE, EM FUNÇÃO DAS AMOSTRAS RETIRADAS DA SEGUNDA RAMIFICAÇÃO, SENDO A PRIMEIRA A ORDENADA E A SEGUNDA A ABCISSA DE UM PONTO REPRESENTADO NUM SISTEMA DE DOIS EIXOS.

RESUMO

"MÉTODO DE GERAÇÃO DE DIAGRAMAS DE OLHO PARAMÉTRICOS EM MODO ASSÍNCRONO"

A presente invenção diz respeito à área das telecomunicações, mais concretamente à área dos sistemas de comunicação digitais, descrevendo-se um novo método de geração de diagramas de olho em modo assíncrono. Este procedimento permite que, sem o uso de técnicas de recuperação e sincronização com o sinal de relógio que normalmente requerem electrónica de alta velocidade e complexos mecanismos de sincronismo, fazer a monitoria da qualidade do sinal (relacionada com as medições do factor de qualidade Q) ou do desempenho (relacionado com o grau de impacto que os impedimentos à transmissão de sinal, como a diafonia entre canais, a dispersão e outros, têm no sistema de comunicação) do canal de comunicação, independentemente do ritmo de transmissão ou do formato de modulação e sem o conhecimento prévio de nenhum dos dois parâmetros referidos. Este método emprega um divisor de potência que divide a potência do sinal de dados em duas partes, enviando cada uma das duas partes para duas ramificações, estando a primeira ligada a um dispositivo de amostragem e representação no ecrã (exemplo osciloscópio) e a segunda a um diferenciador que diferencia o sinal no tempo e o envia também para o dispositivo de amostragem e

representação no ecrã. As amostras capturadas da primeira são representadas, preferencialmente, em função das amostras retiradas da segunda ramificação, sendo a primeira a ordenada e a segunda a abcissa de um ponto representado num sistema de dois eixos.

DESCRIÇÃO

"MÉTODO DE GERAÇÃO DE DIAGRAMAS DE OLHO PARAMÉTRICOS EM MODO ASSÍNCRONO"

Domínio técnico da invenção

A presente invenção diz respeito à área das telecomunicações, descrevendo-se um novo método de gerar diagramas de olho em modo assíncrono.

Descrição do estado da técnica

Um diagrama de olho é uma imagem, construída a partir da sobreposição de vários bits, de onde se retira informação sobre a qualidade do sinal e da performance do canal de comunicações. Usualmente esta imagem é apresentada em osciloscópios.

A Figura 1 apresenta um diagrama de olho com modulação não retorno a zero (NRZ), para um sinal de 40 Gbit/s, obtido em modo síncrono, em que, no eixo vertical, é representada a amplitude do sinal e no eixo horizontal é representado o tempo em segundos. O eixo horizontal está centrado no centro do bit com duração de 25 pico segundos, precisamente o período temporal de um sinal com o ritmo de transmissão de 40 Gbit/s.

A um diagrama de olho normalmente está associada, entre outras características, a altura do olho (1) a largura do olho (2) e a variação da amplitude do bit (3). Esta ultima característica, a variação da amplitude do bit está associada ao ruído do sinal, ou outras formas de distorção do mesmo sinal. Quando o sinal está muito corrompido com ruído ou com outras formas de distorção, o olho tende a fechar. Não tem grande valor informativo a área circunscrita por (4) e (5). Só a área (6) respeitante ao olho, tem valor informativo significativo quando se pretende avaliar, o desempenho do canal ou a qualidade do sinal.

O sincronismo ou assincronismo numa amostragem de um sinal, seja este óptico ou outro, é definido como a característica em que as amostras do sinal são retiradas a uma frequência de amostragem, que é ou não, respectivamente, directamente proporcional à frequência do relógio e em que a transição ascendente do relógio do sinal de dados e do relógio do amostrador, ocorrem ou não, respectivamente, simultaneamente. A frequência de relógio do sinal de dados está relacionada ao ritmo de transmissão.

O conceito de transparência é também uma característica técnica muito importante para avaliar a robustez de um dispositivo de monitoria.

Um dispositivo diz-se transparente a uma determinada característica do sinal, como o ritmo de

transmissão, ou o formato de modulação, se puderem ser feitas medidas e/ou observações, neste sinal, sem ser necessário proceder a alterações físicas ou algorítmicas no dispositivo, devido a mudanças dessas mesmas características.

Normalmente associado à geração de um diagrama de olho síncrono, está um circuito de recuperação de relógio, que normalmente é constituído por um phase-locked loop (PLL), ou por um filtro externo de elevado factor de qualidade Q [George Georgiou et al.: Clock and Data Recovery IC for 40-Gb/s Fiber-Optic Receiver, IEEE Journal Of Solid-State Circuits, Vol. 37, No. 9, September 2002; Tan Kok-Siang et al., "Design of high-speed clock and data recovery circuits", Springer Analog Integrated Circuits and Signal Processing, Vol. 52, No. 1-2, August 2007].

Na Figura 2 está representado um diagrama com um circuito de recuperação de relógio baseado em PLL. A forma de funcionamento deste circuito é a seguinte: um Oscilador Controlado por Tensão (OCT) (22) é executado, inicialmente, perto do ritmo de transmissão de interesse. Uma parcela do sinal do OCT forma uma entrada (14) para um detector de fase (20). A outra entrada (10) para o detector de fase são os dados de entrada. O detector de fase compara as fases das duas entradas e produz uma tensão de saída (11) relacionada com a diferença de fase (o "erro do sinal" (11)). Normalmente este sinal é filtrado (21) de alguma

forma, tornando-se a tensão de controle de freqüência do OCT (12).

As PLLs, utilizam electrónica com elevada exigência ao nível da velocidade de processamento de sinal, quando se tratam de taxas de fluxo de bits também elevadas. O custo também pode ser elevado [Ruben S. Luís et al.: Optical Signal-to-Noise Ratio Estimation Using Reference Asynchronous Histograms, Journal Of Lightwave Technology, Vol. 27, No. 6, March 15, 2009] nestas condições. O uso de recuperação de relógio para geração de diagramas de olho síncronos cria dificuldades ao nível da transparência com o ritmo de transmissão, quando múltiplos sinais com diferentes ritmos de transmissão, operam no sistema de comunicação [R. Luís et al.: Performance Monitoring in Optical Networks Using Asynchronously Acquired Samples With Nonideal Sampling Systems and Intersymbol Interference, Journal Of Lightwave Technology, Vol. 22, No. 11, November 2004]. Isto pode ser verificado pela necessidade de usar um OCT que é executado perto do ritmo de transmissão de interesse.

Outras abordagens constroem um diagrama de olho amostrando o sinal assincronamente, calculando o periodograma do sinal, sem ser necessário proceder a alguma alteração física devido a alterações do ritmo de transmissão, sendo por isso transparente a este [L. Noirie et al.: New transparent optical monitoring of the eye and BER using asynchronous under-sampling of the signal, in

Proc. ECOC2002. PD 2.2.]. O sinal é sincronizado com a componente do espectro, de maior amplitude, obtida a partir do cálculo do periodograma.

Desta forma não se pode dizer que este método seja totalmente assíncrono, dado que alguma espécie de sincronismo é necessário. Esta abordagem é ainda conhecida por usar operações de processamento de sinal complicadas [Ippei Shake et al.: Simple Measurement of Eye Diagram and BER Using High-Speed Asynchronous Sampling, Journal Of Lightwave Technology, Vol. 22, No. 5, May 2004] e por ainda não ter sido demonstrada a sua transparência ao formato de modulação.

Uma técnica baseada em medição de histogramas em diagramas de olho assíncronos foi também desenvolvida. Um exemplo dessa mesma técnica pode ser vista em [Ruben S. Luís et al.: Optical Signal-to-Noise Ratio Estimation Using Reference Asynchronous Histograms, Journal Of Lightwave Technology, Vol. 27, No. 6, March 15, 2009]. Esta técnica tem a vantagem de ser transparente ao ritmo de transmissão e ao formato de modulação, no entanto os diagramas de olho obtidos, tem o problema de obter amostras a meia altura do diagrama de olho assíncrono, que corrompem a medição do factor de qualidade Q e não permitem uma rápida visualização, através da simples observação do diagrama de olho, da qualidade do sinal, como permitem os diagramas de olho abertos [Zhongqi Pan et al: Optical Performance

monitoring for the next generation optical communication networks, Optical Fiber Technology, 2009].

Outra técnica reconstrói o diagrama de olho amostrando o sinal assincronamente, mas requer conhecimento prévio do ritmo de transmissão, para gerar diagramas de olho precisos [Ippei Shake et al.: Simple Measurement of Eye Diagram and BER Using High-Speed Asynchronous Sampling, Journal Of Lightwave Technology, Vol. 22, No. 5, May 2004]. Por este motivo quando o ritmo de transmissão muda é necessário proceder a ajustes do algoritmo que controla o dispositivo, para se adequar a esta mudança. Desta forma esta técnica não é transparente ao ritmo de transmissão.

Alternativa similar à construção de diagramas de olho, para análise da qualidade do sinal e da perfomance do canal óptico, também foi desenvolvida recentemente. É exemplo dessa mesma técnica [Trevor B. Anderson et al: Multi Impairment Monitoring for Optical Networks, Journal Of Lightwave Technology, Vol. 27, No. 16, August 15, 2009], que usa um par de amostras retiradas assincronamente, do mesmo sinal, uma com um tempo de atraso em relação à outra, de um tempo de bit, ou com fracções de tempo de bit. Este par de amostras gera um diagrama em que as amostras do sinal atrasado são colocadas em função das amostras do sinal não atrasado, gerando aquilo que é conhecido na literatura como “phase portraits”, ou diagramas de fase, demonstrados na Figura 2 e Figura 3 de [Trevor B. Anderson et al: Multi Impairment Monitoring for Optical Networks,

Journal Of Lightwave Technology, Vol. 27, No. 16, August 15, 2009], para modulações NRZ e modulações retorno a zero (RZ), respectivamente. Estes diagramas de fase produzem padrões de elevada riqueza a nível informativo com uma complexidade similar aos diagramas de olho, mas sem necessitar de recuperação de relógio [Zhongqi Pan et al: Optical Performance monitoring for the next generation optical communication networks, Optical Fiber Technology, 2009]. Embora estes diagramas não produzam geralmente formas de diagramas de olho, produzem bons indicadores da performance do canal óptico e da qualidade do sinal, sendo alternativas viáveis aos diagramas de olho. Para algumas situações concretas, imagens parecidas com um diagrama de olho são produzidas, como em [Jian Zhao et al:NRZ-DPSK and RZ-DPSK Signals Signed Chromatic Dispersion Monitoring Using Asynchronous Delay-Tap Sampling, Journal Of Lightwave Technology, Vol. 27, No. 23, December 1, 2009], no entanto para diferentes formatos de modulação isso já não se verifica como se pode verificar em [Ken Clarke et al: Monitoring of Chromatic Dispersion for 10 Gbit/s RZ modulation using Asynchronous Sampling, Proceedings of ACOFT/AOS 2006 - Melbourne, Australia, 10 - 13 July 2006], em que é utilizado o mesmo tempo de atraso de meio bit. A análise destes diagramas, requer no entanto o conhecimento prévio do ritmo de transmissão e do formato de modulação [Y. Zhou et al: Identification Using Asynchronous Delay-tap Sampling, ECOC 2008, 21-25 September 2008, Brussels, Belgium]. Além disto é necessário ajustar fisicamente o tempo de atraso, de acordo com o ritmo de transmissão do

sinal. É necessário também, ajustar a análise do diagrama tendo em conta o formato de modulação. Isto implica que esta técnica não é transparente ao formato de modulação, nem ao ritmo de transmissão.

Sumário da invenção

A presente invenção descreve um método de gerar diagramas de olho assíncronos e transparentes ao ritmo de transmissão e formato de modulação.

A presente invenção reduz as necessidades de utilizar circuitos de conversão de analógico para digital, com elevadas demandas ao nível da velocidade de processamento de sinal, permitindo que o sinal seja amostrado a frequências muito abaixo do ritmo de transmissão e sem qualquer relação com o relógio do sinal de dados.

Relativamente às técnicas discutidas na secção "Descrição do estado da técnica", esta técnica gera diagramas de olho completamente assíncronos, ao mesmo tempo que é capaz de gerar diagramas de olho abertos (caso o sinal não esteja corrompido por ruído), sem necessidade de sincronizar com nenhum sinal de relógio obtido seja por recuperação de relógio, ou por periodograma, ou outro, algo não conseguido por nenhuma das técnicas anteriormente descritas.

Para que isso aconteça o método proposto, utiliza um diferenciador.

Descrição geral da invenção

Nesta invenção é proposta uma nova técnica, que gera diagramas de olho em modo assíncrono, sem auxílio de qualquer sinal de relógio ou outro sinal de sincronismo. Para tal deve-se ter em consideração o diagrama da Figura 3, em que o dispositivo de geração de diagramas de olho (1010), está implementado num sistema de comunicações genérico. Este sistema de comunicações genérico é aplicável, a qualquer sistema de comunicações, sejam estes sistemas de comunicações por fibra óptica, sistemas de comunicações rádio, ou outros, onde seja possível propagar ondas acústicas, ou electromagnéticas.

O transmissor (2000) emite numa determinada frequência (ou frequências se o sistema for multicanal), chamada a frequência da portadora. Esta portadora é modulada com a informação que se pretende transmitir e o sinal é enviado através do canal de comunicações (2010), que pode ser uma fibra óptica, ou um par de fios (geralmente de cobre) onde o sinal eléctrico é transportado, ou a água, numa comunicação submarina, onde a informação é transmitida acusticamente, ou o ar, numa comunicação sem fios. Outros canais de comunicação são os discos magnéticos e os discos ópticos [John G. Proakis et al.: COmmunications Systems Engineering, Prentice-Hall International, pp. 13-21, 1994]. O receptor (2020) recebe

a informação e traduze-la, para uma completa compreensão da informação referida. Posteriormente a potência do sinal é dividida, em partes iguais e é enviada num dos braços, para um dispositivo de amostragem e representação num ecrã (2040) (exemplo osciloscópio) e no outro braço, é enviada para um diferenciador (2030). Este diferenciador calcula a derivada do sinal que vem do receptor e envia-a, também, para o osciloscópio (2040).

Formas práticas de implementar um diferenciador foram propostas por [Al-Alaoui, M.A: Novel IIR differentiator from the Simpson integration rule, IEEE Transactions on Circuits and Systems I: Fundamental Theory and Applications, Vol. 41 , No. 2, 1994; Jing Xu et al.: High-speed all-optical differentiator based on a semiconductor optical amplifier and an optical filter, Optics Letters, Vol. 32, No. 13, July , 2007; Zhengyong Li et al.: All-optical differentiator and high-speed pulse generation based on cross-polarization Modulation in a semiconductor optical amplifier, Optics Letters , Vol. 34, No. 6 , March 15, 2009; Pantelis Velanas et al.: High-Speed All-Optical First- and Second-Order Differentiators Based on Cross-Phase Modulation in Fibers, Journal Of Lightwave Technology, Vol. 26, No. 18, September 15, 2008; Mykola Kulishov et al: Long-period fiber gratings as ultrafast optical differentiators, Optics Letters, Vol. 30, No. 20, October 15, 2005; Jing Xu et al.: All-optical differentiator based on cross-gain modulation in

semiconductor optical amplifier, Optics Letters , Vol. 32, No. 20, October 15, 2007].

De uma forma geral o funcionamento do dispositivo de geração de diagramas de olho (1010) compreende a captação de duas amostras, uma do sinal que vem do diferenciador (2030) e a outra que vem directamente do receptor (2020). Estas amostras são capturadas simultaneamente e assincronamente, não tendo o relógio do amostrador, qualquer sincronismo com o relógio do sinal. O valor das duas amostras é representado num sistema de 2 eixos X e Y, como aquele que é apresentado na Figura 12, onde consta um exemplo. O valor da amostra que vem do diferenciador (2030) está representado no eixo X e corresponde à abcissa (52). O valor da amostra que corresponde ao sinal que vem do receptor (2020) está representado no eixo Y e corresponde à ordenada (51). A representação dos valores destas duas amostras em cada um dos eixos, corresponde à representação de um ponto (50) no plano do sistema de dois eixos. O mesmo procedimento é repetido para cada par de amostras. Pontos obtidos de forma semelhante a (50) são representados no plano do sistema de dois eixos gerando uma imagem equivalente a um diagrama de olho.

Descrição dos Desenhos

Este novo conceito de um sistema de geração de diagramas de olho em modo assíncrono é de seguida descrito em pormenor, sem carácter limitativo e a título

exemplificativo, na sua forma de realização preferencial, representada nas figuras anexas, das quais:

- A **Figura 1** representa um diagrama de olho obtido sincronamente, com descrições das suas características.

- A **Figura 2** representa um phase-locked loop (PLL), com as suas partes constituintes.

- A **Figura 3** representa o diagrama de blocos de um sistema de comunicações.

- A **Figura 4** representa uma implementação do sistema de geração de diagramas de olho em modo assíncrono, num sistema de comunicações óptico de um único canal, na situação em que se usa um diferenciador eléctrico e no caso em que se utiliza modulações on-off keying (OOK), como as modulações NRZ-OOK e RZ-OOK.

- A **Figura 5** representa uma implementação do sistema de geração de diagramas de olho em modo assíncrono, num sistema de comunicações óptico de um único canal, na situação em que se usa um diferenciador óptico e no caso em que se utiliza modulações on-off keying (OOK), como as modulações NRZ-OOK e RZ-OOK.

- A **Figura 6** representa uma implementação do sistema de geração de diagramas de olho em modo assíncrono, num sistema de comunicações óptico de um único canal, na

situação em que se usa um diferenciador eléctrico e no caso em que se utiliza modulações deslocamento diferencial de fase (DPSK), como as modulações NRZ-DPSK e RZ-DPSK.

- A **Figura 7** representa uma implementação do sistema de geração de diagramas de olho em modo assíncrono, num sistema de comunicações óptico de um único canal, na situação em que se usa um diferenciador óptico e no caso em que se utiliza modulações deslocamento diferencial de fase (DPSK), como as modulações NRZ-DPSK e RZ-DPSK.

- A **Figura 8** representa uma implementação do sistema de geração de diagramas de olho em modo assíncrono, num sistema de comunicações óptico multicanal, na situação em que se usa um diferenciador eléctrico e no caso em que o canal em análise utiliza modulações on-off keying (OOK), como as modulações NRZ-OOK e RZ-OOK.

- A **Figura 9** representa uma implementação do sistema de geração de diagramas de olho em modo assíncrono, num sistema de comunicações óptico multicanal, na situação em que se usa um diferenciador óptico e no caso em que o canal em análise utiliza modulações on-off keying (OOK), como as modulações NRZ-OOK e RZ-OOK.

- A **Figura 10** representa uma implementação do sistema de geração de diagramas de olho em modo assíncrono, num sistema de comunicações óptico multicanal, na situação em que se usa um diferenciador eléctrico e no caso em que o

canal em análise utiliza modulações deslocamento diferencial de fase (DPSK), como as modulações NRZ-DPSK e RZ-DPSK.

- A **Figura 11** representa uma implementação do sistema de geração de diagramas de olho em modo assíncrono, num sistema de comunicações óptico multicanal, na situação em que se usa um diferenciador óptico e no caso em que o canal em análise utiliza modulações deslocamento diferencial de fase (DPSK), como as modulações NRZ-DPSK e RZ-DPSK.

- A **Figura 12** representa um sistema de dois eixos em que a amostra do sinal (21) e do sinal diferenciado (52), são representados como a ordenada e a coordenada do ponto representado (50).

Descrição das Tabelas

- A **Tabela 1** representa o conjunto de figuras do diagrama de olho em modo assíncrono e do diagrama de olho em modo síncrono em função do formato de modulação
- A **Tabela 2** representa duas figuras do diagrama de olho em modo síncrono e assíncrono com o sinal corrompido com ruído.

Números de referência:

1-> Altura do diagrama de olho síncrono

2-> Largura do diagrama de olho síncrono

3-> Variação da altura do bit

4,5-> Zonas de transição 1-1 no formato de modulação NRZ

6-> Zona que circunscreve o olho

10-> Entrada de dados na PLL (sinal eléctrico)

11-> Sinal de erro (sinal eléctrico)

12-> Sinal de controlo da OCT (sinal eléctrico)

13-> Sinal de relógio recuperado (sinal eléctrico)

14-> Sinal de referência (sinal eléctrico)

20-> Detector de fase

21-> Filtro eléctrico

22-> Oscilador controlado por tensão

2000-> Transmissor de um sistema de comunicações

2010-> Canal de comunicações num sistema de comunicações

2020->Receptor de um sistema de comunicações

2030-> Diferenciador

100-> Transmissor WDM

101, 102, 103, 104, 105, 106, 107, 108, 109-> Ligações por cabo eléctrico

110, 111, 112, 113, 114, 115, 117, 118, 119, 120, 121, 122, 123, 124, 125->Ligações por fibra óptica

116-> Ligação de fibra óptica de longa distância

200, 201, 204, 205-> Gerador de sinal eléctrico modulante

300, 301, 302, 304, 305-> Lasers sintonizados em frequência

400, 401, 402, 404, 405-> Moduladores de fase ou intensidade óptica

500-> Multiplexador óptico em frequência

600-> Amplificador óptico

700-> Detector óptico

800-> Divisor eléctrico de potência

802-> Divisor óptico de potência

900, 2040-> Dispositivo de amostragem e representação no ecrã, das amostras capturadas.

1000-> Diferenciador eléctrico

1001-> Diferenciador óptico

1100-> Filtro óptico

1200-> Interferómetro Mach-Zhender

1010-> Dispositivo de geração de diagramas de olho assíncronos.

801-> Frequência central do filtro óptico

812, 813-> Definem a largura de banda do filtro óptico a -3 dB

822, 823-> Definem a extensão máxima da zona de corte e a largura de banda correspondente

50-> Ponto no sistema de 2 eixos X-Y, que é o resultado da representação do valor da amostra da derivada do sinal que é a coordenada no eixo X e do valor da amostra do sinal que é a ordenada no eixo Y

51->Valor da ordenada no eixo Y que representa o sinal (105)

52-> Valor da abcissa no eixo X que representa a derivada do sinal.

Uma explicação geral do modo de funcionamento do sistema já foi previamente demonstrada quando nos referimos à Figura 3 e seus constituintes. De seguida vamos dar alguns exemplos de aplicação deste método, utilizando as comunicações por fibra óptica como exemplo.

Exemplos:

Os exemplos abaixo demonstrados mostram a aplicação do gerador de diagramas de olho em modo assíncrono, a comunicações por fibra óptica, no entanto o mesmo método é aplicável a outro tipo de comunicações com outro meio de propagação, como já foi anteriormente explicado, quando nos referimos à Figura 3.

Pretende-se gerar um diagrama de olho em modo assíncrono de um sinal com um ritmo de transmissão de 10 Gbit/s e observar o mesmo, estando o dispositivo gerador de diagramas de olho assíncronos, montado num sistema de um único canal óptico como demonstrado na Figura 4. As modulações utilizadas nos exemplos abaixo descritos são citadas a título de exemplo, no entanto, não existe restrições ao nível das modulações possíveis, na medida em que todas as modulações, que são possíveis de ser observadas por um diagrama de olho síncrono, também são possíveis de ser observadas, por um diagrama de olho assíncrono proposto e com formas semelhantes.

O laser (305) está centrado na frequência de 1550 nm e é modulado através do modulador óptico (405), por um gerador de sinal modulante (205) NRZ. Estes compõem o transmissor neste sistema de comunicações. O sinal passa pela fibra óptica de longa distância (116), que representa o canal de comunicações e é amplificado devido ás perdas na fibra por um amplificador óptico (600), sendo posteriormente filtrado, por um filtro óptico (1100). O filtro

óptico (1100) está centrado na frequência de 1550 nm, ou seja, a frequência de transmissão do laser (305). O sinal é detectado por um fotodetector (700), onde o sinal óptico é convertido para um sinal eléctrico. O amplificador óptico (600), o filtro óptico (1100) e o fotodetector (700) compõem o receptor deste sistema de comunicações. A potência do sinal convertido para o domínio eléctrico é posteriormente dividida, preferencialmente, em duas partes iguais, pelo divisor de potência (800). Uma das partes é enviada pela ligação eléctrica (105), para o dispositivo de amostragem e representação num ecrã (900). A outra parte é enviada para o diferenciador eléctrico (1000), pela ligação eléctrica (104), onde o sinal é diferenciado electricamente e enviado, também para o dispositivo de amostragem e representação no ecrã (900). O par de amostras é representado como um único ponto, em que a abcissa é o valor da amostra da derivada retirada do sinal que atravessa (106) e a ordenada é o valor da amostra retirada do sinal que atravessa (105). O diagrama de olho assíncrono e síncrono está representado na Tabela 1. Estes diagramas de olho foram retirados para um OSNR, calculado na ligação (117) igual a 36 dB. Podemos ver um diagrama de olho bem aberto tanto no modo assíncrono, como síncrono. A frequência de amostragem do diagrama de olho assíncrono é 9.14 Giga-amostras/s e a frequência de amostragem do diagrama de olho síncrono é 1.56 Tera-amostras/s.

Um segundo exemplo pode ser retirado se colocarmos modulação RZ no gerador de sinal modulante (205)

e utilizarmos o mesmo aparato da Figura 4, seguindo os mesmos procedimentos e condições referidas para a modulação NRZ. Na Tabela 1 está representado as figuras do diagrama de olho assíncrono e síncrono para este caso.

Os mesmos exemplos anteriores para as modulações referidas podem ser repetidos no aparato da Figura 5. A diferença reside no facto de o sinal permanecer no domínio óptico, após a filtragem do filtro óptico (1100) e no facto de por este motivo não estar presente neste aparato da Figura 5 o fotodetector (700). Deste modo a ligação (117) liga o filtro óptico a um divisor de potência óptico (802). Este divide a potência óptica em duas partes, preferencialmente, iguais, enviando uma parte para o diferenciador óptico pela ligação por fibra óptica (118) e a outra parte pela ligação por fibra óptica (119), a um dispositivo com capacidade para proceder à amostragem óptica do sinal e respectiva representação deste sinal num ecrã (900). A amostragem óptica permite o uso de um detector mais lento. Os resultados anteriormente demonstrados para o caso em que se usa um diferenciador eléctrico são semelhantes aos obtidos com um diferenciador óptico e portanto não estão demonstrados.

As modulações NRZ-DPSK e RZ-DPSK também foram testadas no aparato da Figura 6. Relativamente ao aparato da Figura 4 a diferença reside no facto de se acrescentar um interferómetro Mach-Zhender (1200), para a conversão de modulação de fase, para modulação em amplitude. Os

resultados para estas modulações estão demonstrados na Tabela 1.

Um aparato está demonstrado na Figura 7 para as modulações DPSK, no caso em que se utiliza um diferenciador óptico (802) e no caso em que se faz amostragem óptica. Os resultados obtidos com o aparato da Figura 6 para as modulações DPSK são semelhantes aos obtidos com o aparato da Figura 7 e portanto não estão demonstrados.

A Figura 8, a Figura 9, a Figura 10 e a Figura 11 representam a situação em que se usa um transmissor que emite mais do que uma frequência, ou seja é um transmissor multi-canal. Neste caso o filtro óptico (1100) está centrado na frequência do canal que se deseja observar com um diagrama de olho assíncrono.

A Figura 8 representa um aparato que selecciona um canal que tem modulação OOK e em que é utilizado um diferenciador eléctrico.

A Figura 9 representa um aparato que selecciona um canal que tem modulação OOK e em que é utilizado um diferenciador óptico.

A Figura 10 representa um aparato que selecciona um canal que tem modulação DPSK e em que é utilizado um diferenciador eléctrico.

A Figura 11 representa um aparato que selecciona um canal que tem modulação DPSK e em que é utilizado um diferenciador óptico.

A Tabela 2 mostra um diagrama de olho síncrono e assíncrono degradado em que o OSNR calculado foi de 9 dB. Podemos ver que o grau de degradação do diagrama de olho assíncrono e síncrono é semelhante.

Lisboa, 25 de Outubro de 2011

REIVINDICAÇÕES

1. Método de geração de diagramas de olho paramétricos, em modo assíncrono de modo a proceder à medição de diagramas de olho, sem auxílio do sinal de relógio, ou outro meio de sincronismo com o sinal de dados, obtendo-se diagramas de olho semelhantes no aspecto e no comportamento, quando na presença de ruído ou outra forma de distorção, aos diagramas de olho síncrono, caracterizado por compreender as seguintes etapas:

a. divisão da potência que entra no dispositivo de geração de diagramas de olho, em duas partes, preferencialmente iguais e envio de cada uma das duas partes referidas para cada uma das duas ramificações, que se encontram ligadas ao divisor de potência, estando uma delas ligada directamente a um dispositivo de amostragem e representação do sinal num ecrã e a restante a um diferenciador temporal que se liga também, e paralelamente à anterior, ao dispositivo de amostragem e representação do sinal num ecrã;

b. captação de vários pares de amostras, estando cada elemento deste par de amostras, relacionado com o sinal de cada uma das duas ramificações referidas, ou seja é retirada, uma amostra do sinal e uma amostra desse mesmo sinal, diferenciado no tempo, simultaneamente;

c. representação no ecrã das amostras do sinal, em função das amostras desse mesmo sinal diferenciado no tempo, correspondendo a cada par de amostras um ponto no plano X-Y, sendo preferencialmente, as coordenadas desse ponto

dadas, pelo valor da amostra do sinal de dados na ordenada e a amostra desse mesmo sinal de dados diferenciado no tempo na abcissa.

2. Método de acordo com a reivindicação 1 caracterizado por o ecrã para a representação do sinal ser um osciloscópio.

3. Método de acordo com a reivindicação 1 caracterizado por compreender, um divisor de potência que divide o sinal em duas ramificações, um diferenciador, que diferencia o sinal de uma dessas ramificações e um dispositivo de amostragem e representação do sinal no ecrã, que recolhe pares de amostras, cada uma retirada de cada uma dessas ramificações e as representa, em modo X-Y no ecrã.

4. Método de acordo com a reivindicação 1 caracterizado por o diagrama que se assemelha a um diagrama de olho obtido em modo síncrono e ao qual chamamos diagrama de olho em modo assíncrono, que quando ausente de qualquer espécie de ruído real, ou derivado de distorções do sinal, estar completamente aberto e circular e que quando na presença de ruído tende a fechar, tendo portanto o mesmo comportamento de um diagrama de olho síncrono.

5. Método de acordo com a reivindicação 1 a 3 caracterizado por ter uma amostragem que é assíncrona, relativamente ao relógio do sinal de dados.

6. Método de acordo com a reivindicação 1 e 5 caracterizado por não extrair ou obter de qualquer forma ou técnica, qualquer sinal de relógio de dados, para proceder ao sincronismo com o relógio do amostrador, não tendo necessidade do sinal de relógio de dados, para representar o diagrama de olho em modo assíncrono.

7. Método de acordo com a reivindicação 1, 5 e 6 caracterizado por ser transparente ao ritmo de transmissão.

8. Método de acordo com a reivindicação 1 caracterizado por ser transparente ao formato de modulação.

9. Método de acordo com a reivindicação 1 caracterizado por obter diagramas de olho assíncronos semelhantes no aspecto aos diagramas de olho síncronos, independentemente do formato de modulação utilizado.

10. Método de acordo com todas as reivindicações anteriores caracterizado por ser aplicável a todos os sistemas de comunicação digitais.

Lisboa, 25 de Outubro de 2011

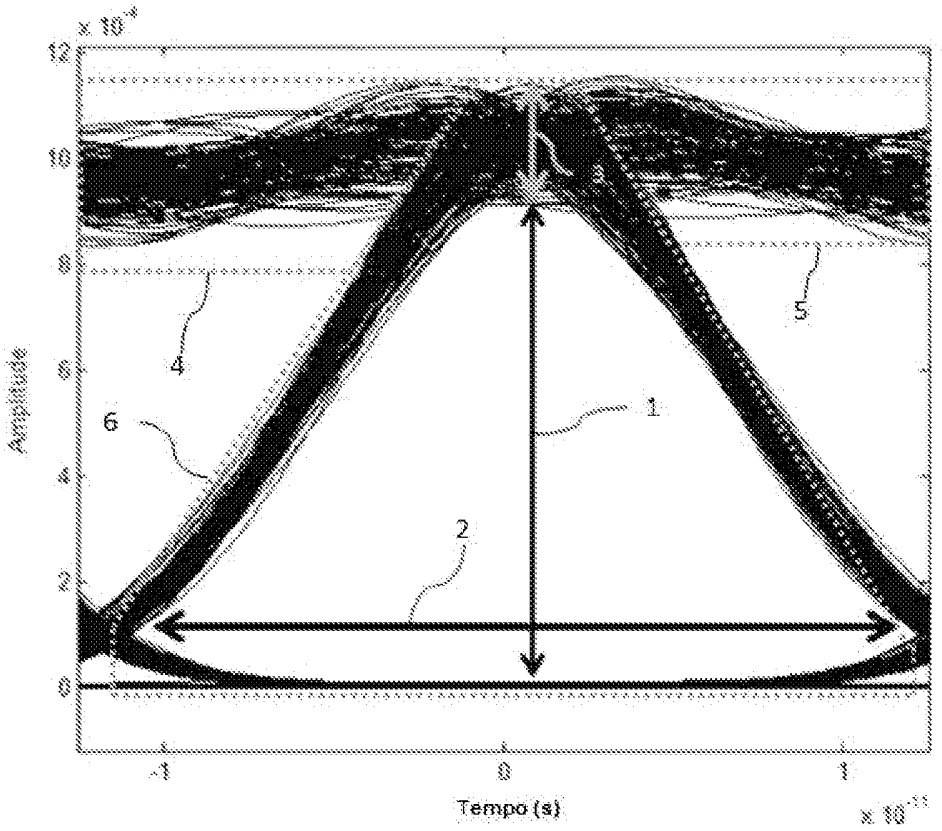

Figura 1

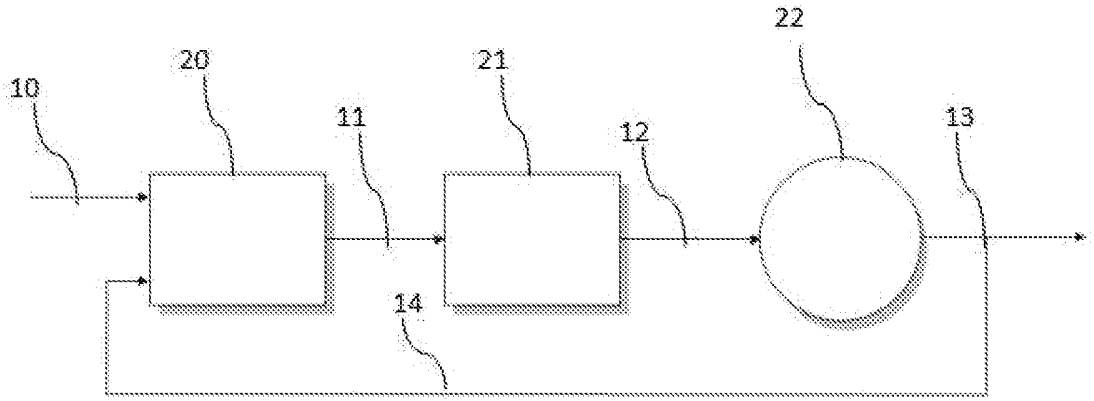

Figura 2

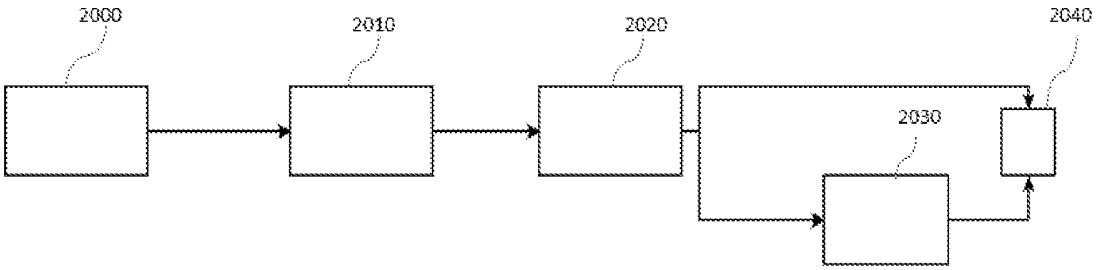

Figura 3

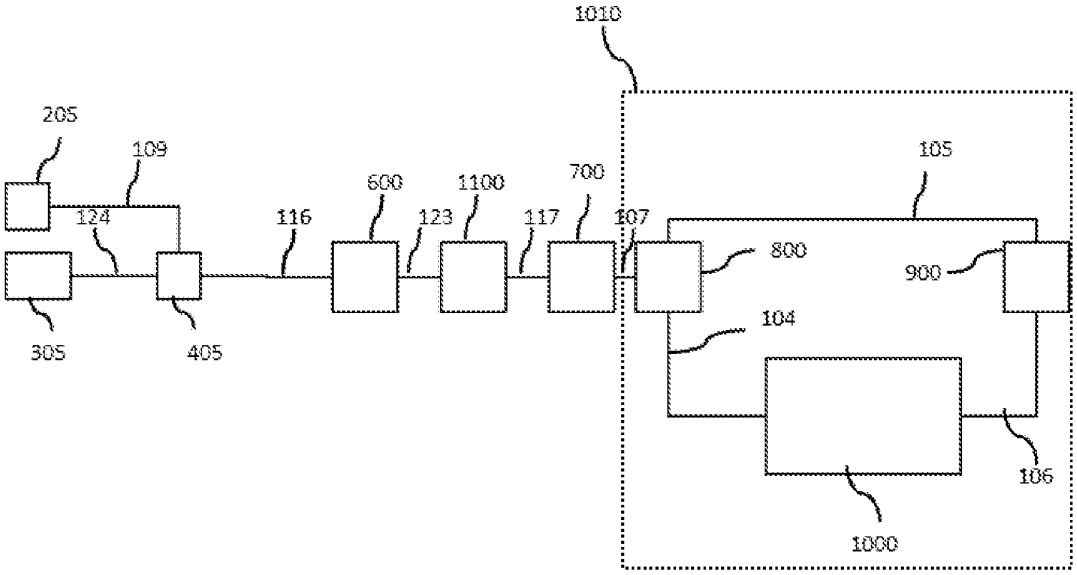

Figura 4

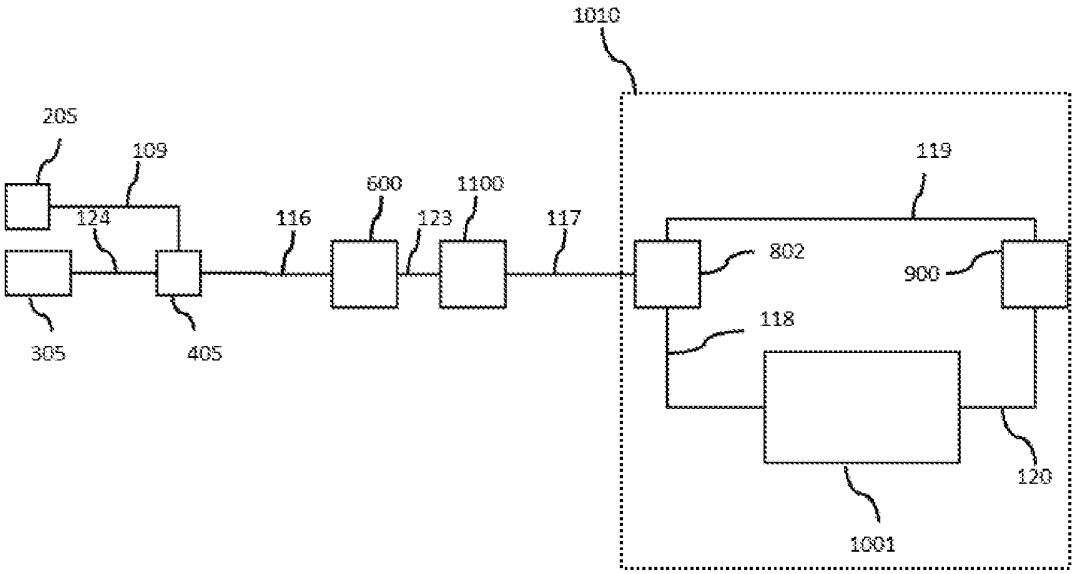

Figura 5

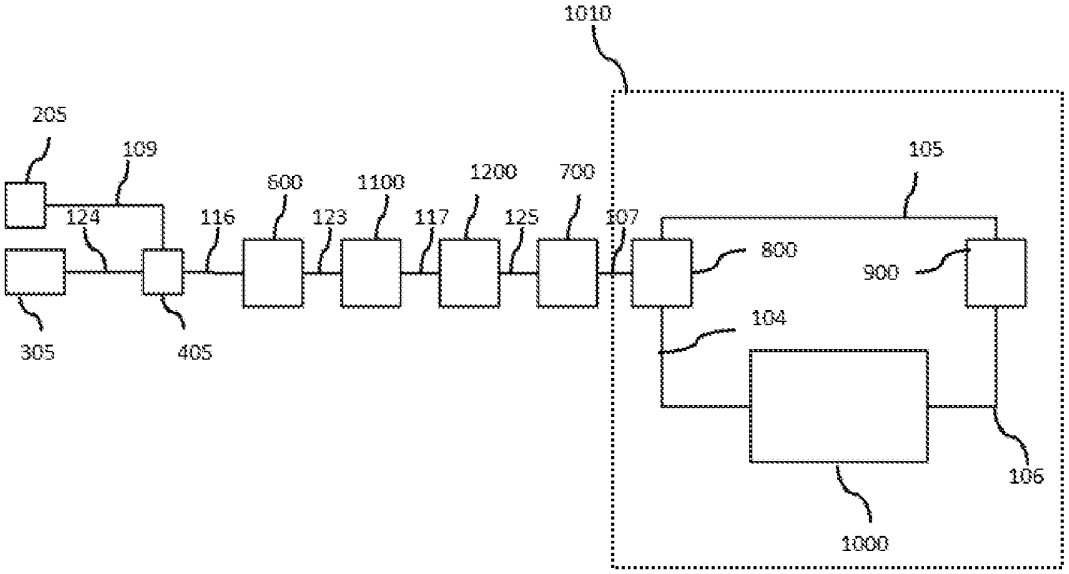

Figura 6

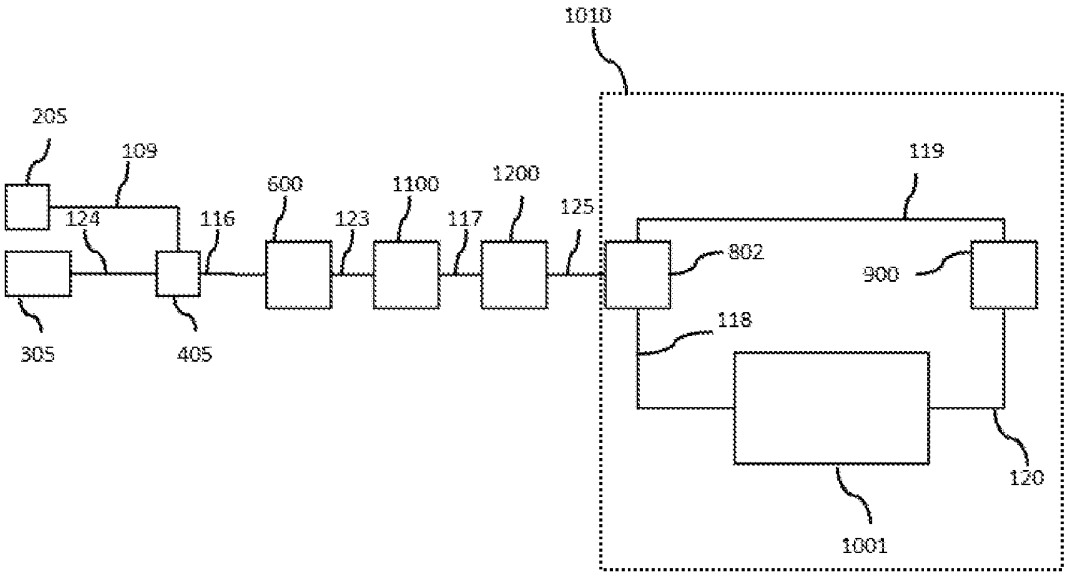

Figura 7

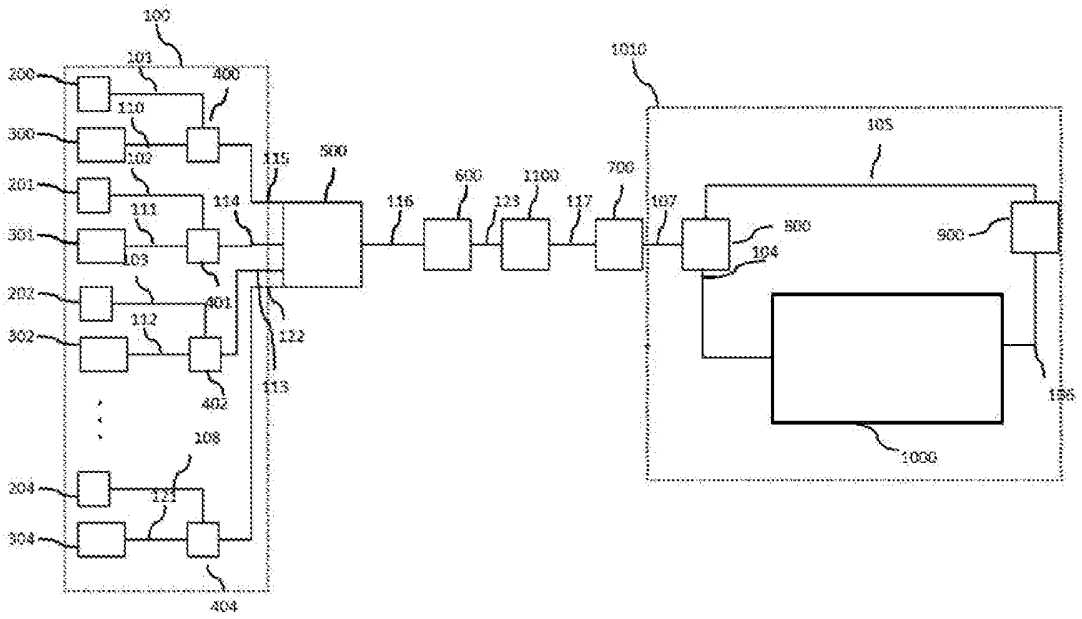

Figura 8

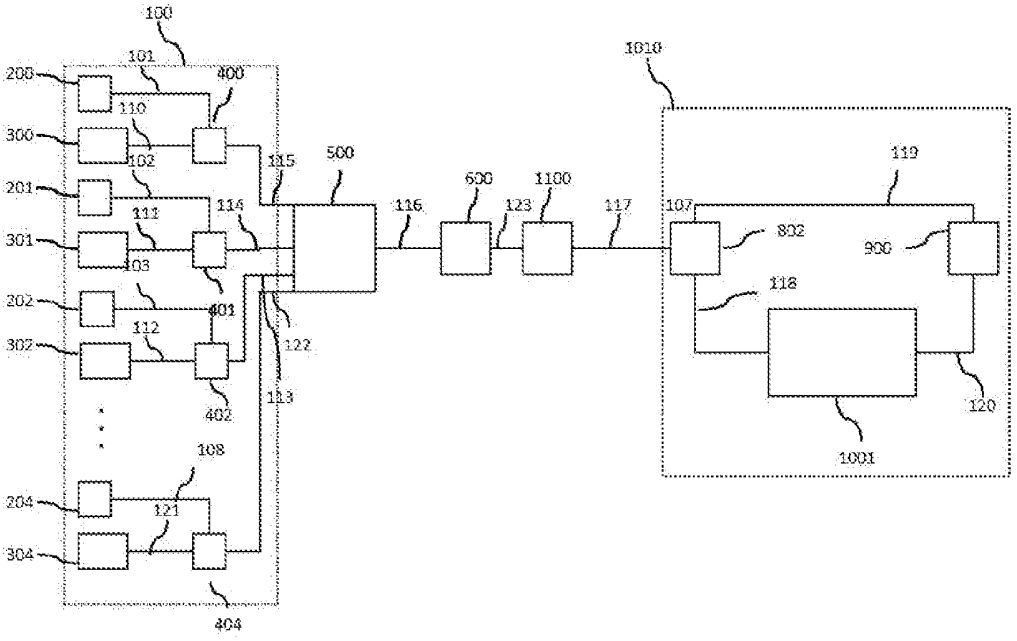

Figura 9

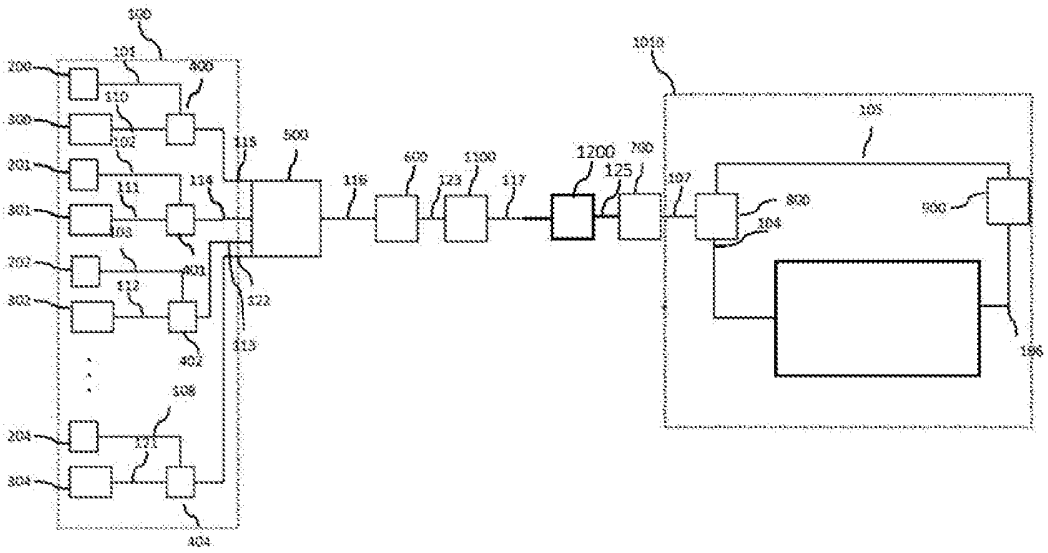

Figura 10

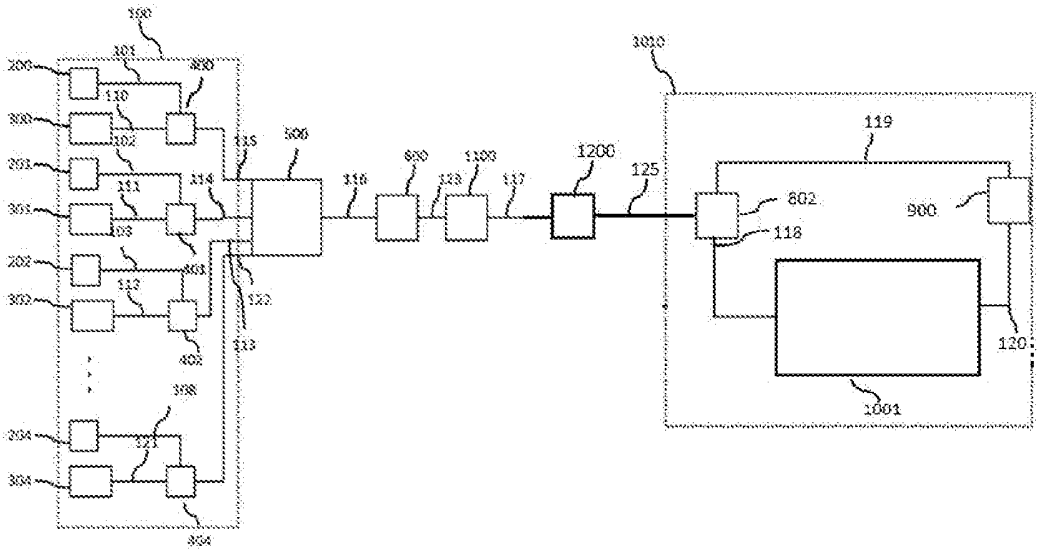

Figura 11

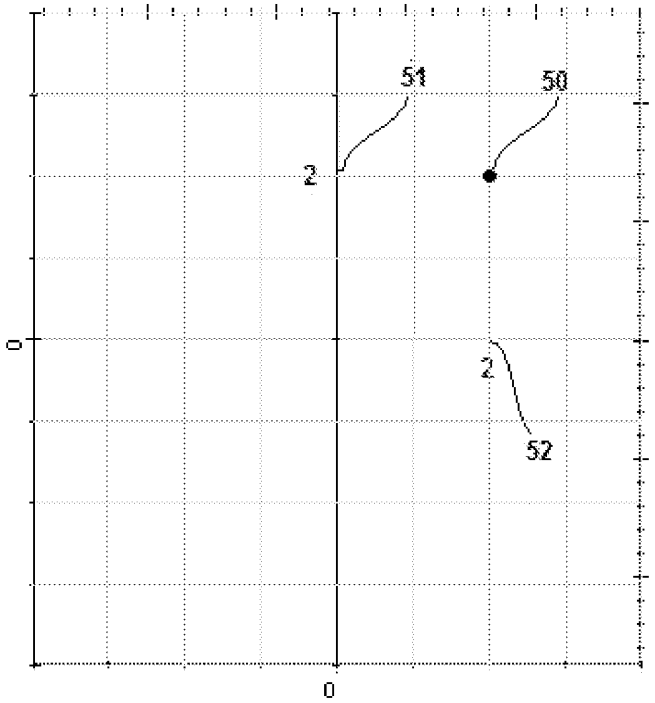

Figura 12

Tabela 1

Formato	Diagrama de olho assíncrono	Diagrama de olho síncrono
NRZ	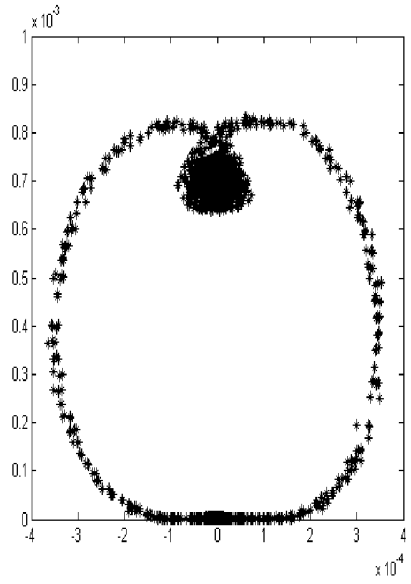	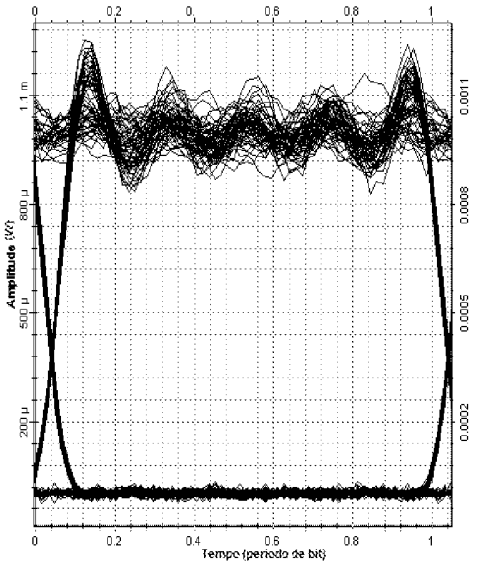
RZ	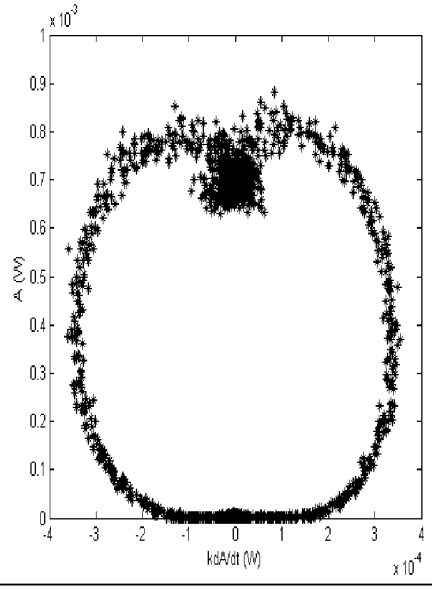	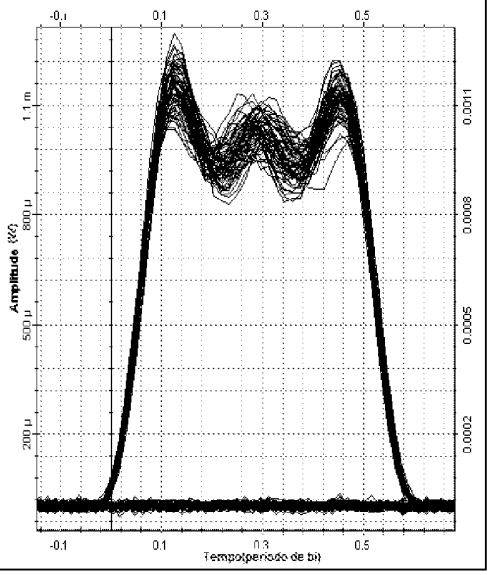

NRZ-DPSK	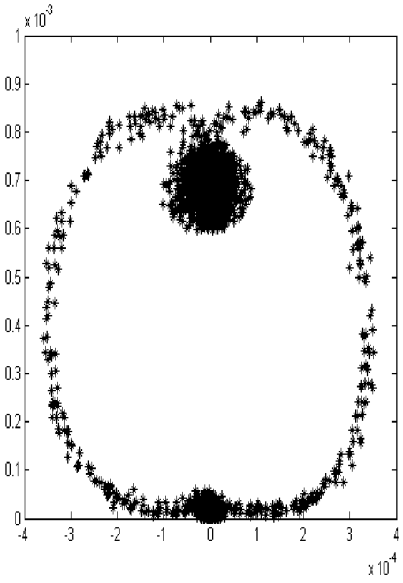	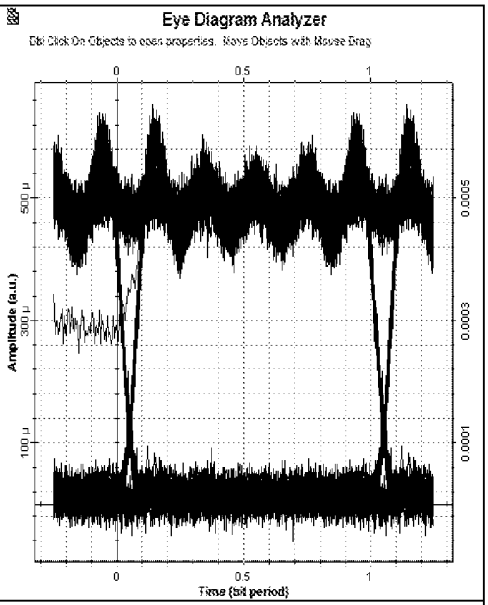
RZ-DPSK	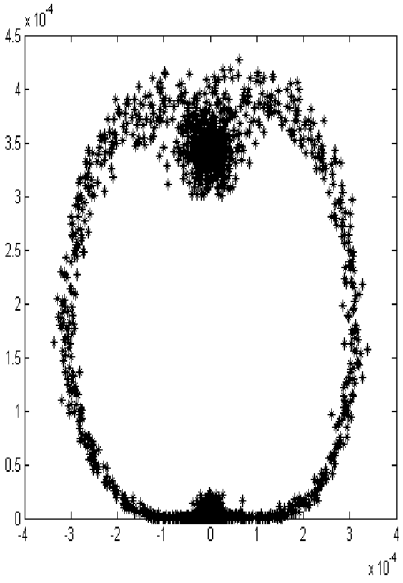	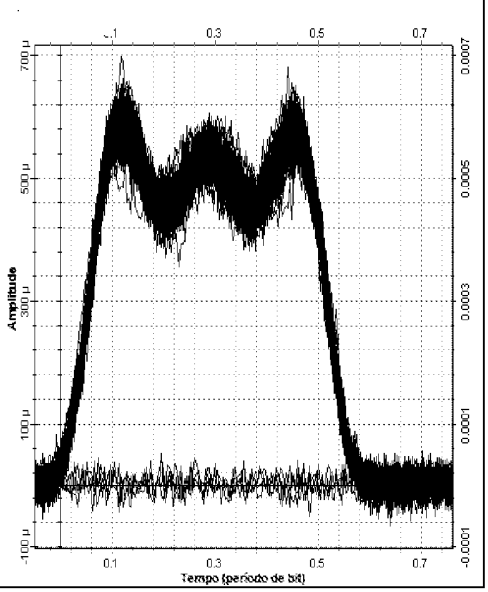

Tabela 2

Formato	Diagrama de olho assíncrono	Diagrama de olho síncrono
NRZ	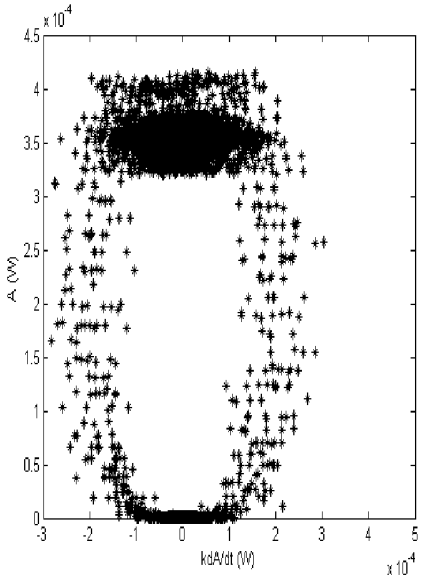	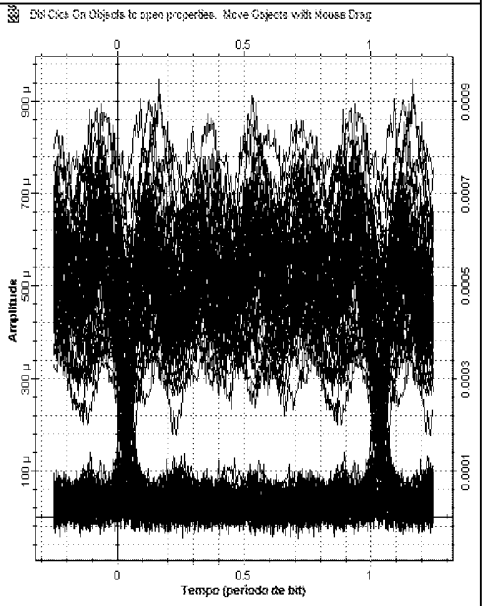

Index of acronyms